5-1-2016

Water Balance and Moisture Dynamics of an Arid and Semi-Arid Soil: A Weighing Lysimeter and Field Study

Jeremy E. Koonce
University of Nevada, Las Vegas, jkoonce@unlv.nevada.edu

WATER BALANCE AND MOISTURE DYNAMICS OF AN ARID AND SEMI-ARID SOIL: A WEIGHING LYSIMETER AND FIELD STUDY

By

Jeremy E. Koonce

Bachelor of Science – Environmental Studies and Geography
University of California, Santa Barbara
1998

Master of Science – Water Resources Management
University of Nevada, Las Vegas
2004

A dissertation submitted in partial fulfillment
of the requirements for the

Doctor of Philosophy – Geoscience

Department of Geoscience
College of Sciences
The Graduate College

University of Nevada, Las Vegas
May 2016

UNLV | GRADUATE COLLEGE

Dissertation Approval

The Graduate College
The University of Nevada, Las Vegas

January 29, 2016

This dissertation prepared by

Jeremy E. Koonce

entitled

Water Balance and Moisture Dynamics of an Arid and Semi-Arid Soil: A Weighing Lysimeter and Field Study

is approved in partial fulfillment of the requirements for the degree of

Doctor of Philosophy – Geoscience
Department of Geoscience

Zhongbo Yu, Ph.D.
Examination Committee Chair

Kathryn Hausbeck Korgan, Ph.D.
Graduate College Interim Dean

Markus Berli, Ph.D.
Examination Committee Member

Michael Nicholl, Ph.D.
Examination Committee Member

Ganqing Jiang, Ph.D.
Examination Committee Member

Dale Devitt, Ph.D.
Graduate College Faculty Representative

ABSTRACT

WATER BALANCE AND MOISTURE DYNAMICS OF AN ARID AND SEMI-ARID SOIL: A WEIGHING LYSIMETER AND FIELD STUDY

by

Jeremy E. Koonce

Dr. Zhongbo Yu, Examination Committee Chair
Professor of Hydrogeology and Hydrology
University of Nevada, Las Vegas

Semi-arid and arid environments are characterized by low precipitation and high evapotranspiration (ET), leaving little water available for discharge into surface water bodies and groundwater recharge. For these water-limited environments, understanding the relationships between precipitation, ET, and soil moisture is critical. These relationships not only affect water resources in these increasingly populated regions but are also necessary to predict the impact of climate change on semi-arid and arid ecosystems.

The overall goal of this dissertation was to shed light on the quantitative relationships between precipitation, evaporation, ET and soil moisture dynamics in an arid and a semi-arid environment. A three-step approach was chosen to (i) quantify soil water fluxes and storage of bare, arid soil in weighing lysimeters, (ii) evaluate a process-based evaporation model using evaporation data from the same bare, arid soil, and (iii) monitor the soil moisture and temperature dynamics of a vegetated, semi-arid soil at a field site. The studies were carried out at two sites in Nevada: (1) The bare arid soil is part of the SEPHAS weighing lysimeter facility, located in Boulder City near Las Vegas, southern NV; (2) The vegetated semi-arid soil with a shallow water table (depth to water < 6 m) is located in Spring Valley near Ely, central Nevada.

In a first step, precipitation, evaporation and infiltration, total soil mass and soil moisture profiles were monitored in three lysimeters over four years (water years 2009-2012). The results showed that 88 out of 180 precipitation events occurred during winter, but the average amount of precipitation per event was the highest during summer. Between 69% and 90% of annual precipitation was found to evaporate back into the atmosphere during the course of a water year (October through September). Water years with large amounts of winter precipitation (water years 2010 and 2011) yielded higher water storage compared to winters with lower amounts of precipitation (water years 2009 and 2012). Throughout spring, summer and autumn, most of the precipitated water evaporated back into the atmosphere, even after high intensity storms.

As for the soil moisture profile, two precipitation thresholds were found. The first threshold ranged between 0.5 and 2 mm total precipitation, representing the smallest amount of precipitation to cause a change in soil moisture content > 0.01 m^3 m^{-3} at 2.4 cm depth. This range depended on season, antecedent conditions, and the amount of time between previous and successive events. Data show that events with less than 1-2 mm total precipitation have little to no impact on moisture content below the immediate soil surface (top inch or so). With respect to soil water storage, water from storms with 1-2 mm total precipitation evaporate within a day, and do not have an impact on long-term soil water storage. The second precipitation threshold could be defined as the smallest amount of total precipitation needed to change soil moisture content at 25 cm depth by > 0.01 m^3 m^{-3}. Only 14 out of the 180 events (or sequence of events) changed soil moisture content at 25 cm depth or deeper. The 10 largest precipitation events (with respect to total amount of precipitation) were analyzed in more detail. Following all 10 events, soil moisture at 25 cm increased by 0.01 m^3 m^{-3} or more with total precipitation, intensity, and duration ranging between 13.2-41.6 mm, 0.6-12.3 mm hr^{-1}, and 1.5-52 hours, respectively. In

addition, there were two additional events and periods of time where multiple events occurred in one or two days that also increased soil moisture at 25 cm by more than 0.01 m^3 m^{-3} (precipitation was 10.4 mm or greater). During the study period, only 7 events (or sequences of events) changed soil moisture content down to 50 cm depth. It took just under 4 years to see an increase in soil moisture at a depth of 250 cm. The moisture profiles in the lysimeters indicate that most of the moisture dynamics (infiltration as well as evaporation) occurs within the top 25 cm. Precipitation that infiltrates below 25 cm seem to remain in the soil and fosters further infiltration during and after storm events while evaporating only slowly in between events.

For the second step, a recently developed process-based evaporation model by Shokri et al. (2009) and Or et al. (2013) was employed to simulate measured evaporation rates from the weighing lysimeter soil already discussed above. The model focusses on water-vapor diffusion-controlled (or Stage II) evaporation and calculates Stage II evaporation rates based on soil texture, total porosity and an initial moisture content profile as input parameters. Simulations of the evaporation rates using readily available soil physical properties agreed well with two out of the three events that were analyzed (evaporation rate RMSEs of 0.093 and 0.141 mm d^{-1}, respectively). For the third event, simulations systematically underestimated measured evaporation rates (RMSE of 0.181 mm d^{-1}). The latter was likely due to considerable differences between the moisture profile in the lysimeter soil compared to the simplified moisture profile that is assumed by the model. Monte-Carlo simulations showed that total porosity and difference in soil moisture content above and below the second drying front are the models most sensitive parameters. Since total porosity can be determined rather accurately, improving the soil moisture profile characterization would likely need more scrutiny to further improve the model predictions for arid soils.

In a third step, moisture and temperature dynamics were monitored for a vegetated, semi-arid soil at a field site in the Great Basin over one year (July 2010 to June 2011). The question was whether any surface water from precipitation or snow melt would percolate all the way to the groundwater table located at five to six meters below the soil surface and would therefore provide groundwater recharge. The soil consisted of a loam / sandy clay loam overlying clayey material containing lenses of sand and silt and was mostly vegetated by phreatephytes and other shrubs. Inter-annual and seasonal precipitation, ET, soil moisture and temperature were determined. With Fiber Optic Distributed Temperature Sensing (FO DTS), a novel technique was employed to measure temperature profiles in the soil at ~1 cm spatial resolution. The results show that moisture from precipitation and snow melt percolates as deep as ~400 cm but does not reach the phreatic zone. Although, the TDR probes were placed in the soil vertically with the addition of backfill different than the surrounding soil, potentially creating a conduit for water flow. Changes in soil moisture content were observed at 500 cm depth but likely due to changes in groundwater table rather than percolating water from the soil above. Soil moisture and ET data show that infiltration leads to soil moisture gain from October to December whereas moisture loss due to ET dominates from March through September. FO DTS results showed diurnal variation of soil temperatures down to ~50 cm depth and seasonal variations down to ~500 cm were observed. Sensors recorded multiple cold wetting fronts in March through April 2011. Changes in soil temperatures were observed that related to changes in soil water storage; however, this occurred only near surface.

In conclusion, this dissertation sheds some light on how arid and semi-arid soils infiltrate, store and evaporate water as functions of precipitation, atmospheric demand and antecedent soil moisture conditions. The studies described above provide a starting point with respect to the

hydraulic behavior of desert soils and a first set of baseline data. The SEPHAS weighing lysimeter has been in operation since 2008 and there are currently seven years of soil, mass, moisture content, matric potential and temperature data. To date, four years of data analysis have been completed but the methods in place can now easily be applied to the entire seven years. Overall, increased knowledge about the role of desert soils in the hydrologic cycle will serve as well in the long run, in particular with the ever increasing pressure on water resources globally, the anticipated shifts in precipitation patterns due to climate change as well as the increasingly frequent and longer droughts.

Data sets used in this project were unusually large, and are reported in their entirety as supplementary materials as Appendices A and B. In Appendix A, supplementary data include multiple files from the SEPHAS Weighing Lysimeter Facility. Files are organized into folders by Lysimeter (1-3) or Other (meteorological). Data files in Lysimeter 1-3 folders are named by lysimeter number, instrument, hydrologic year, and data type. For example, theta data (also known as water content data using TDR probes) from Lysimeter 1 during the hydrologic year 2008-2009 would be in the Excel file titled "Lysimeter 1_TDR_Hydro Year_2008-2009_Theta.xlxs". The one data file in the Other folder titled "Meteorological Station_2008-2012_Meteorological Data.xlxs" includes four years of meteorological data (wind speed, air temperature, vapor density, relative humidity, precipitation, net radiation, atmospheric pressure, and air density). Supplementary data in Appendix B includes five Excel spreadsheets for the Spring Valley Site SV6. These files are titled via site, instrument, time period, and data type. For example, water content data using TDR probes from 2010-2011 would be in the Excel file titled "SV6_TDR_2010-2011_Water Content.xlxs".

ACKNOWLEDGMENTS

I owe my gratitude to so many people that have made this dissertation possible. I am very fortunate to have had this opportunity to work with a committee with a large array of disciplines. Therefore, I would like to thank Zhongbo Yu, Markus Berli, Mike Nicholl, Ganqing Jiang, and Dale Devitt. In particular, I would like to thank them for their patience, support, and assistance in my endeavors as a graduate student, as well as their assistance in obtaining funding throughout my academic endeavors. I would also like to thank my colleagues from Desert Research Institute for their help in data analysis, field work, and funding. Specifically I would like to thank Michael Young (now with University of Texas, Austin), John Healey, Karletta Chief (now with University of Arizona), Mark Hausner, Brad Lyles, Lynn Fenstermaker, Rose Shillito, Jim Thomas, Tom Giuliano, Emily Kaminski, Karen and Stephen Gray, Amy Russel, Suzanne Hudson, Betty Kim (no longer with DRI), Richard Jasoni, Jay Arnone, Jeff Daniels (no longer with DRI), and Karl Pohlmann. I would also like to thank my colleagues from the Department of Geoscience and College of Sciences at UNLV for their support including Nicholle Booker (no longer with College of Sciences), Maria Figueroa, Andrew Hanson, Ala Kiko, Liz Smith, Terry Spell, and Michael Wells. I would also like to acknowledge Peter Lehmann for his valuable comments and contributions to the discussion of Chapter 3.

My existence as a PhD student would not be possible without the financial support from UNLV as a teaching assistant during the Spring 2008 semester (GEOL 101L), Desert Research Institute for the 2008 summer work conducted at the lysimeter facility in Boulder City (NSF EPSCoR grant # EPS-0447416), Gayle Dana and the NSF EPSCoR Climate Component-Based (Water) Graduate Research Assistantship from Autumn 2008 through Winter 2012 (Cooperative Support Agreement EPS-0814372), and teaching five semesters of Introduction to Physical

Geology (GEOL 101) and one semester of Physical Geography of the Earth's Environment (GEOG 103).

A special and deep-hearted thank you needs to go out to my parents Gary and Vicki Koonce and my girlfriend Renee Turner; they have given me so much support and love. I would like to thank them from the bottom of my heart. Lastly, I would like to thank all of my friends for their companionship and encouragement during my stint as a PhD student. I would like to provide special mention to Millie Abeyta, Michele Arnwine, Nick Barkley, Heath Bloomquist, Josh and Aubrey Bonde, Marc Boozer, Erin Byrne, Seth and Jaime Chaffee, Zach Cook, Lita Fice, Chrystal and Terry Hunter, Jeevan Jayakody, Brian Kraklow, Brandy Little, Chris Martini, Nathan Warner, Amanda Wagner, and Eric Weismann.

TABLE OF CONTENTS

ABSTRACT iii

ACKNOWLEDGMENTS viii

LIST OF TABLES xiii

LIST OF FIGURES xv

CHAPTER 1 DISSERTATION OVERVIEW 1

CHAPTER 2 DETERMINING THE MOISTURE DYNAMICS OF AN ARID SOIL USING WEIGHING LYSIMETERS 5

2.1 Introduction 5

2.2 Materials and Methods 7

2.2.1 The SEPHAS Weighing Lysimeters: Design, Construction and Instrumentation 7

2.2.2 Climate 12

2.3 Results and Discussion 13

2.3.1 Precipitation (Tipping Bucket Measurements) 13

2.3.2 Evaporation and Infiltration (Lysimeter Measurements) 16

2.3.3 Lysimeter Soil Water Dynamics 27

2.4 Summary and Conclusions 36

CHAPTER 3 QUANTIFYING EVAPORATION FROM BARE ARID SOIL: LYSIMETER MEASUREMENTS AND MODEL CALCULATIONS 40

3.1 Abstract 40

3.2 Introduction 41

3.3 Theoretical Considerations 42

3.4 Materials and Methods 44

3.4.1 Lysimeter Facility 44
3.4.2 Study Area 46
3.4.3 Near-Surface Soil Moisture, Temperature and Atmospheric Measurements 46
3.4.4 Evaporation Measurements 47
3.4.5 Event Selection and Model Application 47
3.5 Results and Discussion 48
3.5.1 Stage II Evaporation: Measurements and Simulations 48
3.5.2 Sensitivity Analysis of Individual Variables 53
3.5.3 Sensitivity Analysis using Monte Carlo Simulations 59
3.6 Conclusions 63
3.7 Acknowledgements 65
CHAPTER 4 SOIL MOISTURE AND TEMPERATURE AS A FUNCTION OF PRECIPITATION, ET, AND GROUNDWATER LEVEL IN SPRING VALLEY, NV 66
4.1 Abstract 66
4.2 Introduction 67
4.3 Study Area 70
4.4 Field Methods and Data Collection 72
4.4.1 Soil Moisture and Groundwater Monitoring 72
4.4.2 Soil Temperature 73
4.4.3 Soil Sampling and Analysis 76
4.4.4 Atmospheric and Weather Measurements 76
4.4.5 Field Complications 77
4.5 Results 77

4.5.1 Soil Texture 77
4.5.2 Precipitation and Evapotranspiration 78
4.5.3 Soil Moisture 81
4.5.4 Depth to Groundwater 84
4.5.5 Air-Soil Temperature Profiles (Spring and Summer 2011) 86
4.6 Discussion 88
4.6.1 Inter-Annual Variation in Soil Water along the Soil-Plant-Atmosphere Continuum 88
4.6.2 Spring and Summer Soil Temperature 92
4.7 Conclusions 94
4.8 Acknowledgements 96
CHAPTER 5 CONCLUSIONS 97
APPENDIX A SEPHAS WEIGHING LYSIMETER FACILITY DATA ON CD ROM 102
APPENDIX B SPRING VALLEY DATA ON CD ROM 103
APPENDIX C SEPHAS BACKGROUND, STATISTICAL VERIFICATION, AND ADDITIONAL TIME SERIES DATA 104
APPENDIX D SPRING VALLEY FIELD SITE SV6 SYNTHESIS 121
REFERENCES 136
CURRICULUM VITAE 146

LIST OF TABLES

Table 1. Instrumentation type, depth, quantity, and measurement frequency at the SEPHAS Weighing Lysimeter Facility. 11

Table 2. Largest 10 precipitation events in terms of total precipitation with date, intensity, duration, daily evaporation and season. 16

Table 3. Average monthly infiltration / evaporation ratios from Lysimeters 1-3, for the four year observation period (November 2008 to September 2012). Gray cells represent "dry" months with lower infiltration than evaporation (ratio < 1). White cells represent "wet" months with higher infiltration than evaporation (ratio > 1). 20

Table 4. End-of-the-year soil water storage in terms of annual lysimeter mass gain divided by cumulative precipitation for Lysimeters 1-3, including Lysimeter average, and cumulative precipitation. 26

Table 5. Events 1-3 RMSE for diffusive evaporation including initial simulations (dark bold) using available data and sensitivity analysis using three separate values for four variables (one variable at a time) in Equations (3.1) and (3.2) (t, ξ, φ, and $\Delta\theta$). All results are in units of mm d^{-1}. 51

Table 6. Events 1-3 RMSE for Monte Carlo sensitivity analysis using 1000 realizations for three variables (ξ, φ, and $\Delta\theta$) in Equations (3.1) and (3.2). Only the top 5% and 1% RMSE are shown with the variable's respective ranges. In addition, RMSE (and variable ranges) for the last ten days of diffusive evaporation were also included. 64

Table 7. Monthly and yearly measured precipitation (P) and ET, and P/ET ratios, for the study period of 1 July 2010 through 30 June 2011 79

Table 8. Individual lift soil properties measured during installation of soil in Lysimeters 1-3 (Chief et al., 2009; Shillito, R., unpub. data, 2015). Lift #1, the first to be installed, begins at the base of the lysimeter. 105

Table 9. RMSE statistics for initial and 2008 October 1 moisture contents using 6 different Topp's Coefficients obtained during TDR calibration. 110

LIST OF FIGURES

Figure 1. Study area with Eldorado Valley Excavation Site of SEPHAS Weighing Lysimeter Facility, and WRCC Station #261071. 8

Figure 2. Cross sectional view of (a) underground tunnel with rooms for Lysimeters 1-3 and (b) design of the individual lysimeters at the SEPHAS Weighing Lysimeter Facility (modified from Chief et al., 2009)..... 9

Figure 3. Measured monthly precipitation for 2008 through 2012 (blue, red, green, and purple bars, respectively). 14

Figure 4. SEPHAS facility precipitation events as defined by Osborn (1983) showing storm intensity as a function of duration (log-log scale). Events are color coded representing winter (black box), spring (red circle), summer (blue upward triangle), and autumn (pink downward triangle) with the 10 largest events (in total precipitation) shown (solid fill) in chronological order as Events 1-10..... 15

Figure 5. Monthly infiltration and evaporation as measured by Lysimeters 1-3 (average of all three lysimeters) for (a) winter, (b) spring, (c) summer, and (d) autumn. 19

Figure 6. Daily precipitation and lysimeter (1-3) mass representing soil water storage during the 4-yr study period. First precipitation event occurred on 9 November 2008. 25

Figure 7. Total daily precipitation (as measured by the tipping bucked rain gauge) with Events 1-10 (a), and Lysimeter 1 daily average soil moisture at (b) 2.4, 10, and 25 cm depth, (c) 50, 75, and 100 cm depth, and (d) 150, 200, and 250 cm depth for the study period of 1 October 2008 through 30 September 2012. 30

Figure 8. The physics of evaporation [adapted from Lehmann et al. (2008), Shokri and Or (2011), and Or et al. (2013)] showing (a) atmospheric controlled evaporation with both large and small pores filled with water shortly after a precipitation event, (b) water-filled capillaries (small pores) reaching the soil surface from the primary (1°) drying front, and (c) soil controlled diffusive evaporation beginning when liquid water recedes from the soil surface to a vapor diffusion length of ξ creating a secondary (2°) drying front. 45

Figure 9. Methods to determine the time of onset of Stage II evaporation, t_0, plotting (a) the inverse of evaporation rates squared as a function of time (Brutsaert and Chen, 1995) and plotting (b) the logarithm of the inverse evaporation rates squared as a function of time (Shokri and Or, 2011). 48

Figure 10. Daily precipitation as measured by the SEPHAS facility rain gauge (bar), daily evaporation rates as measured by Lysimeter 1 (triangle), and simulated evaporation rates using Equations 3.1 and 3.2 (line) for Events 1-3. 50

Figure 11. Inverse of evaporation rate squared plotted on a log scale versus time to determine the onset of Stage II evaporation as proposed by Shokri and Or (2011). 52

Figure 12. Lysimeter 1 measured (triangle) and simulated evaporation rates using Equations 3.1 and 3.2 (lines) showing differences in estimated onset of Stage II evaporation, t_0, for Events 1-3. 54

Figure 13. Lysimeter 1 measured (triangle) and simulated evaporation rates for Events 1-3 and vapor diffusion length, ξ, ranging from 3 to 14 mm. 55

Figure 14. Lysimeter 1 measured (triangle) and simulated evaporation rates using Equations 3.1 and 3.2 (line) for Events 1-3 and porosity, φ, ranging from 0.2 to 0.4. 57

Figure 15. Lysimeter 1 measured (triangle) and simulated evaporation (line) for different values of $\Delta\theta$ for Events 1-3. 58

Figure 16. Lysimeter 1 soil profiles of moisture content distribution from 12-250 mm following Events 1-3. 60

Figure 17. Map of the Great Basin Region and Site SV6 located in Spring Valley, Nevada..... 71

Figure 18. Instrumentation plan (a) and cross sectional (b) views of Site SV6 (not to scale)..... 74

Figure 19. Measured daily precipitation and ET for the study period of 1 July 2010 through 30 June 2011. 80

Figure 20. Measured soil moisture content at (a) 0.3 and 1.0 m, (b) 2.0 and 3.0 m, and (c) 4.0 and 5.0 m at Site SV6 from 1 July 2010 through 30 June 2011. 83

Figure 21. Depth to groundwater at Site SV6 from 1 July 2010 through 30 June 2011. Using linear regression, slopes (negative value represents decreasing water table in m d^{-1}) and R2 values were calculated for three periods of time during the decreasing trend: 18 October 2010 to 2 March 2011, 3 March to 9 May 2011, and 10 May to 12 June 2..... 85

Figure 22. Air (0.01 m above land surface) and soil temperature (0.03 and 0.12 – 6.0 m bgs) profiles using Tc's and FO DTS for spring at (a) 4:00 and (b) 16:00, from 24 March - 25 April 2011 (early spring). 87

Figure 23. Air (0.01 m above land surface) and soil temperature (0.03 and 0.12 – 6.0 m bgs) profiles using Tc's and FO DTS for summer at (a) 4:00 and (b) 16:00 from 29 May - 30 June 2011 (early summer 2011). 88

Figure 24. Comparison of daily precipitation using a rain gauge and flux using lysimeters for (a) Lysimeter 1, (b) Lysimeter 2, and (c) Lysimeter 3. Solid red line is best-fitted regression line, and dashed line is 1:1 line (regression line equation R^2, and three outliers included)..... 107

Figure 25. Comparison of initial volumetric moisture contents (calculated from gravimetric moisture samples and bulk density) prior to start of this study and daily average volumetric moisture content (using TDR probes) on 1 October 2008 for (a) Lysimeter 1, (b) Lysimeter 2, and (c) Lysimeter 3. Error bars with 1 standard deviation included for volumetric moisture contents on 1 October 2008. 111

Figure 26. Daily average Lysimeter 1 soil moisture content at 1.2, 3.6, and 4.8 cm using TPHP sensors for the study period of 1 October 2008 through 30 September 2012..... 112

Figure 27. Daily average Lysimeter 2 soil moisture content at (a) 10 and 25 cm, (b) 50, 75, and 100 cm, and (c) 150, 200, and 250 cm using TDR sensors for the study period of 1 October 2008 through 30 September 2012. 113

Figure 28. Daily average Lysimeter 3 soil moisture content at (a) 10 and 25 cm, (b) 50, 75, and 100 cm, and (c) 150, 200, and 250 cm using TDR sensors for the study period of 1 October 2008 through 30 September 2012. 114

Figure 29. Daily average Lysimeter 1 matric potential at (a) 5, 10 and 25 cm, (b) 50, 75, and 100 cm, and (c) 150, 200, and 250 cm using HDU sensors for the study period of 1 October 2008 through 30 September 2012. 115

Figure 30. Daily average Lysimeter 2 matric potential at (a) 5, 10 and 25 cm, (b) 50, 75, and 100 cm, and (c) 150, 200, and 250 cm using HDU sensors for the study period of 1 October 2008 through 30 September 2012. 116

Figure 31. Daily average Lysimeter 3 matric potential at (a) 5, 10 and 25 cm, (b) 50, 75, and 100 cm, and (c) 150, 200, and 250 cm using HDU sensors for the study period of 1 October 2008 through 30 September 2012. 117

Figure 32. Daily average Lysimeter 1 soil temperature at (a) 5, 10 and 25 cm, (b) 50, 75, and 100 cm, and (c) 150, 200, and 250 cm using HDU sensors for the study period of 1 October 2008 through 30 September 2012. 118
Figure 33. Daily average Lysimeter 2 soil temperature at (a) 5, 10 and 25 cm, (b) 50, 75, and 100 cm, and (c) 150, 200, and 250 cm using HDU sensors for the study period of 1 October 2008 through 30 September 2012. 119
Figure 34. Daily average Lysimeter 3 soil temperature at (a) 5, 10 and 25 cm, (b) 50, 75, and 100 cm, and (c) 150, 200, and 250 cm using HDU sensors for the study period of 1 October 2008 through 30 September 2012. 120
Figure 35. Map of the subdivision outlined by Hunt (1967) and location of SV6. 122
Figure 36. Conceptual diagram of the Great Basin rain shadow. 125
Figure 37. Middle Paleozoic Era (Silurian) of the Great Basin with marine deposition along a passive continental margin (modified from Blakely, 1997 and Welch et al., 2007). 127
Figure 38. Great Basin conceptual groundwater flow model (modified from Welch et al., 2007) 132

CHAPTER 1

DISSERTATION OVERVIEW

Water is a limited resource in the semi-arid and arid environments that cover up to 1/3 of the Earth's land surface (Kalma and Franks, 2003; Simmers, 2003). With increasing population (Dregne, 1991), sensitive nature to desertification (Middleton and Thomas, 1997), and potential gap increase between water supply and demand due to climate change (Vorosmarty et al., 2000; Vorosmarty et al., 2010; Garnier et al., 2015), desert areas world-wide are sensitive, particularly from an ecohydrologic perspective. In order to predict the direction and magnitude of hydrologic changes in semi-arid and arid environments, we need a better understanding of the underlying mechanisms. In particular, we need to better understand how soils influence basic hydrologic processes, such as: infiltration, evapotranspiration (ET) and potential groundwater recharge.

Precipitation, soil water infiltration, and ET are the key processes that control the desert water balance. Semi-arid and arid environments are characterized by low mean annual precipitation (i.e., 80-500 in winter and 200-800 mm in summer) that exhibit inter-annual variability of 25-100% (Simmers, 2003). In contrast, potential evaporation may exceed precipitation by a considerable margin, thus allowing very little precipitation to remain in the near surface soil or infiltrate deeper to recharge an aquifer. Measurements from three deserts in the western United States (Las Cruces, NM, Beatty, NV, and Hanford, WA) yielded ET between 1600-2390 mm (Gee et al., 1994).

Evapotranspiration has been studied extensively to better understand the impact of plants on water percolation below the root zone (e.g., Gee et al., 1994; Andraski, 1997; Scanlon et al., 2005); hydro-ecological effects of water table drawdown on the connection between

phreatophytes and groundwater (e.g., Nichols, 1994; Cooper et al., 2006; Patten et al., 2008; Devitt et al., 2010; Kray et al., 2012); and the use of deep arid vadose zones as a barrier for waste disposal (e.g., Winograd, 1981; Jones and Skaggs, 1989). Studies dealing with ET for vegetated arid soils show that, in general, ET returns virtually all precipitated water back to the atmosphere (Gee et al., 1994; Andraski, 1997; Scanlon et al., 2003; Scanlon et al., 2005). Conversely, for non-vegetated ("bare") arid soils, 3% to 50% of annual precipitation remains in the soil and can potentially percolate deeper into the subsurface (Gee et al., 1994; Andraski et al., 1997; Xu et al., 1998). With plant cover typically less than 50% in arid environments (Wythers et al., 1999), bare soil evaporation can play a large role in the water balance.

This dissertation provides an in-depth analysis of inter-annual soil moisture dynamics, and response to precipitation, evaporation and ET at two field sites: (1) a bare arid soil at a weighing lysimeter facility; and (2) a vegetated semi-arid soil with a shallow water table (depth to water < 6 m). The overall goals for Chapters 2-4 include: (i) examine the water balance and the evolution of soil moisture in a bare arid soil, (ii) examine the evaporative dynamics in a bare arid soil using a model that simulates diffusive Stage II evaporation, and (iii) examine the moisture dynamics and soil temperature profile of a semi-arid, vegetated soil, respectively.

Chapter 2 describes a 4-yr baseline study (1 October 2008 through 30 September 2012) of precipitation, evaporation, soil water storage, and volumetric soil moisture content data to better understand the moisture dynamics of a non-vegetated arid soil under natural precipitation conditions. In addition to the baseline study, Chapter 2 addresses the following series of open questions related to the hydrology of an arid soil including: (i) what fraction of the total annual precipitation evaporates and what fraction remains in the soil; (ii) what is a typical moisture

profile of a bare arid soil and how does it evolve over time; and (iii) how do storm intensity and duration affect the soil moisture profile?

Chapter 3 focusses on three of the 180 precipitation events analyzed in Chapter 2 to evaluate diffusive evaporation from Lysimeter 1. The three events were chosen because of their high-intensity, short duration, and a subsequent period of 2-3 weeks with no precipitation. This study evaluates a process-based model by Shokri et al. (2009) and Or et al. (2013) on an arid soil under natural precipitation and evaporation conditions. Measured evaporation rates from Lysimeter 1 were compared to simulated evaporation rates after the three storm events hypothesizing that this model simulates ET well during the drying out phase of the soil. Two sensitivity analyses, one including an analysis of individual parameters and the other a two-step Monte Carlo analysis of multiple parameters, were performed to identify the most sensitive parameters of the evaporation model. Chapter 3 was prepared for submission to Vadose Zone Journal.

Chapter 4 addresses the increased complexity when moving from a lysimeter study with well controlled initial and boundary conditions (as described in Chapters 2 and 3) to the field, with the addition of a relatively shallow water table (depth of less than 6 m) that is hydraulically connected to a plant community of phreatophytes. This 1-yr study (1 July 2010 and 30 June 2011) was conducted in a semi-arid environment where daily ET, precipitation, volumetric soil moisture, and depth to groundwater were evaluated to examine seasonal trends within Spring Valley of the Great Basin (Site SV6). Although this study was invasive, installing instrumentation in both the vadose and phreatic zones, it provided insight on the processes that affect soil water and temperature from a shallow water table to near surface and the effects of inter-annual precipitation and ET variability. One of the instruments installed was fiber optic distributed temperature sensing system (FO DTS), allowing for greater spatial resolution while

maintaining excellent temporal resolution (Selker et al., 2006a; Tyler et al., 2009). It was used during early spring and summer seasons of 2011 when ET is at its highest. The goals of this project include: analyze inter-annual and seasonal precipitation and ET with changes in soil water storage; determine depth of wetting front and whether or not it reaches the phreatic zone during the study period; determine the efficacy of FO DTS to determine changes in soil moisture; and determine soil temperature extinction depths.

Data sets used in this project were unusually large, and are reported in their entirety on the attached CD ROMs (Appendix A – SEPHAS Weighing Lysimeter Facility Data on CD ROM; Appendix B – Spring Valley Data on CD ROM). Additional data outside the scope of this research are also included in the CD ROM. Appendix C provides general information regarding the lysimeters, including lysimeter soil information (i.e., texture, bulk density, particle density), statistical analyses (i.e., rain gauge and lysimeter verification, soil moisture verification), and time-series graphs outside the scope of this dissertation (i.e., Lysimeters 2-3 soil moisture, Lysimeters 1-3 soil temperature and matric potential). Appendix D provides a synthesis of the physical characteristics for Site SV6 and surrounding area. Characteristics include physiography, climate, geology, hydrology, and plant community and are described in the context of both regional and local scales.

CHAPTER 2

DETERMINING THE MOISTURE DYNAMICS OF AN ARID SOIL USING WEIGHING LYSIMETERS

2.1 Introduction

Arid environments are characterized by low precipitation and high evapotranspiration (ET), leaving little potentially available for groundwater recharge. Reference ET can exceed the average annual precipitation by an order of magnitude; for example, in North Las Vegas, a 2-yr average reference ET from turfgrass was 174 cm and annual precipitation is 10 cm (Wright et al., 2012). Desert vegetation have adapted to such water-limited conditions. One strategy is to take advantage of storm events, whereas another is to access soil water from previous events, including groundwater (Noy-Meir, 1973; Ehleringer et al., 1991). From an ecohydrology perspective, the key questions are: (i) how does the soil moisture profile respond to a single storm, or sequence of storms, at a specific time of the year; and (ii) how does the soil moisture profile change during inter-storm periods? In both cases, knowledge of the soil moisture dynamics (water infiltration, storage, redistribution and ET) and its connection to meteorological conditions in the Mojave Desert, particularly precipitation or lack thereof, is critical.

There are a few studies that have provided insight into the moisture dynamics of arid soils. For example, using lysimeter data from three desert sites, Gee et al. (1994) showed that 10% to greater than 50% of annual precipitation drains deep into bare, sandy soils; however, if soils are vegetated and/or silty loam, deep drainage is eliminated. Andraski (1997) addressed soil moisture, matric potential and temperature at the Amargosa Desert Research Site (ADRS), a commercial waste-burial facility near Beatty, NV, under natural-site (undisturbed) and simulated

waste-site (disturbed) conditions from the soil surface down to 5.25 m. The study measured soil moisture content using neutron probes on a monthly basis and after precipitation, but only for events with precipitation of 5 mm or more. In addition, the study addressed changes in soil water storage calculated from moisture content data. Andraski (1997) found no long-term soil water accumulation or downward penetration of precipitation at the vegetated site but found that 3-6% of water (by volume) remains in the soil for the non-vegetated sites. Work by Garcia et al. (2011) addressed soil water movement due to thermal gradients at the ADRS using the HYDRUS-1D numerical code. They found that during a 4.7-yr period, percolation and plant water uptake occurs within the upper 30 cm of the soil even after above-average precipitation, yet non-vegetated soil showed increased water storage within the upper 100 cm of soil. Scanlon et al. (2005) monitored the water balance of both bare and vegetated arid soil at the Nevada National Security Site (or NNSS; formerly known as NTS) within the upper portion of the Mojave Desert over an 8-yr monitoring record, and included the largest El Nino event during the last century. They found that even during times of high precipitation, such as the El Nino event in 1997-1998, vegetation productivity increased rapidly and subsequently reduced soil water by half of what a non-vegetated soil would. A recent report that summarizes weighing lysimeter and vadose zone monitoring activities at the NNSS found that summer evaporation from bare soil eventually exceeds ET from vegetated soil due to increased storage in the bare soil (National Security Technologies, 2015). Yet, through all of these studies, our understanding of water dynamics in near surface arid soils is rather limited.

This study aims to improve our understanding of the moisture dynamics of a non-vegetated arid soil under natural precipitation conditions in the Mojave Desert. Specifically, we use data from a unique lysimeter facility to address a series of open questions related to arid-zone

hydrology including: (i) quantifying the apportionment of annual precipitation, between evaporative loss and infiltration; (ii) evolution of the moisture profile for a bare soil at the yearly scale; and (iii) short-term impacts of storm intensity and duration on the soil moisture profile. Total soil mass and soil moisture profiles were monitored under natural precipitation conditions over a 4-yr period (1 October 2008 to 30 September 2012) in three weighing lysimeters located in the Mojave Desert of the Southwestern U.S.

2.2 Materials and Methods

2.2.1 The SEPHAS Weighing Lysimeters: Design, Construction and Instrumentation

The study was carried out at the recently established SEPHAS Weighing Lysimeter Facility in Boulder City, Nevada (35.96°N, -114.85°W; https://www.dri.edu/sephas). The study area is located in Boulder City, NV, approximately 40 km southeast of Las Vegas, NV, in the eastern part of the Mojave Desert (Figure 1). The core of the facility consists of three cylindrical stainless steel tanks of 2.26 m inner-diameter, 3.0 m depth and 6.4 mm wall thickness (type 304, Moore's Blacksmith Shop, Red Bluff, CA) each placed on scales (Model FS-8, Cardinal Scale Manufacturing Co., Webb City, MO) (Figure 2a) and housed underground in individual rooms connected by an access tunnel (Figure 2b). The load cells of the lysimeter scales measure changes in lysimeter mass as a change in force between the scale lever and the ground with a resolution of 0.047 N or better, equating to a lysimeter scale mass resolution of 471.5 g or better. Lysimeter scales measure (average) mass in 15 minute intervals. Refer to Chief et al. (2009) for a more detailed description on the design and construction of the lysimeter facility.

Figure 1. Study area with Eldorado Valley Excavation Site of SEPHAS Weighing Lysimeter Facility, and WRCC Station #261071.

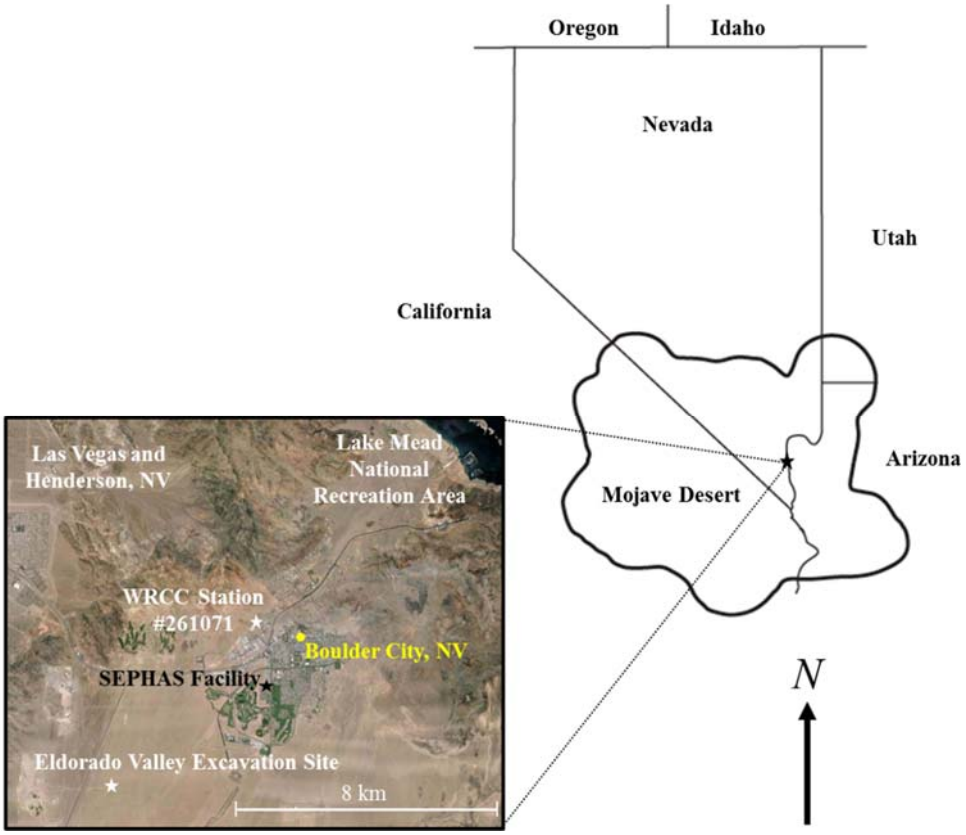

Soil used to fill the lysimeters originates from an excavation site in Eldorado Valley, about 8 km southwest of Boulder City and was classified as a sandy-skeletal, mixed, thermic Typic Torriorthents (Soil Survey Staff, 1993) of the Arizo soil series (Chief et al., 2009). The soil developed on a south-facing, shallow sloped alluvial fan (0-15% slope angle) composited of volcanic material (Chief et al., 2009) fluvially deposited from the nearby McCullough and Highland Ranges. The soil profile (excavation) from Eldorado Valley consisted of a poorly structured Aeolian-deposited sand within the uppermost section and then grades into a loamy sand w/ gravel; the profile was also calcareous with limited root growth below 120-160 cm (Chief et al., 2009).

Figure 2. Cross sectional view of (a) underground tunnel with rooms for Lysimeters 1-3 and (b) design of the individual lysimeters at the SEPHAS Weighing Lysimeter Facility (modified from Chief et al., 2009).

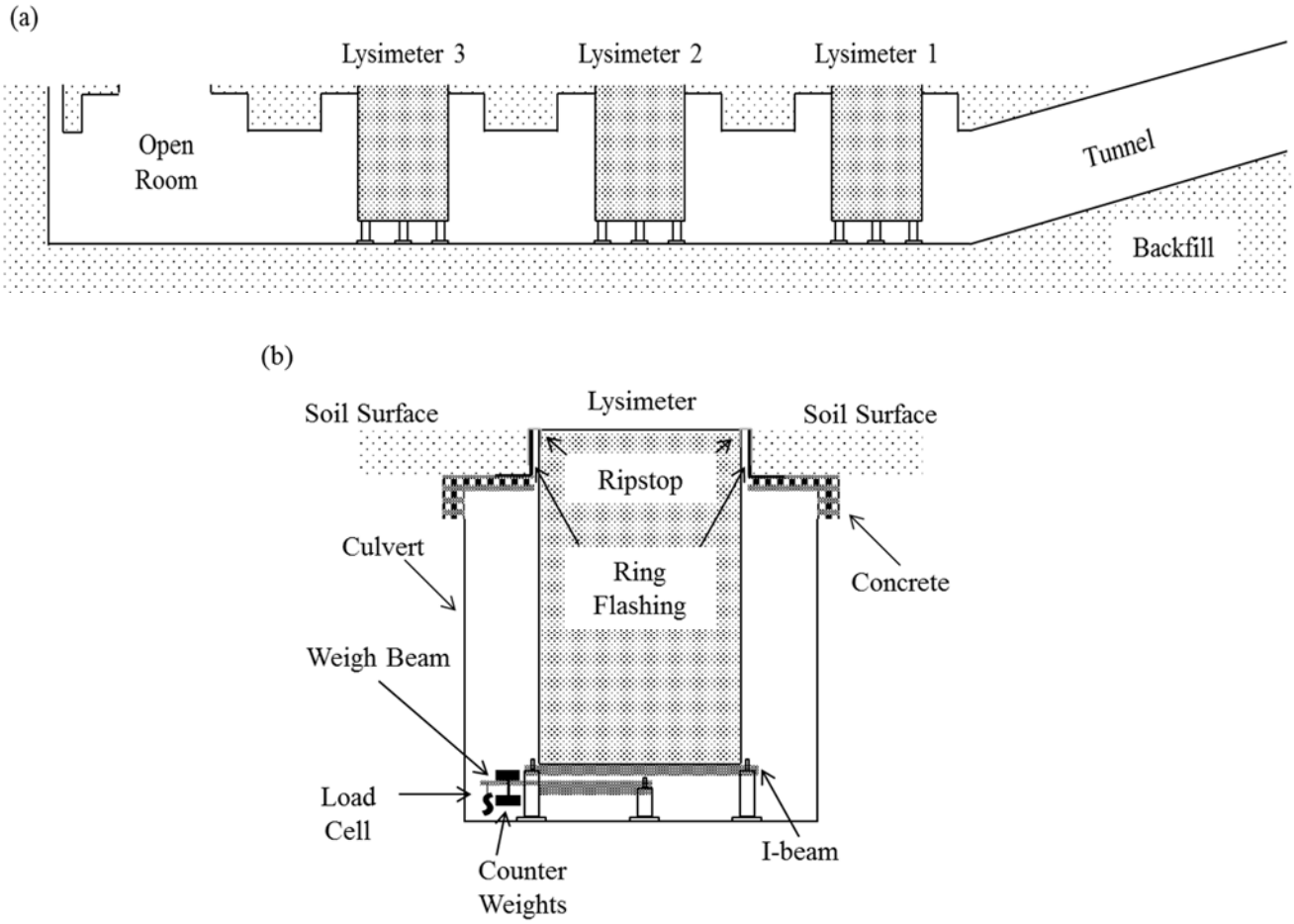

The lysimeter soils were installed in individual lifts (2-22 cm thicknesses) packed to bulk density values similar to that measured in the undisturbed Eldorado Valley soil (Chief et al., 2009). Average (oven-dry) total bulk densities (including gravel and fines) for all lifts in Lysimeters 1-3 were 1.75, 1.77, and 1.75 g cm^{-3}, respectively; which yielded average total porosities of 0.30, 0.30, and 0.31, respectively (Shillito, R., unpub. data, 2015). For Lysimeter 1, the soil was homogenized before repacking, which yielded a nearly uniform texture of gravelly fine sand from 0-300 cm. For Lysimeters 2 and 3, the five designated Arizo soil horizons (Soil

Survey Staff, 1993; Chief et al., 2009) were collected separately and repacked in five horizons from 0-25, 25-80, 80-120, 120-160 and 160-200 cm separately with the goal to maintain the lithology and chemistry of the Eldorado Valley soil. The bottom 100 cm of Lysimeters 2 and 3 (200-300 cm depth) were filled with the same homogenized soil as in Lysimeter 1 (Chief et al., 2009).

The SEPHAS lysimeters are instrumented to measure edaphic properties such as volumetric moisture content, matric potential, and temperature (for details, see Chief et al., 2009). This study focuses on volumetric moisture content, which has been monitored in 2.4 cm depth using a triple-probe heat-pulse (TPHP) sensor (East 30 Sensors, Inc., Pullman, WA) and in 10, 25, 50, 75, 100, 150, 200, and 250 cm depth using time domain reflectometry (TDR) sensors (model CS605, Campbell Scientific Inc., Logan, UT). Additional TPHP sensor data (1.2, 3.6, and 4.8 cm; for Lysimeter 1 only) and heat dissipation unit (HDU) sensors (model 229, Campbell Scientific Inc., Logan, UT) used to measure soil matric potential and soil temperature are provided in Appendices A (data on CD ROM) and C (time series graphs). For details on instrument theory, one is referred to Campbell et al. (1991) and Bristow et al. (1994) for TPHP sensors, Topp et al. (1980) for TDR sensors, and Reece (1996) and Scanlon et al. (2002) for HDU sensors. Analysis and calibration for TPHP, TDR, and HDU sensors were described by Young et al. (2008), Young et al. (1997), and Bilskie (2007), respectively.

All sensors were installed horizontally inside each lysimeter at each depth, except TPHP sensors (placed only in the southeast quadrant), and with two to four replications per depth placed in the four quadrants of each depth (northeast, southeast, southwest, and northwest). Details on depth, number of sensors, and reading frequency in this study are provided in Table 1. All sensors were connected either directly to Campbell Scientific CR3000 dataloggers or

indirectly via multiplexers (Chief et al., 2009). Data were collected at 1- to 3-hr time intervals (depending on sensor depth) from 1 October 2008 through 30 September 2012, which constitutes four 'Water Years'.

Table 1. Instrumentation type, depth, quantity, and measurement frequency at the SEPHAS Weighing Lysimeter Facility.

	Instrument Quantity		
Depth (cm)	TDR CS605*	TPHP**	Met Station
5	--	4	
10	4	--	
25	4	--	
50	4	--	
75	4	--	1
100	2	--	
150	4	--	
200	2	--	
250	2	--	
	Data Processing Frequency		
5	--	1 h (SE)	
10	1 h (NE, SE, SW, NW)	--	
25	1 h (NE, SE, SW, NW)	--	
50	1 h (NE, SE) and 3 h (SW, NW)	--	
75	3 h (NE, SE, SW, NW)	--	30 min
100	3 h (NE, SW)	--	
150	3 h (NE, SE, SW, NW)	--	
200	3 h (SE, NW)	--	
250	3 h (NE, SW)	--	

* - Per lysimeter

** - 4 sensors at 6-18, 18-30, 30-42, and 42-54 mm in Lysimeter 1 only (Lysimeters 2 and 3 not used in study)

NE - northeast quadrant; SE - southeast quadrant; SW - southwest quadrant; NW - northwest quadrant

A full meteorological station is located at the SEPHAS facility (Chief et al., 2009) and was operational during data collection for this study. A tipping bucket precipitation gage (model TE525WS-L, Campbell Scientific, Inc., Logan, UT) located approximately 2.0 m above ground

surface and 28.5 m west of the southern midpoint of lysimeter 1 recorded data every 30 minutes (Table 1).

Water flux in (infiltration) and out (evaporation) of the lysimeters is estimated from measured changes in lysimeter mass over 1-hr (hour to hour) to 24-hr periods (midnight to midnight). Flux (mm of H_2O) was calculated by dividing the mass change by water density (assumed to be 1,000 kg m^{-3}) and lysimeter surface area (4.022, 4.021, and 4.019 m^2 for Lysimeters 1-3, respectively). Lysimeter water storage was similarly calculated as flux, but cumulatively added over time. Although the study period begins on 1 October 2008, small amounts of soil were added on 2 October 2008 and construction was conducted inside the tunnel through most of October; therefore, 8 November 2008 was used as the first day of lysimeter analysis, as this is before the first precipitation event on record (9 November 2008). Data were then 'zeroed' so that any changes beginning on 8 November 2008 were due to precipitation and evaporation and not from human influence.

2.2.2 Climate

According to Houghton et al. (1975), the climate is considered a low-latitude desert characterized by mild winters and very hot summers. Over the 73 year record (1931-2004) at the nearest Western Regional Climate Center meteorological station (Station # 261071; 35.98º, 114.85 º; approximately 2 km north and 48 m elevation change from the site), mean daily temperatures range from 13.7 °C to 25.4 °C, and mean annual precipitation is 141 mm (WRCC, 2009). Winter precipitation is typically brought on by light to moderate intensity, high duration storms associated with Pacific fronts moving inland, while summer precipitation is brought on by monsoonal storms of moist tropical air moving northeast from the Gulf of Mexico and tropical Pacific and combining with strong surface heating in S. Nevada resulting in a typical pattern of

high-intensity, short-duration storms (Houghton et al., 1975; Rundel and Gibson, 1996; Redmond, 2009).

2.3 Results and Discussion

The results and discussion of Chapter 2 are grouped into the following three sub-sections: precipitation (tipping bucket measurements), evaporation, infiltration, soil water storage (lysimeter measurements), and soil water dynamics. The section on precipitation focuses on precipitation measured using the rain gauge (yearly, monthly, and daily) as well as defines a precipitation event. The amount, duration, and intensity of each event is also included. The section on evaporation, infiltration and soil water storage provides a look at the mass balance of an arid soil with water: what goes in, what goes out, and what remains using changes in lysimeter mass. Lastly, the section on soil water dynamics looks at the soil moisture profile (moisture content only) prior to, during, and after precipitation.

2.3.1 Precipitation (Tipping Bucket Measurements)

A total of 521.1 mm precipitation was recorded from 1 October 2008 to 30 September 2012 (48 months). Annual precipitation for the 2009, 2010, 2011 and 2012 water years were 88.3, 140.3, 153.8, and 138.7 mm, respectively. The 4-yr annual average of 130.3 mm was approximately 7.6% below the 73-yr average of 141.0 mm measured at WRCC Station # 261071. Monthly precipitation totals show that most activity occurred in the winter and summer (Figure 3). There is also a high degree of year-to-year variability, which is typical for desert environments (Simmers, 2003). It is worth noting that during the month of June, there was not a single precipitation event recorded using the tipping bucket during the four year study

period; however, there were two small events measured using the lysimeters (discussed in Section 2.3.2).

Figure 3. Measured monthly precipitation for 2008 through 2012 (blue, red, green, and purple bars, respectively).

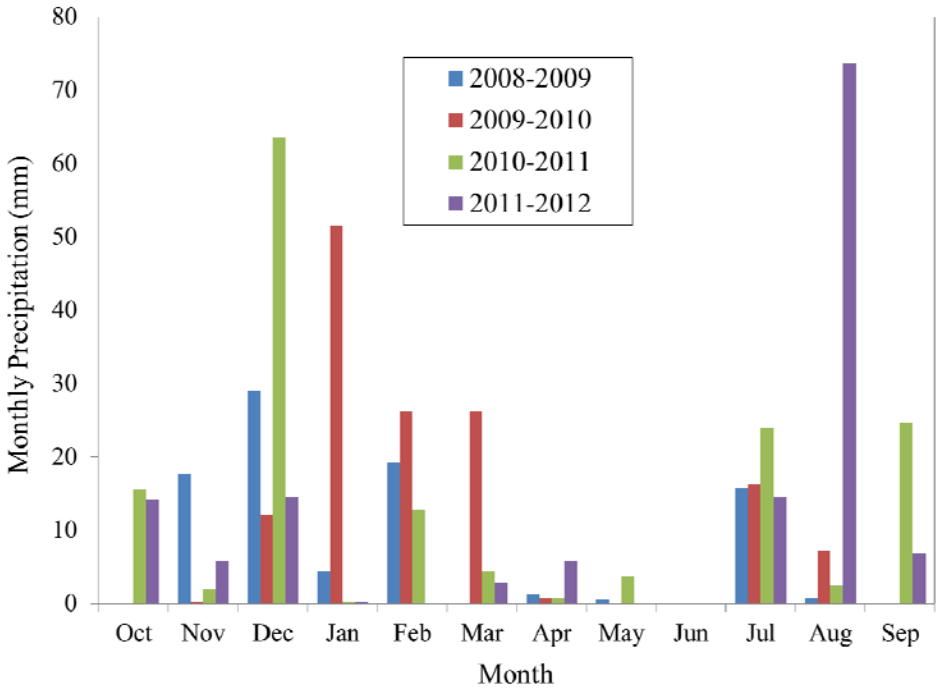

During the study period, 180 precipitation events were recorded. Each event was defined as a period of continuous precipitation separated by a minimum of 1 hr without precipitation (Osborn, 1983). Average intensity ranged from 0.1 to 12.3 mm hr^{-1} and duration from 0.5 to 52 hrs (Figure 4). The 10 largest events (in total precipitation) are outlined in Figure 4 and listed in Table 2. It's important to note that during Event 7 (22-24 December 2010) the rain gauge read 30.9 mm total precipitation whereas Lysimeters 1-3 read an averaged 51.1 mm for the same 52 hr time period. This indicates that the rain gauge probably did not capture all the precipitation during that time

period and the total amount of precipitation was likely around 51 mm rather than 30.9 mm. A comparison of the precipitation data from the lysimeters with data from rain gauges located in and near Boulder City, showed that for Event 7, the precipitation data from the lysimeters is more accurate than the data from the rain gauge at the SEPHAS facility.

Figure 4. SEPHAS facility precipitation events as defined by Osborn (1983) showing storm intensity as a function of duration (log-log scale). Events are color coded representing winter (black box), spring (red circle), summer (blue upward triangle), and autumn (pink downward triangle) with the 10 largest events (in total precipitation) shown (solid fill) in chronological order as Events 1-10.

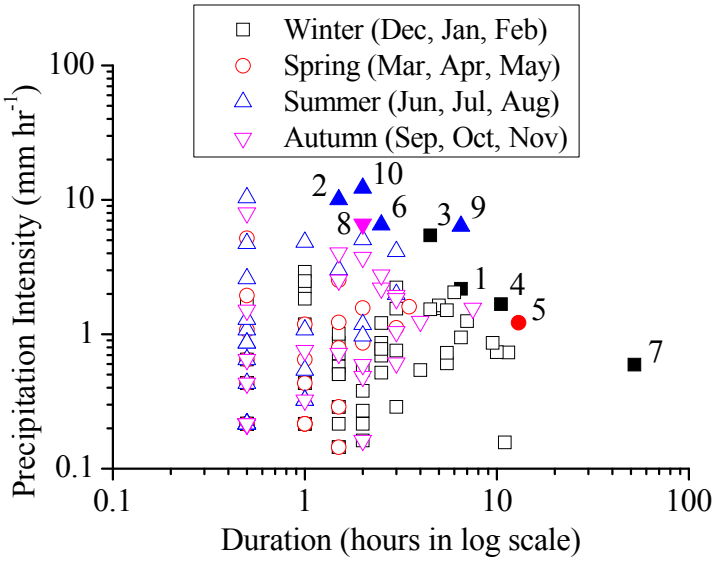

The average intensity for precipitation events was generally highest during summer (2.6 mm hr^{-1}), whereas average duration was highest in the winter (2.9 hrs). Close to half of all events (88 out of 180) occurred during winter. The rest were split between spring (27 events), summer (32 events) and autumn (33 events). The average amount of precipitation per event was the highest during summer (4.8 mm per Event) and lowest during spring (1.7 mm per Event). Four out of the ten largest events took place during winter (Table 2) and four more in the summer.

Table 2. Largest 10 precipitation events in terms of total precipitation with date, intensity, duration, daily evaporation and season.

		Precipitation			**Daily	
		Total	Intensity	Duration	Evaporation	
Event #	Date	(mm)	(mm hr^{-1})	(hours)	(mm d^{-1})	Season
Event 1	2/7/2009	14.1	2.2	6.5	1.0	Winter
Event 2	7/3/2009	15.1	10.1	1.5	2.7	Summer
Event 3	1/19/2010	24.5	5.4	4.5	0.0	Winter
Event 4	1/21/2010	17.6	1.7	10.5	1.2	Winter
Event 5	3/7/2010	15.9	1.2	13.0	1.9	Spring
Event 6	7/30/2010	16.3	6.5	2.5	2.6	Summer
Event 7*	12/22/2010	30.9	0.6	52.0	1.2	Winter
Event 8	9/16/2011	13.2	6.6	2.0	3.2	Autumn
Event 9	8/22/2012	41.6	6.4	6.5	3.5	Summer
Event 10	8/29/2012	24.5	12.3	2.0	3.9	Summer

* = based on local rain gauges and Lysimeters 1-3 mass increase, the amount of precipitation is closer to 50 mm.

** = First full day of evaporation for Lysimeter 1 following precipitation event

2.3.2 Evaporation and Infiltration (Lysimeter Measurements)

Evaporation from Lysimeter 1 ranged between 1.0-3.9 mm d^{-1} over the first full day following 9 of 10 largest events (Event 3 was not evaluated due to proximity to event 4; Table 2). Evaporation rates were highest immediately after precipitation events and during what is considered Stage I evaporation (e.g., Idso et al., 1974; van Brakel, 1980; Yiotis et al., 2006). The largest amount of daily evaporation observed occurred after Event 10 on 30 August 2012 with a rate of 3.9 mm d^{-1}. Evaporation rates for winter Events 1, 4, and 7 were 1.0, 1.2, and 1.2 mm d^{-1}, respectively. Evaporation rates within one day after summer Events 2, 6, 9, and 10 were 2.7, 2.6, 3.5, and 3.9 mm d^{-1}, respectively. Similarly, another summer event discussed in Chapter 3 (7 August 2010), saw a high rate of 2.7 mm d^{-1} one day after precipitation, although this event was smaller than those shown in Table 2. As for spring (Event 5) and autumn (Event 8), evaporation rates within one day after the storm were 1.9 and 3.2 mm d^{-1}, respectively. Two additional events

discussed in Chapter 3, one in spring (13 April 2012) and the other in autumn (11 September 2012), showed similar rates of evaporation one day after precipitation (1.4 and 2.8 mm d^{-1}, respectively) as the spring and autumn events introduced in Table 2.

Stage I evaporation rates are controlled by atmospheric demand and is therefore no surprise that the evaporation rates following summer events are higher than those during winter as the driving atmospheric forces (net radiation, temperature, humidity etc.) are stronger during the summer. Also, spring and autumn generally show higher Stage I evaporation rates compared to winter. An interesting find was that no constant evaporation rates were found right after the storm events, in contrast to several studies on Stage I evaporation (Van Brakel, 1980; Scherer, 1990; Yiotis et al., 2006). Instead evaporation rates decreased within a day after the end of the individual storm events, dropping by an order of magnitude from the 1 mm d^{-1} range during day one to the 0.1 mm d^{-1} range within the following days indicating a pretty rapid transition from Stage I to Stage II evaporation. Evaporation rates in the range of 0.1 mm d^{-1} are typical for Stage II evaporation where atmospheric conditions remain the driver for evaporation but the latter becomes limited by water vapor diffusion through the near-surface soil rather than atmospheric demand (Shokri et al., 2009). See Chapter 3 for more details on Stage I and Stage II evaporation.

As will be shown later on in Chapter 3, the onset of Stage II evaporation could be determined a few days after an event (2-4 days). As for Events 1-10 introduced in Table 2, the onset of Stage II has not been determined in detail; however, summer evaporation rates following Events 2 and 10 (for six days) ranged between 0.3-0.4 mm d^{-1} and 0.3-0.8 mm d^{-1}, respectively. For the winter, there were multiple events; however, from 2-20 January 2011 (a period of time after Event 7) evaporation rates ranged between 0.1-0.5 mm d^{-1}. Based on the findings reported herein, and Chapter 3, Stage II evaporation can be expected to occur within six days or less after the an

event. Since arid environments are precipitation-free throughout most of the year, Stage II evaporation dominates over Stage I evaporation with respect to duration for most of the year. Average Stage II evaporation rates (over 15 days) following the three events discussed in Chapter 3 were 0.3, 0.2, 0.4 mm d^{-1} (events during summer, spring, and autumn, respectively) indicating that Stage II evaporation from a soil as described in this study will likely be in the range of about 0.1 mm d^{-1}. Support for 0.1 mm d^{-1} as a "steady state" Stage II evaporation rate in the Mojave Desert also comes from measured evaporation rates of 0.1, 0.1, 0.2, and 0.1 mm d^{-1}, during June 2009, 2010, 2011, and 2012, respectively. In particular since during the months of June, the soil surface remained mostly dry (no events recorded via tipping bucket, but 2 small events recorded via lysimeter).

To compare infiltration with evaporation, Figure 5 shows measured monthly infiltration and evaporation for winter, spring, summer, and autumn averaged for Lysimeters 1-3. The amount of winter infiltration (257.7 mm) during the study period was more than two times the amount of winter evaporation (121.7 mm) for the same time period, whereas the opposite held true for spring (105.1 mm of evaporation compared to only 47.4 mm of infiltration). As for summer, infiltration (157.2 mm) exceeded evaporation (117.6 mm) while autumn shows similar amounts of infiltration (100.3 mm) and evaporation (103.7 mm). Average infiltration recorded from lysimeter mass gain during winter months during the four water years were 53.8, 92.4, 95.0, and 16.5 mm, respectively, while average lysimeter evaporation were 34.3, 32.5, 33.2, and 21.6 mm showing that winter infiltration consistently exceeds evaporation. Note that during water year 2012, winter infiltration and evaporation were lower than the three previous water years. As for spring, infiltration (4.0, 28.8, 6.5, and 8.1 mm) was consistently lower than evaporation (23.1, 40.0, 27.6, and 14.3 mm) for the four water years. Similar amounts of infiltration (18.7, 22.3,

Figure 5. Monthly infiltration and evaporation as measured by Lysimeters 1-3 (average of all three lysimeters) for (a) winter, (b) spring, (c) summer, and (d) autumn.

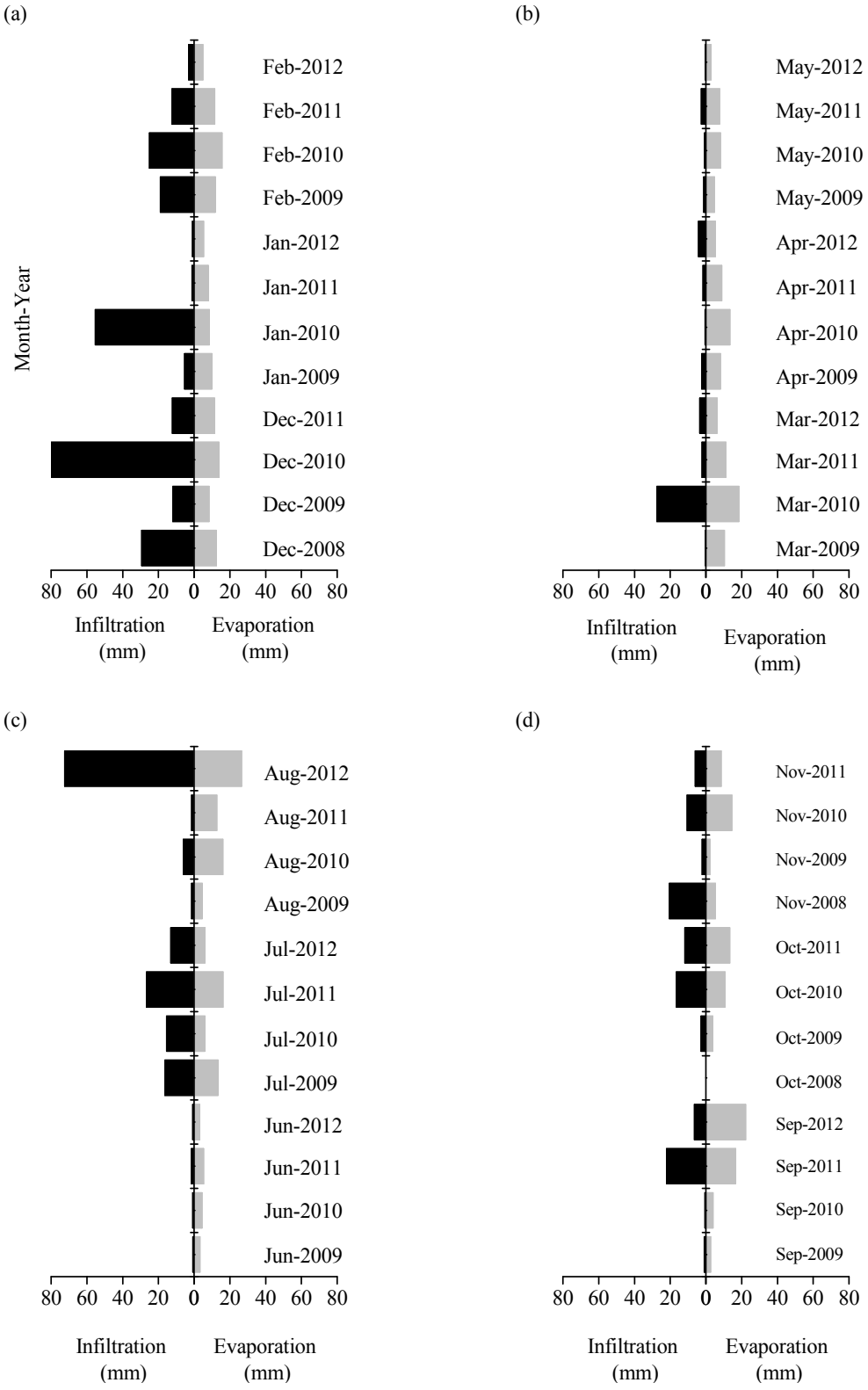

29.7, and 86.4 mm) and evaporation (21.2, 26.6, 34.2, and 35.6 mm) were observed for summer months. For autumn, infiltration of 5.8, 27.6, and 39.9 mm, and evaporation of 8.7, 29.1, and 38.4 mm were recorded for water years 2009 to 2011. Note that summer and autumn can be "wet" (more infiltration than evaporation) as well as "dry" (less infiltration than evaporation), depending on the year.

In a second step, monthly infiltration and evaporation for the four water years was related to soil water storage using ratios between monthly average infiltration and evaporation as shown in Figure 5 (Table 3). An infiltration to evaporation ratio >1 represents a monthly net influx of water to the soil (increase in water storage) whereas a ratio <1 represents a monthly net outflux of water from the soil (decrease in water storage). Devitt et al. (2010) uses a similar approach, calculating the ratio between precipitation and reference ET, to reflect a supply and demand relationship.

Table 3. Average monthly infiltration / evaporation ratios from Lysimeters 1-3, for the four year observation period (November 2008 to September 2012). Gray cells represent "dry" months with lower infiltration than evaporation (ratio < 1). White cells represent "wet" months with higher infiltration than evaporation (ratio > 1).

Year	Jan	Feb	Mar	Apr	May	Jun	Jul	Aug	Sep	Oct	Nov	Dec
2008											3.8*	2.4
2009	0.6	1.6	0.0	0.3	0.3	0.0	1.2	0.3	0.4	0.7	0.9	1.4
2010	6.5	1.6	1.5	0.0	0.1	0.0	2.6	0.4	0.1	1.6	0.7	5.9
2011	0.1	1.1	0.2	0.2	0.3	0.3	1.6	0.1	1.3	0.9	0.7	1.1
2012	0.2	0.6	0.6	0.8	0.1	0.0	2.2	2.7	0.3			
Average:	1.9	1.2	0.6	0.3	0.2	0.1	1.9	0.9	0.5	1.1	1.6	2.7

* Due to work inside the tunnel, the ratio only includes data from 9-30 November 2008

As expected, there is considerable inter-annual variability; however, there are also some general trends that were observed. Thirty of the forty-seven months (64%) showed infiltration to evaporation ratios less than 1, indicating more soil water loss than gain, which is characteristic for an arid environment. The analysis also shows that ratios between infiltration and evaporation are the lowest during spring and early summer and, therefore, most of the water loss is occurs during this time of year. For all four years of the study period, March, April, May, and June consistently had ratios below 1, ranging from 0.0 to 0.8. The only exception was March 2010 with a ratio of 1.5 caused by an unusually high precipitation event that month. The 4-yr average ratios for March, April, May, and June were 0.6, 0.3, 0.2, and 0.1, respectively. These results can be explained by the fact that during early spring (March and April), moisture from winter storms is still available in the near surface soil and evaporation increases concurrently with increasing atmospheric demand during that time of the year. Due to decreasing amount of soil moisture and, concurrently, low precipitation, evaporation then decreases from May to June, causing the infiltration to evaporation ratios to remain low because of the low level of precipitation. Quite surprisingly, no storm events were recorded with the tipping bucket rain gauge during the month of June for the entire study period (Figure 3). Upon further analysis, two minor events were recorded with the lysimeters in June 2011 but not the tipping bucket rain gauge leading to a infiltration to evaporation ratio of larger than 0 for June 2011; however, lack of precipitation for the month of June for all four years led to very low infiltration to evaporation ratios (Table 3).

In July, infiltration to evaporation ratios are consistently above 1 with values ranging from 1.2 to 2.6. This result was surprising since July has one of the highest levels of atmospheric demand (data not shown). The result indicates that actual evaporation is much smaller than potential evaporation in July. In other words, even though atmospheric conditions remain the

drivers of evaporation, they no longer control actual evaporation. For a more detailed analysis of evaporation processes after storm events, see Chapter 3. The other reason for the high infiltration to evaporation ratios in July is the increase in precipitation from summer monsoon storms. Figure 5 shows a consistent amount of infiltration ranging from 15-27 mm per month for all four years. August 2009, 2010 and 2011 showed only small amounts of infiltration and, subsequently, lower infiltration to evaporation ratios of 0.1 to 2.7, with 0.9 as the 4-yr average. August, however, also shows the highest amount of precipitation variability. For example, in August 2009 only 1.5 mm of precipitation was recorded whereas in August 2012 Events 9 and 10 alone brought 66.1 mm of precipitation.

With decreasing atmospheric demand during autumn, evaporation decreases while infiltration increases causing the 4-yr average ratios to increase from 0.5 in September to 1.6 in November. The ratio further increases to 2.7 in December due to the low amount of atmospheric demand and highest amount of average infiltration (Figure 5). It is worth noticing that the 4-yr average ratio between infiltration and evaporation for July is in between those of October through February. I.e. based on the infiltration to evaporation ratio, mid-summer soil conditions in July are similar to mid-winter conditions in January. The reasons for these high ratios, however are different (lower atmospheric demand and higher precipitation in autumn and winter months, particularly December, and high atmospheric demand and high precipitation in July). For January, the 4-yr average ratio between infiltration and evaporation is 1.9 and surprisingly low (although still above a ratio of 1), considering the low amount of atmospheric demand. The variability between the annual ratios is also high ranging from 0.1 (January 2011) to 6.5 (January 2010) and primarily controlled by considerable variability in total infiltration. There was very little in January 2009 (5.4 mm), 2011 (1.2 mm), and 2012 (1.0 mm), but a large amount in 2010 (55.3

mm). February shows a 4-yr average ratio between infiltration and evaporation of 1.2, probably due the rather consistent precipitation pattern (Figure 5) and the still rather low atmospheric demand.

Overall the analysis of infiltration and evaporation ratios shows that water is mostly added to the soil in winter and removed in spring. This result is in agreement with previous studies on the water balance of arid soils (Gee et al., 1994; Andraski, 1997; Xu et al., 1998; Scanlon et al., 2005). In other words, winter storms provide the necessary soil moisture and, under bare soil conditions, the greatest potential for deeper percolation and groundwater recharge. According to Andraski (1997) and Scanlon et al. (2005), under vegetated conditions, the roots would prevent most of this water, if not all, from percolating below the root zone by the time spring begins (considered to be the growing period for many plants). In the bare soil, moisture is removed during spring as well; however, since there are no roots, the potential is greater for water in late winter to percolate below a depth where atmospheric conditions control on the amount of evaporation. Rather surprising was the finding that also in July, moisture is added to rather than removed from the soil indicated by infiltration to evaporation ratio consistently greater than 1. This finding needs to be further analyzed with respect to soil moisture dynamics. Chapter 3 covers one aspect of it by further studying the processes governing Stage II evaporation.

In a third step, soil moisture storage as a result of precipitation and evaporation was analyzed. Figure 6 provides daily precipitation (as measured by the tipping bucket rain gauge) and the corresponding change in lysimeter mass representing soil water storage for the 4-yr study period. Precipitation events and mass gains occur concurrently and the amount of precipitation agrees very well with the increase in lysimeter mass for each precipitation event (except Event 7, as described earlier in Section 2.3.1). Precipitation free periods concur with periods of decreasing

lysimeter mass due to evaporation and, therefore, decreasing water storage. As expected based on the infiltration and evaporation data presented in Figure 5, the amount of water remaining in the soil is considerably less than cumulative precipitation over the four year observation period, as characteristic for arid environments. As can be seen for most storm events (Figure 6), lysimeter mass eventually returns to a pre-storm levels (or even below) until the next large event (i.e., high intensity and/or high duration) provides enough water to infiltrate deep into the soil profile. For example, Event 2 (3 July 2009) increases water storage in Lysimeter 1-3 by 14.8, 14.7, and 14.8 mm, respectively; however, by 6 December 2009, all of this soil water, and more, was removed from all the three lysimeters (Figure 6). Precipitation in December 2008 is a bit of an outlier due to limited soil water in Lysimeter 1-3 and that some of the precipitation was a mixture of snow and rain; otherwise, soil water storage returned to pre-storm levels or below.

Table 4 provides end-of-the-year soil water storage relative to cumulative precipitation. Percentages were calculated by dividing lysimeter mass gain (expressed in mm water storage) by cumulative precipitation from the rain gauge (in mm) recorded for each water year. As Table 4 shows, the smallest amount of water storage (the largest amount of water returned back into the atmosphere via evaporation) occurs during the 2009 and 2012 water years with Lysimeters 1-3 soils withholding between 10.2-15.0% (Table 4). This first water year was the first year of soil water measurements with antecedent conditions drier than the next three years. In addition, it was the driest year of the study period (88.3 mm). The 2012 water year, on the other hand, had a similar amount of precipitation (138.7 mm) as the 2010 water year (140.3 mm). However, the 2010 water year had higher amounts of soil water storage (26.8-29.7% for Lysimeters 1-3), very similar to the wettest water year 2011 of the study period (153.8 mm precipitation and 31.0%, 26.4-31.0% for Lysimeters 1-3). The reason for the differences in soil water storage of the four

water years is most likely the amount of winter precipitation. Except for the 2009 water year, where the dry moisture conditions remaining from soil installation in spring 2008 still had an effect on soil water storage. During water year 2009, 52.6 mm of precipitation was measured during the months of December through February, whereas in the winter of water year 2012 only 14.9 mm were recorded. As for water years 2010 and 2011, the two years with the highest end-of-the-year soil water storage, 89.7 and 76.5 mm of winter precipitation was measured. These numbers suggest that annual water storage is more affected by the occurrence of large winter storms than large summer storms. With a range of 10 to 31% of total precipitation remaining in the lysimeters per year, 69-90% of total precipitation evaporates back into the atmosphere even under bare soil conditions (i.e. without transpiration by plants).

Figure 6. Daily precipitation and lysimeter (1-3) mass representing soil water storage during the 4-yr study period. First precipitation event occurred on 9 November 2008.

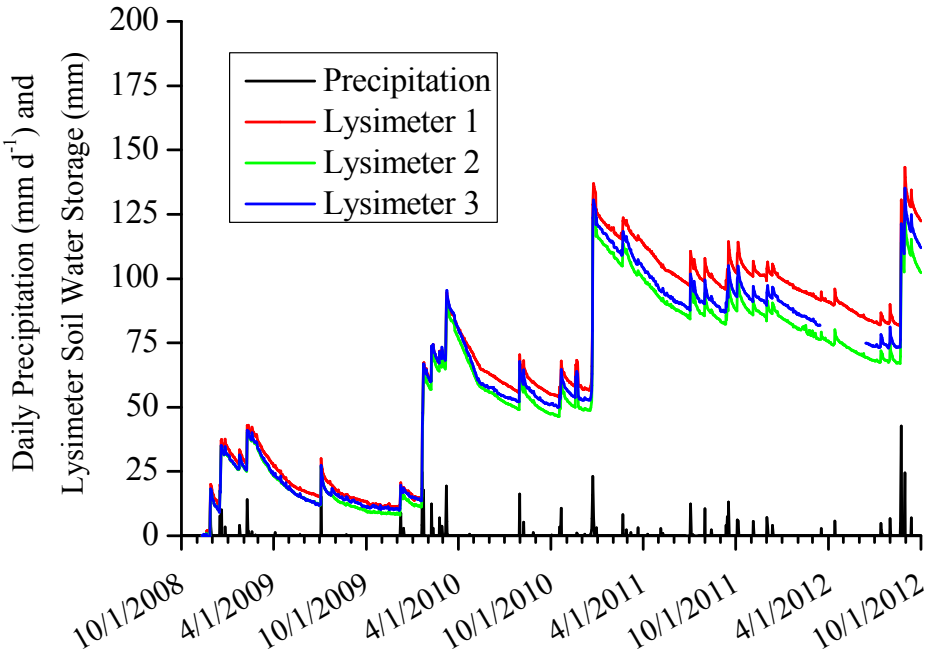

Figure 6 and Table 4 show the differences in lysimeter mass (water storage) over time for the three lysimeters. Differences in water storage between Lysimeter 1, 2 and 3 are to be expected since Lysimeter 1 contains homogenized soil whereas in Lysimeters 2 and 3 five individual horizons were reconstructed by repacking with soil from the corresponding five individual horizons at the excavation site. Since Lysimeters 2 and 3 were built as "identical twins", similar hydraulic behavior was expected but different behavior compared to Lysimeter 1. Figure 6 shows that mass for Lysimeters 2 and 3 track very similarly and that there is a difference in mass versus time compared to Lysimeter 1. Lysimeter 1 appears to dry out less after individual storms compared to Lysimeters 2 and 3. With respect to storage, however, Lysimeters 2 and 3 are not necessarily more similar than Lysimeter 1, except that they both store less water than Lysimeter 1. So from a water storage perspective, there is a clear difference between the three lysimeters but not between the homogenized soil (Lysimeter 1) and "stratified" soils (Lysimeters 2 and 3).

Table 4. End-of-the-year soil water storage in terms of annual lysimeter mass gain divided by cumulative precipitation for Lysimeters 1-3, including Lysimeter average, and cumulative precipitation.

Hydrologic Year	Lysimeter 1	Lysimeter 2	Lysimeter 3	Lysimeter Ave (StDev)	Cumulative Precipitation (mm)
2008-2009*	15.0%	11.1%	12.6%	12.9% (2.0%)	88.3
2009-2010	29.7%	26.8%	28.5%	28.3% (1.5%)	140.3
2010-2011	31.0%	26.4%	27.5%	28.3% (2.4%)	153.8
2011-2012	14.3%	10.2%	13.4%**	12.6% (2.1%)	138.7

* Not a complete hydrologic year (storage calculations begin for Lysimeters 1-3 on 9 November 2008 due to work conducted in lysimeter tunnel

** Data not collected between 16 March through 12 June 2012; used Lysimeter 2 storage difference between 15 March and 13 June (6.9 mm of evaporation) and subtracted from Lysimeter 3 total storage on 15 March 2012

2.3.3 Lysimeter Soil Water Dynamics

This section focuses on the soil water dynamics after individual storm events with emphasis on Events 1 to 10 (Figure 4 and Table 2). The analysis presented here uses soil moisture data from Lysimeter 1 only, but can be easily extended to the data from Lysimeters 2 and 3. Lysimeters 2 and 3 are similar in setup, but are slightly different in soil texture, porosity, and bulk density (for soil water data measured in Lysimeters 2 and 3, the reader is referred to Appendices A and C). Figure 7 shows four years of daily total precipitation (Figure 7a), pointing out Events 1-10, and corresponding moisture content time series at multiple depths from 2.4 cm to 250 cm throughout the soil profile of Lysimeter 1 (Figures 7b-7d).

As expected, near-surface soil moisture increased following precipitation and then decreased due to evaporation and/or redistribution within the soil. As discussed in Section 2.3.2, average monthly infiltration was more than two times higher than the amount of evaporation during winter months, while evaporation was more than two times higher than infiltration during spring months indicating winter as the optimum season for added water storage and potential recharge. However, high intensity events typically occur during the summer while long duration events typically occur during the winter. Subsequently, a question arises regarding what are the characteristics of a precipitation event (e.g., season, intensity, duration, and total precipitation) that lead to increased soil moisture content deeper into the soil profile. The following sections provide a discussion of soil moisture seasonal trends in shallow (2.4, 10, and 25 cm), moderate (50, 75, 100 cm), and deep (150, 200, 250 cm) zones of the lysimeter soil profile (Figure 7b-7d, respectively) to better understand soil water dynamics in arid soils.

2.3.3.1 Winter Soil Moisture Redistribution

During winter months 88 precipitation events were recorded by the tipping bucket rain gauge. Figure 7a shows that in general winter events larger than 0.5 mm of total precipitation increase soil moisture in 2.4 cm depth by at least 0.01 m^3 m^{-3}. A limited amount of events smaller than 0.5 mm were found to increase soil moisture at 2.4 cm, but they were all either part of a group of multiple events that occurred over a short period of time or preceded by a larger event. Since winter events smaller than 0.5 mm of precipitation generally do not infiltrate deeper than 2.4 cm, these small events can likely be ignored for water storage and recharge considerations deeper in the soil; however, these small events might be critical in establishing near-surface soil features such as biocrusts, altering the rates of evaporation.

From the total of 88 winter events, 11 events increased soil moisture by more than 0.01 m^3 m^{-3} at 10 cm depth. From the latter, seven (although Events 3 and 4 were 2 days apart) increased soil moisture down to 25 cm. Four of these six were Events 1, 3, 4, and 7, which were among the ten largest events (in terms of total precipitation) that occurred during the 4-yr study (Table 2). Event 1 (7 February 2009) was ranked as the 9th largest precipitation event that occurred and was the first single event to provide enough water to increase soil moisture at 50 cm depth. Soil moisture had already began to slowly increase from the beginning of January 2009 (0.03 m^3 m^{-3}) to mid-February 2009 (0.04 m^3 m^{-3}); however, by the end of February, soil moisture at 50 cm depth reached 0.07 m^3 m^{-3}, largely due to Event 1. Soil moisture remained at 0.07 m^3 m^{-3} until mid-May 2009, before decreasing to 0.05 m^3 m^{-3} by December 2009. It is unclear whether Event 1 had an effect all the way down to 75 cm depth. If it had, it would have been an increase of less than 0.01 m^3 m^{-3}. Subsequently, no soil moisture increases were observed deeper than 50 cm until shortly after Events 3 and 4 (January 2010). These two events

occurred within three days of each other and were the 3rd and 5th largest events in total precipitation, respectively. Based on daily average soil moisture, water percolated down to depths of 50 and 75 cm, increasing soil moisture to 0.15 m^3 m^{-3} by 23 January 2010 and 0.12 m^3 m^{-3} by 14 February 2010, respectively. By 25 March 2010, soil moisture at 100 cm increased up to 0.13 m^3 m^{-3}, likely driven by Events 3 and 4 but also influenced by the spring storm (Event 5) discussed later. There were additional events that added soil water between Events 4 and 5 such as a 12.3 mm event on 6 February, a 2.5 mm event on 9 February, a 6.9 mm event on 22 February, and two events (1.7 and 1.9 mm) on 27 February 2010. However, only the 6 February 2010 event increased soil moisture by more than 0.01 m^3 m^{-3} at 10 and 25 cm.

The 2nd largest event in terms of total precipitation and largest event in terms of duration (Event 7) occurred in December 2010. Due to the severity of the storm, and problems with the tipping bucked rain gauge, the actual amount of precipitation registered by the lysimeters was higher than the values read by the rain gauge. For this analysis, we therefore rely on the precipitation data measured by Lysimeter 1. Between 17 and 23 December 2010, Lysimeter 1 measured 80.3 mm in total precipitation. Consequently, large increases in soil moisture occurred at depths of 2.4, 10, 25, 50, 75, and 100 cm between 17 and 25 December 2010. In early January 2011, soil moisture in 150 cm depth began to increase from 0.05 m^3 m^{-3} (the antecedent moisture content when the soil was installed in spring 2008) to a maximum of 0.12 m^3 m^{-3} by early February 2011, likely due to Event 7. There were some smaller events that occurred in late December 2010 and early January 2011, but they were only reflected in soil moisture increases at 2.4 and 10 cm depth. No changes in soil moisture were observed in 200 depth until mid-March 2011 and in 250 cm depth until mid- to late-February 2012, respectively (Lysimeter 1 only).

Figure 7. Total daily precipitation (as measured by the tipping bucked rain gauge) with Events 1-10 (a), and Lysimeter 1 daily average soil moisture at (b) 2.4, 10, and 25 cm depth, (c) 50, 75, and 100 cm depth, and (d) 150, 200, and 250 cm depth for the study period of 1 October 2008 through 30 September 2012.

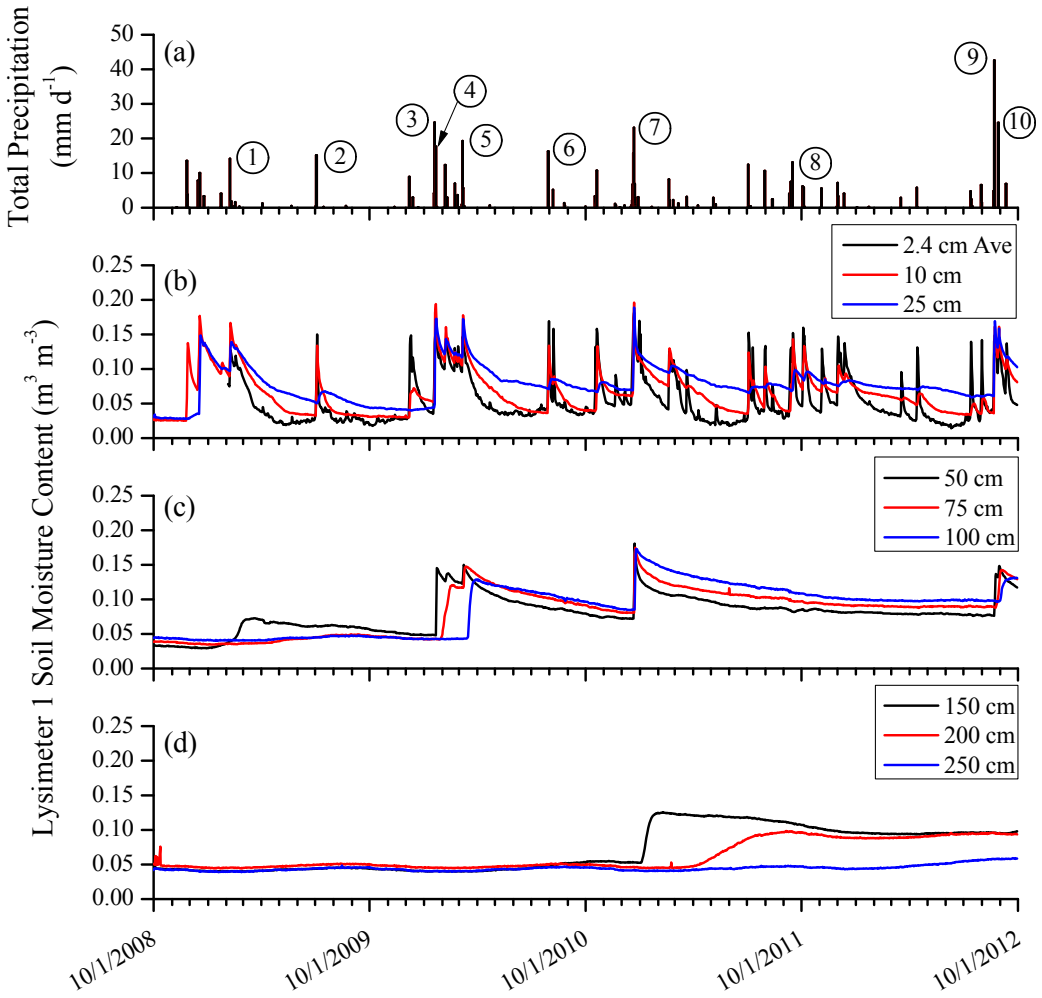

2.3.3.2 Spring Soil Moisture Redistribution

There were 27 precipitation events that occurred during the spring months. Evaporation was more than two times the amount of infiltration during spring (Figure 5b; Table 3) indicating that spring is the season of maximum evaporation and, in turn, minimum increase in water storage

(most of the precipitation evaporates). Based on daily average soil moisture measurements at 2.4 cm (Figure 7b), spring events with total precipitation larger than 1 mm increase soil moisture by 0.01 m^3 m^{-3} or more. As expected, there are exceptions to the 1 mm threshold. For example, after a small event on 3 April 2009 with 1.2 mm precipitation and of 0.8 mm hr^{-1} intensity, there was no increase higher than 0.01 m^3 m^{-3} in 2.4 cm depth. This might be related more to the low antecedent moisture content at the beginning of the study period, as very similar size event two years later on 7 March 2011 (precipitation of 1.2 mm and intensity of 1.2 mm hr^{-1}) caused an increase in soil moisture of 0.01 m^3 m^{-3} at 2.4 cm. There were also a few exceptions involving multiple events occurring within 24 hrs with precipitation less than 1.0 mm causing increases in soil moisture. For example, on 9 May 2011, there were four events ranging between 0.1 and 0.4 mm (total of 0.9 mm within 24 hrs) increasing soil moisture at 2.4 cm by 0.03 m^3 m^{-3}.

Out of the 27 spring precipitation events, only two primary events (largest within a group of multiple events within a few days) increased soil moisture at a depth of 10 cm (Figure 7b), and one of these (Event 5) increased soil moisture at depths below 50 cm (Figures 7c and 7d). As mentioned previously, winter storms have a bigger impact on soil moisture than spring storms. This is due to both more precipitation as well as lower evaporation during winter compared to spring. Although there is evaporation during the winter, spring is the time for evaporation due to the small number and short duration of storms. Moisture from most spring storms did not reach 25 cm. However, near surface soil moisture typically decreased during spring, reaching 0.07 m^3 m^{-3} or lower down to 25 cm depth. The two events causing soil moisture increases of 0.01 m^3 m^{-3} or more at 10 cm included Event 5 and one event that occurred on 13 April 2012 (precipitation of 5.6 mm and intensity of 1.6 mm hr^{-1}). The latter event only increased soil moisture by 0.02 m^3 m^{-3} at 10 cm depth, while Event 5 increased soil moisture by 0.07 m^3 m^{-3} at

10 cm and 0.06 m^3 m^{-3} at 25 cm depth. There was a slight increase in soil moisture at 25 cm following the April 2012 event, but the increase was less than 0.01 m^3 m^{-3}. Event 5 also increased soil moisture at 50, 75, and 100 cm; although, the amount of soil water at 50 (0.15 m^3 m^{-3} in January 2010) and 75 cm (0.12 m^3 m^{-3} in February 2010) were high due to 10 events in January (including Events 3 and 4) and 9 events in February 2010 (Events 3 and 4). The additional water brought on by Event 5 was enough to redistribute soil moisture down to 100 cm and increase soil moisture from 0.04 m^3 m^{-3} on 7 March 2010 to 0.13 m^3 m^{-3} on 25 March 2010.

2.3.3.3 Summer Soil Moisture Redistribution

During the 4-yr study, summer infiltration exceeded evaporation by about 1.5 times, but is probably due to the fact that four of the largest precipitation events (Events 2, 6, 9 and 10) occurred during summer. There were 32 precipitation events during the summer months, but only a few increased soil moisture at depths below 50 cm (Figures 7c and 7d). Most soil moisture increases occurred within the near surface soil (Figure 7b) as far as 2.4 and 10 cm depths. During June, soil moisture decreased throughout the four years since no precipitation occurred based on the tipping bucket rain gauge (although section 2.3.1 references two small events that were measured by the lysimeters in June 2011). Evaporation rates from Lysimeter 1 averaged 0.1, 0.1, 0.2, and 0.1 mm d^{-1}, during June 2009, 2010, 2011, and 2012, respectively; which is characteristic of diffusive Stage II evaporation (Chapter 3).

Based on daily average soil moisture at 2.4 cm, summer events with total precipitation between 1 and 2 mm can increase soil moisture by 0.01 m^3 m^{-3} or more. As expected, the 1-2 mm limit is dependent on atmospheric conditions, however, the range was fairly consistent and a "precipitation threshold" for the increase in soil moisture at 2.4 cm depth is likely to be found closer to 2 mm than to 1 mm. There were a few exceptions involving multiple events with

precipitation less than 1.0 mm with soil moisture in 2.4 cm depth increasing by more than 0.01 m^3 m^{-3}. But they were either preceded or followed by one or more events with precipitation larger than 2 mm. For example, on the morning of 4 July 2011, soil moisture at 2.4 cm increased by 0.10 m^3 m^{-3} following a 0.5 mm event; however, this event was preceded by an evening storm on 3 July 2011 measuring 12.4 mm (3.0 hr duration). Similarly, there were 3 events on 13 July 2012 which two events were only 0.1 mm each (0.5 hr duration) and a third measuring 4.5 mm (1.5 hr duration). An additional event occurred on 14 July 2012 measuring 2.4 mm (0.5 hr duration). Soil moisture at 2.4 cm increased by 0.03 m^3 m^{-3} on 13 July and an additional 0.08 m^3 m^{-3} by 14 July 2012.

Although there were 32 precipitation events measured during the summer months, only nine of them increased soil moisture by 0.01 m^3 m^{-3} or more at 10 cm depth and only 4 at 25 cm depth. Events reaching a depth of 10 cm included total precipitation ranging between 4.5-41.6 mm and intensities ranging between 2.0-10.2 mm hr^{-1}. Intensities during Events 2, 6, 9 and 10, were 10.1, 6.5, 6.4, and 12.3 mm hr^{-1}, respectively. These events increased soil moisture at 10 cm by 0.10, 0.06, 0.13, and 0.04 m^3 m^{-3}, respectively; however, for Event 10 the soil was still moist from prior to the event thus explaining why soil moisture only increased by 0.04 m^3 m^{-3}. Two additional events, with lower total precipitation (as compared Events 2, 6, 9 and 10), occurred on 7 August 2010 and 31 July 2011 (intensities of 10.2 and 5.1 mm hr^{-1}, respectively) and increased soil moisture by 0.01 and 0.06 m^3 m^{-3}, respectively, at 10 cm. Another event occurred on 3 July 2011 (total precipitation of 12.4 mm; intensity of 4.1 mm hr^{-1}) increasing soil moisture by 0.08 m^3 m^{-3}. The last two events occurred on 13 and 31 July 2012. These two events were typically smaller in both total precipitation (4.5 and 5.9 mm, respectively) and intensity (3.0 and 2.0 mm hr^{-1}, respectively) for causing greater than 0.01 m^3 m^{-3} soil moisture increases at 10

cm depth; however, the July 13th event was followed by a 2.5 mm (intensity of 4.8 mm hr^{-1}) precipitation event on the 14th while the July 31st event was preceded by a 1.5 mm (intensity of 1.0 mm hr^{-1}) on the same day. Soil moisture increased by 0.02 m^3 m^{-3} for both events.

As for soil moisture increases at 25 cm depth and deeper, only Events 2, 6, 9 and 10 provided enough moisture to infiltrate down to 25 cm and increase soil moisture by more than 0.01 m^3 m^{-3}. Measured daily average increases in soil moisture at 25 cm depth for these four events were 0.01, 0.01, 0.11, and 0.03 m^3 m^{-3}, respectively. Infiltration and redistribution of water from these four events were further dampened deeper within the profile. Only Events 2 and 6 provided enough water to increase soil moisture at 50 cm by less than 0.01 m^3 m^{-3}; otherwise, no soil moisture increases were observed below 50 cm. Only the combination of Events 9 and 10 provided enough water to see changes in soil moisture at 50, 75, and 100 cm. Soil moisture increases of 0.07, 0.05, and 0.03 m^3 m^{-3} were observed at these respective depths. Considering size and timing of Events 9 and 10 (first and third largest events in terms of total precipitation and only one week apart) the two events did not infiltrate as deep as it could have been expected. Based on available data, this indicates that summer storm events, even if sizeable, do not infiltrate as deep as winter events and, therefore increase water storage less than winter events.

2.3.3.4 Autumn Soil Moisture Redistribution

Very little storm activity occurred during autumn, particularly in 2009 and 2010; however, with atmospheric demand decreasing, smaller storm events infiltrate to 2.4 cm or deeper than in spring and summer. Based on daily average soil moisture at 2.4 cm (Figure 7b), autumn events with total precipitation between 0.4 and 1 mm can increase soil moisture by 0.01 m^3 m^{-3} or more. For example, one event on 20 November 2010 (total precipitation of 1.1 mm and intensity of 0.7 mm hr^{-1}) infiltrated down to 2.4 cm and increased soil moisture by 0.04 m^3 m^{-3} by 21

November 2010. There were some events with total precipitation below 0.4 mm which caused an increase in soil moisture at 2.4 cm depth. But these events were preceded or followed by multiple other events. An exception was the 5 October 2011 event with total precipitation of 5.8 mm followed by an increase in moisture content of only 0.01 m^3 m^{-3} at 2.4 cm depth. On 4 October 2011, daily average soil moisture at 2.4 cm was 0.16 m^3 m^{-3}; then soil moisture decreased to 0.14 m^3 m^{-3} on 5 October and increased to 0.15 m^3 m^{-3} (~ 0.01 m^3 m^{-3}) by 6 October. So the small increase in soil moisture due to the 5 October event was likely due to the already high antecedent moisture content.

There were a total 33 storm events during the autumn months of the 4-yr study period. Only six events or group of events (one large event followed and/or preceded by multiple smaller events) provided enough water for infiltration down to 10 cm (increases in moisture content of 0.01 m^3 m^{-3} or higher); while only one group of multiple events and one event increased soil moisture at 25 cm by more than 0.01 m^3 m^{-3}. A group of 5 events between 19 and 20 October 2010 increased soil moisture only by 0.01 m^3 m^{-3} at 25 cm (total precipitation during these two days was 11.9 mm, with events ranging between 0.1-5.5 mm). The largest of the storms in total precipitation occurred on 16 September 2011 (Event 8) with total precipitation of 13.2 mm and an intensity of 6.6 mm hr^{-1}. Not only was this a large event (ranking the 10^{th} largest of all events during the 4-yr period), it was also the 5^{th} highest intensity storm. Furthermore, it was preceded by the fourth largest event in terms of intensity that occurred on 11 September (total precipitation of 4.0 mm and intensity of 8.0 mm hr^{-1}) and another event on 13 September (total precipitation of 7.5 mm and intensity of 3.7 mm hr^{-1}). Soil moisture at 2.4 cm depth increased from 0.03 (10 September) to 0.15 m^3 m^{-3} (17 September), 0.04 to 0.14 m^3 m^{-3} at 10 cm (same dates), and 0.07 (10 September) to 0.10 m^3 m^{-3} (21 September) at 25 cm. In addition, another set of 5 events

occurred shortly afterwards between 3 and 5 October 2011 ranging between 0.1 and 6.0 mm in total precipitation (intensities ranged between 0.2 and 4.0 mm hr^{-1}). These October 2011 events increased soil moisture at both 2.4 and 10 cm by 0.11 and 0.06 m^3 m^{-3}, respectively. Despite the multiple events between 11 September and 5 October 2011 (total of 8 events), soil moisture did not increase by 0.01 or more at depths below 25 cm. Soil moisture actually levels off following these storms reaching relatively constant soil moisture of 0.08, 0.09, and 0.10 m^3 m^{-3}, respectively.

2.4 Summary and Conclusions

The overall goal of this study was to improve our understanding of the moisture dynamics (water infiltration, storage, redistribution, and evaporation) of a bare arid soil system. The study was conducted on data from the SEPHAS Weighing Lysimeter Facility where total soil mass and soil moisture profiles were monitored under natural precipitation conditions over a 4-yr period (1 October 2008 to 30 September 2012).

During the four year observation period, 180 precipitation events were recorded with a 4-yr annual average of 130.3 mm, which is 7.6% below the 73-yr average of 141.0 mm measured by WRCC Station # 261071. From the 180 events total, the "top ten" events in terms of total precipitation were selected, ranging between 13.2 and 41.6 mm. Precipitation intensity was generally higher during summer whereas precipitation duration was higher in the winter. The average intensities for winter, spring, summer, and autumn events were 0.7, 1.0, 2.6, and 1.4 mm hr^{-1}, respectively, while the average durations were 2.9, 1.6, 1.2, and 1.6 hrs, respectively. Close to half of all events (88 out of 180) occurred during winter. The other half occurred during spring (27 events), summer (32 events) and autumn (33 events). The average amount of precipitation

per event was the highest during summer (4.8 mm per Event) and lowest during spring (1.7 mm per Event), while winter and autumn were similar (2.7 and 2.6 mm per Event, respectively). Eight out of the ten largest events took place during winter (4 events) and summer (4 events). Only one "top ten" event took place during spring and autumn, respectively.

Between 69% and 90% of annual precipitation was found to evaporate back into the atmosphere during the course of the water year. The least amount of evaporation occurs in winter (December through February) with an average ratio of precipitation to evaporation of 1.9. The highest amount of evaporation was observed during spring (March through May) with an average ratio of precipitation to evaporation of 0.4. Summer (June through August) and autumn (September through November) showed average precipitation to evaporation ratios of 1.0 for both seasons. Evaporation rates between 1 and 3.9 mm d^{-1} were measured during the first day after storm events (Stage I evaporation) and between 0.1 and 1.0 mm d^{-1} within six days or less after the end of the event till the next storm event (Stage II evaporation). It was interesting to see that for the month of June, which was precipitation free for the entire study period (with the exception of two small events in 2011), monthly averaged Stage II evaporation rates were at 0.1 mm d^{-1} for water years 2009, 2010 and 2012 with the exception of 0.2 mm d^{-1} for water year 2011. The latter provides a guideline for any evaporation predictions off bare, sandy soil under similar climatic conditions. In other words, 37 mm of evaporation per year (33% of average annual evaporation in Las Vegas) likely occur as some sort of "baseline evaporation", unrelated to storm events. 67% of the evaporation, however, seems to occur within hours to weeks after a storm event and is likely related to precipitation provided from that storm. Which indicates that evaporation in such an arid environment may remain driven by atmospheric demand but is

primarily controlled by water supply in the form of precipitation (i.e. "no rain, nor evaporation, even if you have high atmospheric demand) followed by soil and atmospheric conditions.

From the total annual precipitation recorded, between 10% and 31% remained in the soil as soil water storage. Low annual water storage was attributed to dry antecedent soil moisture conditions (water year 2009) and, more importantly, limited winter precipitation (water years 2009 and 2012). High annual water storage was related to the occurrence of large winter storms in water years 2010 and 2011. In January 2010, two events occurred totaling in 17.6 and 24.5 mm of precipitation while in December 2010, one event occurred totaling in 30.9 mm. No other winter event matched the amount of total precipitation during these 3 events. Although large increases in soil water storage occurred late in August 2012 following two events totaling 24.5 and 41.6 mm, their impact on soil water storage in water year 2012 was surprisingly small. Additional research is needed to determine why large summer events contribute less to annual soil water storage than larger winter events.

As for the soil moisture profile, two precipitation thresholds were found during the 4-yr study: (1) the smallest amount of precipitation necessary to see an effect in soil moisture (daily average values > 0.01 m^3 m^{-3}) at 2.4 cm depth, and (2) the smallest amount of precipitation needed to reach 25 cm and below (daily average values > 0.01 m^3 m^{-3}). The former is important since it defines the smallest amount of precipitation that has an effect on the soil beyond the immediate surface. The latter indicates the smallest amount of precipitation that might lead to deeper infiltration into the soil (below the "evaporation depth"). The first threshold ranged between 0.5 and 2 mm, but depended on season, antecedent conditions, and the amount of time between previous and successive events. Events with this amount of precipitation can be ignored as water will evaporate soon after thereby not increasing soil water storage. There were 10

precipitation events that were analyzed in more detail in this study as these were the largest events in total precipitation to occur. Soil moisture at 25 cm increased by 0.01 m^3 m^{-3} or more following all 10 events with total precipitation, intensity, and duration ranging between 13.2-41.6 mm, 0.6-12.3 mm hr^{-1}, and 1.5-52 hours, respectively. No matter the size of precipitation event, other than the first year (due to antecedent conditions), soil moisture at 25 cm would eventually reach a low of 0.07 m^3 m^{-3}. The amount of precipitation needed to see changes of soil moisture at 50 cm and deeper ranged differently for the four seasons. 7 out of these 10 events increased soil moisture at 50 cm and below, with 4 occurring during the winter, 2 occurring during the summer and 1 occurring during the spring (none during autumn). Total precipitation for these 7 events ranged between 14.1-30.9 mm for winter storms, 24.5-41.6 mm for summer storms, and 15.9 mm for spring. It took just under 4 years to see an increase in soil moisture at a depth of 250 cm in only one lysimeter. Furthermore, years with high winter precipitation show the largest amount of soil water storage at the end of a year. Summer storms were typically evaporated back into the atmosphere; although, more time is needed to see how the last two storms of August 2012 may change this. The facility has been in operation since 2008, with data only analyzed up to 2012. Currently, there are 3.5 additional years of data to analyze to continue this ongoing work.

CHAPTER 3

QUANTIFYING EVAPORATION FROM BARE ARID SOIL: LYSIMETER MEASUREMENTS AND MODEL CALCULATIONS

3.1 Abstract

Arid land covers between 20-34% of the Earth's surface but little is known about the hydrology of arid soils, in particular the processes governing evaporation. Shokri et al. (2009) and Or et al. (2013) developed a process-based model to simulate vapor diffusion-controlled (or Stage II) evaporation off a bare soil. The goal of this study was to evaluate the Shokri and Or models on an arid soil system, using measured evaporation data from a weighing lysimeter in the Mojave Desert. Simulated Stage II evaporation rates after three storm events were compared to measured evaporation rates and showed good agreement for the first two out of three events (evaporation rate RMSEs of 0.093 and 0.141 mm d^{-1}, respectively). For the third event, simulations systematically underestimated measured evaporation rates (RMSE of 0.181 mm d^{-1}). The latter was likely due to differences between the soil moisture profiles in the lysimeter and assumed by the model. A sensitivity analysis showed that total porosity and difference in soil moisture content above and below the secondary drying front are the models most sensitive parameters. Because total porosity can be determined rather accurately, improving the soil moisture profile characterization would likely need more scrutiny to further improve the model predictions for arid soils.

3.2 Introduction

At this time, little is known about the hydrology of arid soils, particularly with respect to water flow and storage (Hendrickx et al., 2003). Low annual precipitation (80-150 mm; e.g., Simmers, 2003) and atmospheric demand that exceeds precipitation by ratios ranging between 5 and 33.3 (UNESCO, 1979) strongly suggest a lack of infiltration. However, a number of authors (e.g., Gee et al,. 1994; Xu et al., 1998; Andraski et al., 1997) have concluded that between 3% and 50% of annual precipitation remains in desert soils under non-vegetated ("bare") conditions and does not evaporate. A recent four-year study (Chapter 2) showed that between 10.2-31.0% of annual precipitation (130 mm average) remained in the bare, sandy soil of three weighing lysimeters installed in the Mojave Desert of Southern Nevada, US. It was also found that during the driest time of the year (March through June) nearly all evaporation stems from the upper 25 cm of the soil (volumetric moisture content of ≤ 0.07 m^3 m^{-3}), leaving the deeper soil relatively moist. This likely occurs because dry soil restricts the movement of liquid water, thus limiting evaporative loss to vapor phase transfer from within the soil profile (Heitman et al., 2008a, 2008b; Lehmann et al., 2008).

In laboratory experiments, Lehmann et al. (2008) and Shokri et al. (2009) found that evaporation becomes water vapor diffusion-controlled after the hydraulic conductivity from the soil surface is disrupted – this disconnect signifies the onset of Stage II evaporation. Shokri et al. (2009) developed a mechanistic model to predict Stage II fluxes as a function of the depth of the drying front, and Or et al. (2013) predicted the time-variable depth of this front as Stage II evaporation proceeds. In this study, we combine these models (Shokri et al., 2009; Or et al., 2013) to examine Stage II evaporation from an arid soil under natural precipitation and evaporation conditions. Measured evaporation rates from a weighing lysimeter were compared to

simulated evaporation rates after three high-intensity, short-duration storm events to determine the efficacy of the models in bare arid soils. Two sensitivity analyses, one including an analysis of individual parameters and the other a two-step Monte Carlo analysis of multiple parameters, were performed to identify the most sensitive parameters of the evaporation model.

3.3 Theoretical Considerations

Current understanding of the physical processes that control evaporation from bare soil (Lehmann et al., 2008; Shokri and Or, 2011; Or et al., 2013) is summarized in Figure 8. At the close of a precipitation event, water evaporates directly from the soil surface (Figure 8a). In this first phase, evaporation rates are high and controlled by atmospheric demand (e.g., Idso et al., 1974; van Brakel, 1980; Yiotis et al., 2006). As the near-surface soil dries, the larger pores drain, while the smaller pores continue to provide liquid water to the soil surface (Figure 8b), which is influenced by soil texture and pore size distribution. Concurrently, the primary (1°) drying front develops as an evaporation plane located below the surface (Shokri et al., 2009).

As drying progresses, direct liquid connections to the soil surface become constrained to pores of increasingly smaller diameter. While the capillary gradient driving water upwards increases with decreasing pore size, the ability of those pores to transport water decreases. Therefore, flux to the surface is greatly decreased. This second phase is typically short-lived, and characterized by a rapid decrease in evaporation rate (Lehmann et al., 2008; Shokri et al., 2009; Or et al., 2013).

As soil continues to dry, liquid water connection to the soil surface is lost (Figure 8c), creating a dry layer between the soil surface and a secondary (2°) drying front at a vapor diffusion length ξ (Lehmann et al., 2008; Shokri et al., 2009; Or et al., 2013). This third and final

phase is controlled by vapor diffusion, and is characterized by slowly decreasing evaporation rates (Lehmann et al., 2008; Shokri et al., 2009; Or et al., 2013). Some authors (e.g., Idso et al., 1974) have treated the short-lived second phase as a distinct stage (i.e., evaporation Stages I-III), while others have treated it as a transition between Stage I (atmospheric demand) and Stage II (diffusion-controlled) evaporation (e.g., Lehmann et al., 2008; Shokri et al., 2009; and Or et al., 2013); here, we follow the latter convention.

Shokri et al. (2009) predict Stage II evaporation rates using a modified version of Fick's law:

$$J = \frac{\theta_a^{2.5}}{\varphi} D_o \frac{C_{sat} - C_\infty}{L_{dried}(t)} \qquad (3.1)$$

where J is evaporation rate [mm d^{-1}], θ_a is volumetric air content [m^3 m^{-3}], φ is total porosity [m^3 m^{-3}] of the soil, and D_o is the diffusion coefficient of water vapor in free air [m^2 s^{-1}]. The saturated water vapor density within the soil above the 2°drying front, C_{sat} [kg m^{-3}], is estimate from the ideal gas law, using soil temperature and relative humidity inside the soil pores. The water vapor density in the atmosphere at the soil surface, C_∞ [kg m^{-3}], is also estimated from the ideal gas law, using atmospheric relative humidity and temperature. At the onset of Stage II evaporation, the depth of the 2º drying front, L_{dried} [mm], is equal to the vapor diffusion length, ξ (i.e., initial depth of the 2º drying front). As evaporation progresses, $L_{dried,}$ increases as a function of time, or $L_{dried}(t)$, following the onset of Stage II (Or et al., 2013):

$$L_{dried}(t) = \sqrt{\xi^2 + t \frac{2\frac{\theta_a^{2.5}}{\varphi} D_o (C_{sat} - C_\infty)}{\Delta\theta}} \qquad (3.2)$$

where $\Delta\theta$ is the moisture content difference between the wet zone (soil between the 1° and 2° drying fronts) and the dry zone (soil above the 2° drying front). Note that for $t = 0$, Equation (3.2) yields the vapor diffusion length, ξ, as the depth of the 2º drying front.

Equations (3.1) and (3.2) allow for the calculation of Stage II evaporation rates based on only a few relatively easy to determine atmospheric (relative humidity, temperature) and near-surface soil physical properties (total porosity, volumetric soil moisture content, temperature). The vapor diffusion length, ξ, is difficult to measure in the field, but can be estimated from Figure 6 in Shokri and Or (2011). Or et al. (2013) also suggested that θ_a and φ above the 2° drying front can be assumed to be equal. Limitations of this approach (Equations 3.1 and 3.2) include an assumption that water primarily evaporates at the 2° drying front and diffuses upward to the soil surface. Second, it is implicitly assumed that soil vapor diffusivity follows the model proposed by Moldrup et al. (2000).

3.4 Materials and Methods

3.4.1 Lysimeter Facility

This study was carried out with data from Lysimeter 1 at the SEPHAS facility (https://www.dri.edu/sephas; Chief et al., 2009) in Boulder City, Nevada (35.96°N, -114.85°W). Lysimeter 1 is a 2.26 m diameter stainless steel tank that extends from ground surface to a depth of 3.0 m. The lysimeter is housed in an individual room and rests on a highly accurate scale (Model Z-100, Cardinal Scale Manufacturing Co., Webb City, MO). The lysimeter was filled from bottom to top in individual layers (between 2-22 cm layer thicknesses) with soil excavated from nearby Eldorado Valley (see below). The soil in Lysimeter 1 has a homogenous texture profile with an average gravel content of 18.9% and fine fraction (< 2 mm) consisting of 93.0% sand, 5.5% silt and 1.5% clay (low clay content due to limited weathering). The lysimeter soil was packed to an average total bulk density of 1.75 g cm^{-3} (porosity of 0.30). The uppermost

layer in Lysimeter 1, where both the 1º and 2º drying fronts form, has a depth of 60 mm and a bulk density of 1.90 g cm^{-3} (from which a porosity of 0.24 m^3 m^{-3} was calculated).

Figure 8. The physics of evaporation [adapted from Lehmann et al. (2008), Shokri and Or (2011), and Or et al. (2013)] showing (a) atmospheric controlled evaporation with both large and small pores filled with water shortly after a precipitation event, (b) water-filled capillaries (small pores) reaching the soil surface from the primary (1°) drying front, and (c) soil controlled diffusive evaporation beginning when liquid water recedes from the soil surface to a vapor diffusion length of ξ creating a secondary (2°) drying front.

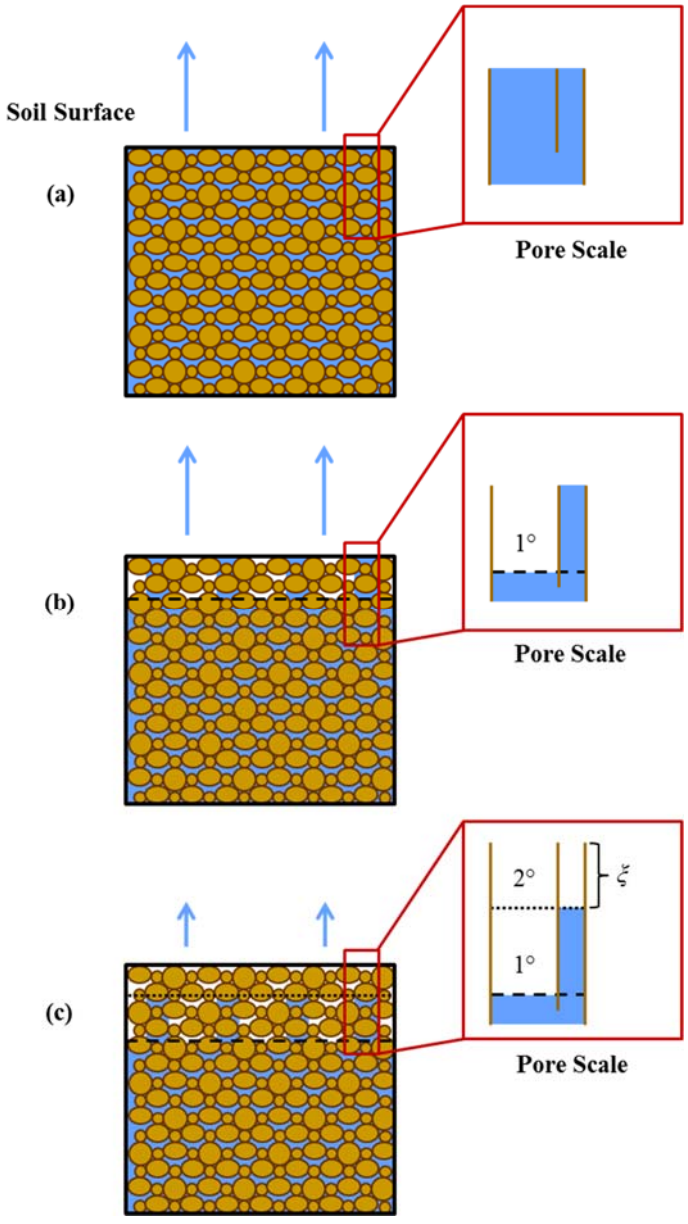

3.4.2 Study Area

The lysimeter facility is located in Boulder City, NV, approximately 40 km southeast of Las Vegas, NV, in the eastern part of the Mojave Desert. The soil originates from Eldorado Valley, about 8 km SW of Boulder City and was classified as a sandy-skeletal, mixed, thermic Typic Torriorthents (Soil Survey Staff, 1993) of the Arizo soil series (Chief et al. 2009). According to Chief et al. (2009), the soil at the study site developed on a South-facing, shallow sloped alluvial fan (0-15% slope angle), deposited from the nearby McCullough and Highland Ranges. From a nearby weather station (WRCC Station # 261071; 35.98°N, -114.85°W), the average annual minimum and maximum temperatures are 13.7°C and 25.4°C, respectively, and the average annual total precipitation is 141.0 mm over a 73-year record (1 September 1931 through 31 July 2004) (WRCC, 2009).

3.4.3 Near-Surface Soil Moisture, Temperature and Atmospheric Measurements

Near surface soil temperature and volumetric moisture content were measured at hourly intervals using Three Probe Heat Pulse (TPHP) sensors (Campbell et al., 1991; Bristow et al., 1994) installed at 12, 24, 36, and 48 mm depths within the lysimeter. The difference in soil moisture content above and below the 2° drying front, $\Delta\theta$, was assumed to be the equivalent to the volumetric moisture content at 48 mm depth measured during the observation period. This equivalence is based on the assumptions that (a) the second drying front will not move deeper than 48 mm during the observation period and (b) air-filled porosity above the second drying front is equal to the total porosity. These assumptions also imply a moisture content profile in the shape of a step function as assumed by Shokri and Or (2011). Finally, volumetric water contents at depths of 100 and 250 mm were measured using time domain reflectometer (TDR) probes (Model CS605, Campbell Scientific Inc., Logan, UT).

Atmospheric temperature and relative humidity were measured 10 cm above the soil surface using a micro-meteorological tower instrumented with relative humidity and temperature sensors (model SHT-75, Sensirion, Westlake Village, CA). Precipitation was monitored using a tipping bucket rain gage (model TE525WS-L, Campbell Scientific, Inc., Logan, UT) located approximately 28.5 m west of the lysimeter. Soil water content, soil temperature, atmospheric relative humidity, and air temperature were recorded at hourly intervals. Precipitation was recorded at 30-min intervals.

3.4.4 Evaporation Measurements

Because the lysimeter does not have a bottom drain, daily evaporation can be determined from measured changes in lysimeter mass over a 24-h period. Change in lysimeter mass was converted to depth of water by dividing the mass change by water density (1,000 kg m^{-3}) and lysimeter surface area (4.022 m^2) and multiplying by a conversion of 1,000 mm m^{-1}.

3.4.5 Event Selection and Model Application

Daily evaporation rates were determined for three precipitation events on 7 August 2010, 13 April 2012, and 11 September 2012 (hereafter referred to as Events 1-3, respectively). These three events were selected from a pool of approximately 180 events recorded between October 2008 and 2012 (analyzed in Chapter 2), and chosen because they exhibited high-intensity, short duration, and each was followed by 2-3 weeks of zero precipitation.

The onset of Stage II evaporation, when t=0 (or t_0), was followed using the method proposed by Brutsaert and Chen (1995). The inverse square of measured evaporation rate was plotted as a function of time (Figure 9a). The intercept between a linear fit to the "steep" part of the time-axis is then taken as t_0. Shokri and Or (2011) proposed an alternative method where the inverse

square of evaporation is plotted on log-scale, and resulting discontinuity in the data is taken as t_0 (Figure 9b).

Figure 9. Methods to determine the time of onset of Stage II evaporation, t_0, plotting (a) the inverse of evaporation rates squared as a function of time (Brutsaert and Chen, 1995) and plotting (b) the logarithm of the inverse evaporation rates squared as a function of time (Shokri and Or, 2011).

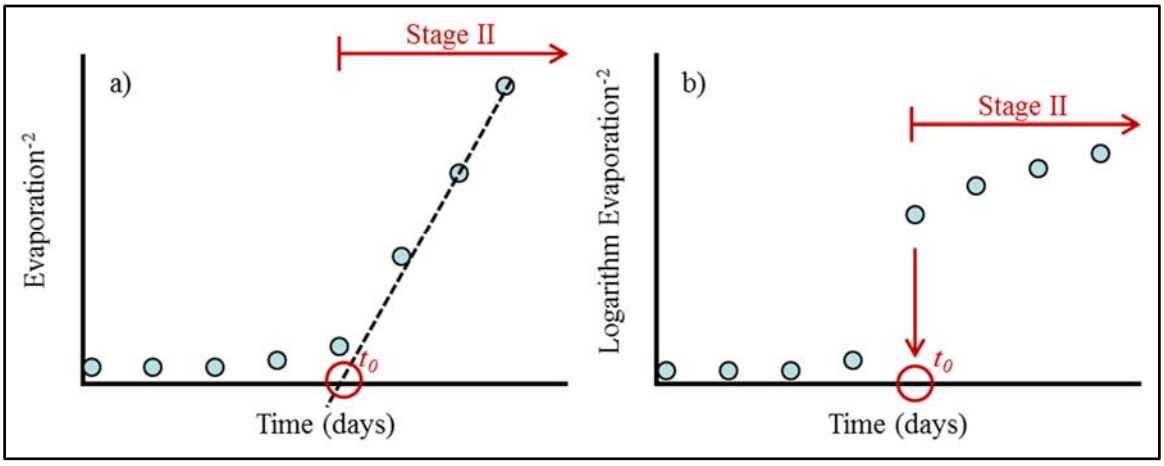

Vapor diffusion length (ξ) for a sandy soil is 6.3 mm (Shokri and Or, 2011) and soil porosity in the upper lift of the lysimeter is 0.24 m^3 m^{-3} (calculated using bulk density in Chief et al. [2009]). Change in water content ($\Delta\theta$) was calculated using water content measured at 48 mm, assuming a water content of 0 m^3 m^{-3} above the 2° drying front. The value of D_0 was determined using air temperature and Table 2.3 in Hillel (1998).

3.5 Results and Discussion

3.5.1 Stage II Evaporation: Measurements and Simulations

Measured daily evaporation rates for Events 1-3 were high (1.4-2.8 mm d^{-1}) on the day immediately following the precipitation event, and then decreased soon after to an average of 0.6

mm d^{-1} (Figure 10). Initial evaporation rates were higher for Events 1 and 3 (2.7 and 2.8 mm d^{-1}, respectively) than for Event 2 (1.4 mm d^{-1}). This difference cannot be explained by magnitude of the associated precipitation events, and is therefore attributed to higher atmospheric demand. Surface air temperatures were considerably higher following Events 1 and 3 (27.1-28.4°C and 24.4-29.0°C, respectively) than for Event 2 (7.7-13.7°C) and vapor pressure deficits were much higher (2.4-3.2 kPa and 1.6-3.6 kPa versus 0.4-0.9 kPa for Event 2). High initial evaporation was followed by a rapid decrease towards an apparent steady-state value of 0.3, 0.2, and 0.4 mm d^{-1} for Events 1-3, respectively, during Days 5-19. In each case, atmospheric demand remained fairly constant, suggesting that observed behavior reflected a transition from atmospheric controlled (Stage I) to diffusion-controlled (Stage II).

The onset of Stage II evaporation was estimated using the method proposed by Shokri and Or (2011). The squared logarithm of the inverse evaporation is plotted as a function of time, and the bend in the resulting plot is taken as the onset of Stage II (Figure 11); 9 August 2010, 17 April 2012, and 14 September 2012 for Events 1-3, respectively. Equations 3.1 and 3.2 were then used to estimate Stage II evaporation (Figure 10). Following Shokri and Or (2011) the vapor diffusion length was estimated as 6.3 mm. Measured lysimeter porosity values (Chief et al., 2009) provided a representative estimate of 0.24. Change in moisture content, $\Delta\theta$, was calculated from the moisture content measured at 48 mm. Following the suggestion by Or et al. (2013), we assumed the air-filled porosity above the second infiltration front to be equal to the total porosity.

Figure 10. Daily precipitation as measured by the SEPHAS facility rain gauge (bar), daily evaporation rates as measured by Lysimeter 1 (triangle), and simulated evaporation rates using Equations 3.1 and 3.2 (line) for Events 1-3.

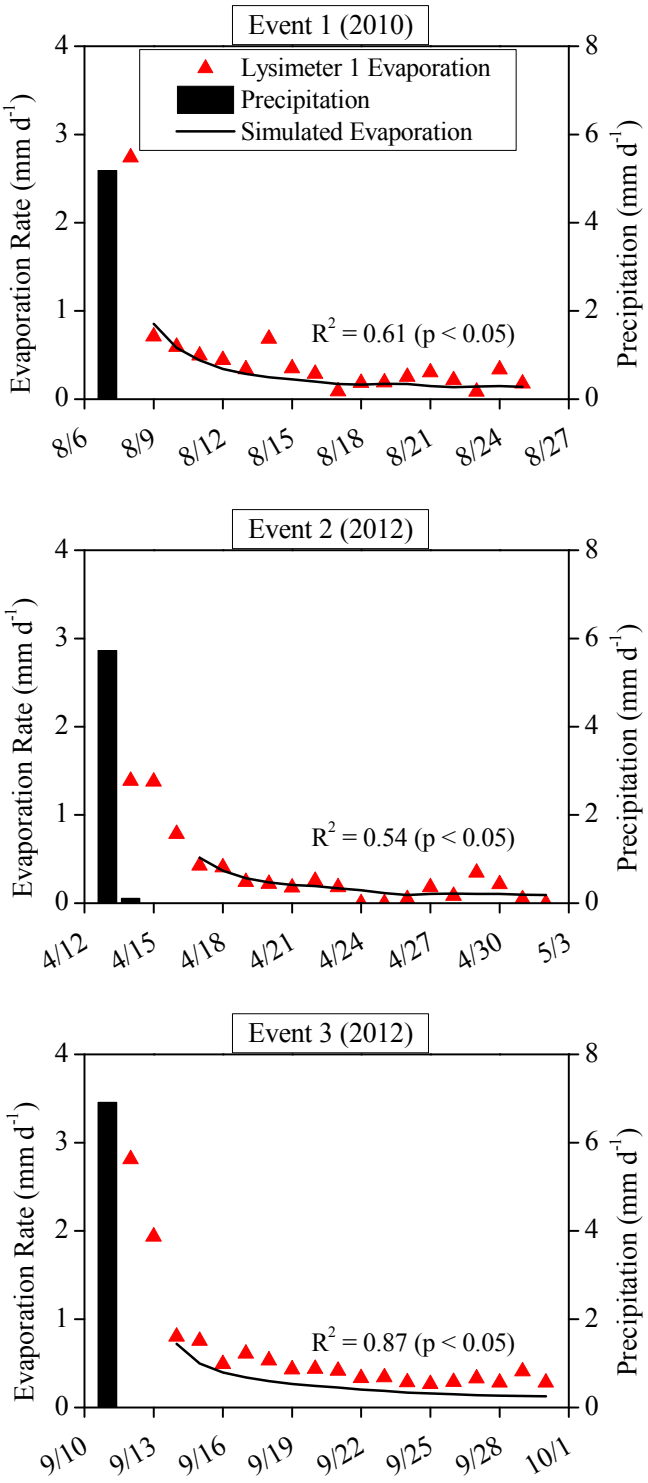

Calculated evaporation rates showed the best agreement with measured data for Event 2 and the least for Event 3 (Figure 10). Root-mean-square errors (RMSE) ranged between 0.093 and 0.181 mm d^{-1} (Table 5). For Events 1 and 2, equations 3.1 and 3.2 simulated the general trend of Stage II evaporation and some fluctuations associated with atmospheric demand, but were unable to capture short term (i.e., single day) changes in evaporation, as evident in R^2 values of 0.61 and 0.54, respectively ($p < 0.05$). For Event 3, the model consistently underestimates evaporation rates for the entire observation period ($R^2 = 0.87$; $p < 0.05$). Possible reasons for this are addressed in the sensitivity analysis below, but might be related to the difference between the actual soil moisture profile and the assumed soil moisture profile, as well as soil moisture not accounted for above the 2° drying front (Yiotis et al., 2006).

Table 5. Events 1-3 RMSE for diffusive evaporation including initial simulations (dark bold) using available data and sensitivity analysis using three separate values for four variables (one variable at a time) in Equations (3.1) and (3.2) (t, ξ, φ, and $\Delta\theta$). All results are in units of mm d^{-1}.

		Onset time of Stage II Evaporation (t_0)			Vapor Diffusion Length (ξ)		
Event	**Initial Simulation**	Prior Day	Day After	2 Days After	3.0 mm	9.0 mm	14 mm
1	**0.141**	0.496	0.150	0.158	0.164	0.139	0.153
2	**0.093**	0.125	0.106	0.133	0.109	0.091	0.098
3	**0.181**	0.351	0.157	0.156	0.177	0.194	0.222

	Porosity (φ)			Soil Moisture Difference ($\Delta\theta$)		
Event	0.20	0.30	0.40	-0.02 m^3m^{-3}	+0.02 m^3m^{-3}	+0.04 m^3m^{-3}
1	0.159	0.148	0.217	0.162	0.128	0.121
2	0.094	0.110	0.165	0.098	0.099	0.109
3	0.221	0.144	0.134	0.204	0.162	0.145

Figure 11. Inverse of evaporation rate squared plotted on a log scale versus time to determine the onset of Stage II evaporation as proposed by Shokri and Or (2011).

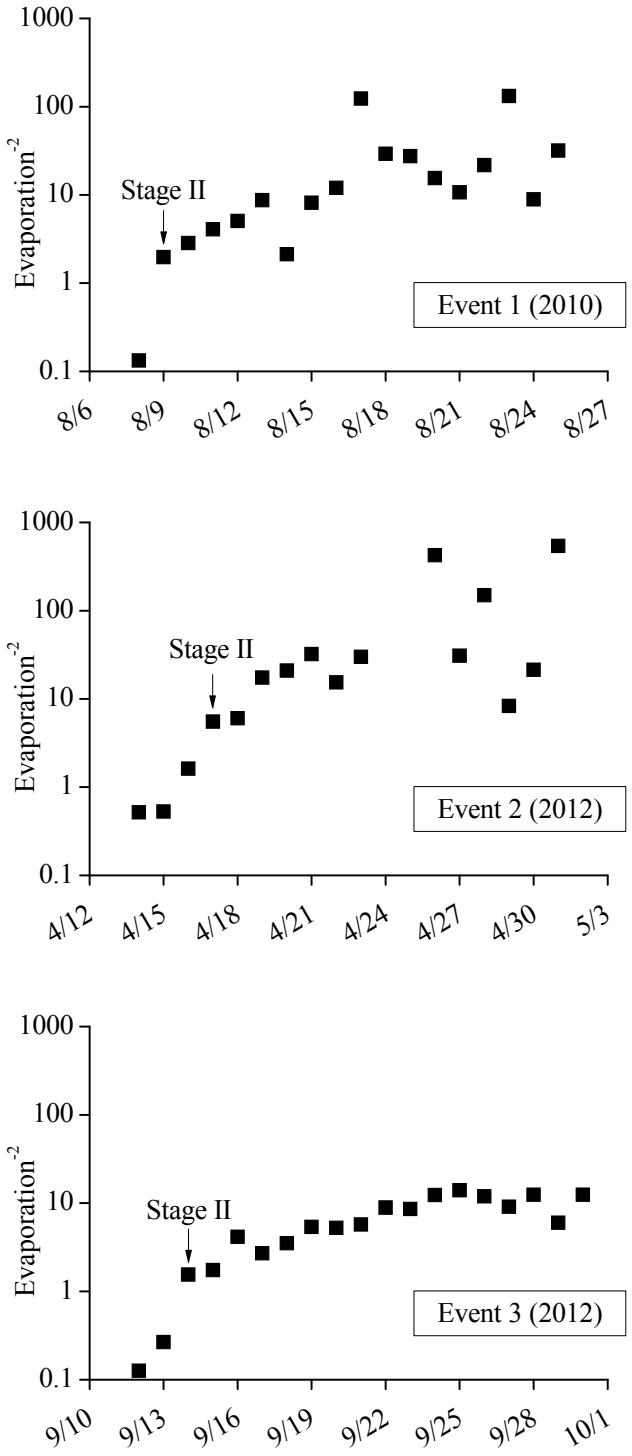

3.5.2 Sensitivity Analysis of Individual Variables

A sensitivity analysis was performed in order to determine how small errors in estimating input parameters to equations 3.1 and 3.2 (t_0, ξ, φ, and $\Delta\theta$) may have affected the results presented in Figure 10. Beginning with our base case, we considered 3 values for t_0; results are shown in Figure 12 and Table 5. For Events 1 and 2, our base case provided a better fit than the alternative values (lowest RSME). Conversely, for Event 3 the RSME decreased slightly when t_0 was delayed by 1-2 days. These results suggest that the method proposed by Shokri and Or (2011) for estimating the onset of Stage II evaporation provides a good first-order estimate that should be used with caution. For all three events (Figure 12), the significance of t_0 decreases rapidly with increasing time. Over the last 10 days for each event period, predicted evaporation rate differ by < 0.05 mm d^{-1} between different values of t_0. We also note that the sensitivity analysis for t_0 did not explain underestimation of evaporation rates in Event 3.

Sensitivity to the vapor diffusion length, ξ (Figure 13) was evaluated by considering values (3.0, 9.0, 14.0 mm) that cover the range given by Shokri and Or (2011). The goodness-of-fit (Table 5) improved slightly for Events 1 and 2 by increasing ξ to 9.0; for Event 3, an improved RMSE was observed by decreasing ξ to 3.0 mm. Similar to t_0, ξ affects evaporation rates primarily during the first few days after the onset of Stage II evaporation. Evaporation rates of the last ten days of the study period for Events 1-3 differ by less than 0.02 mm d^{-1} for the full range of ξ = 3 to 14 mm (Figure 13).

Figure 14 shows the result of varying soil porosity, φ. Although the total porosity of the upper 60 mm of the lysimeter is known, small-scale heterogeneities due to the initial re-packing of the soil and structure formation over time may affect porosity at the millimeter scale; this is the scale at which soil porosity affects Stage II evaporation rates. Additionally, the evaporation

Figure 12. Lysimeter 1 measured (triangle) and simulated evaporation rates using Equations 3.1 and 3.2 (lines) showing differences in estimated onset of Stage II evaporation, t_0, for Events 1-3.

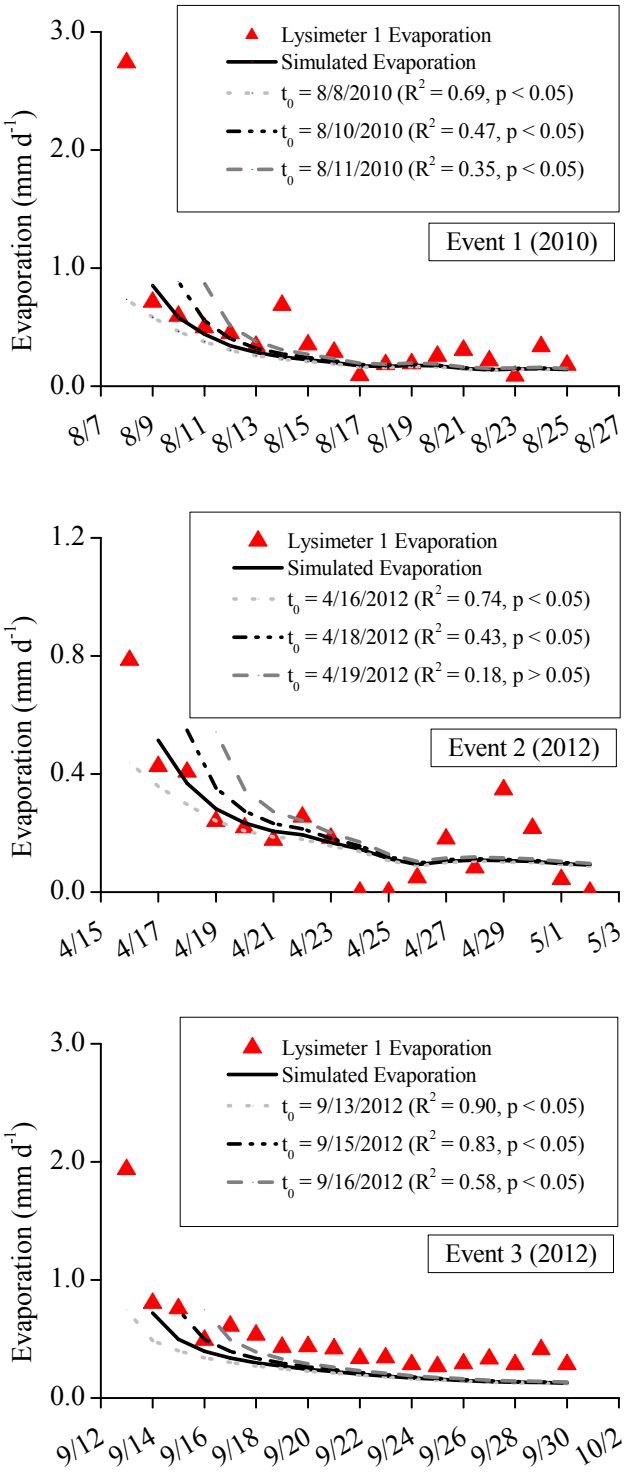

Figure 13. Lysimeter 1 measured (triangle) and simulated evaporation rates for Events 1-3 and vapor diffusion length, ξ, ranging from 3 to 14 mm.

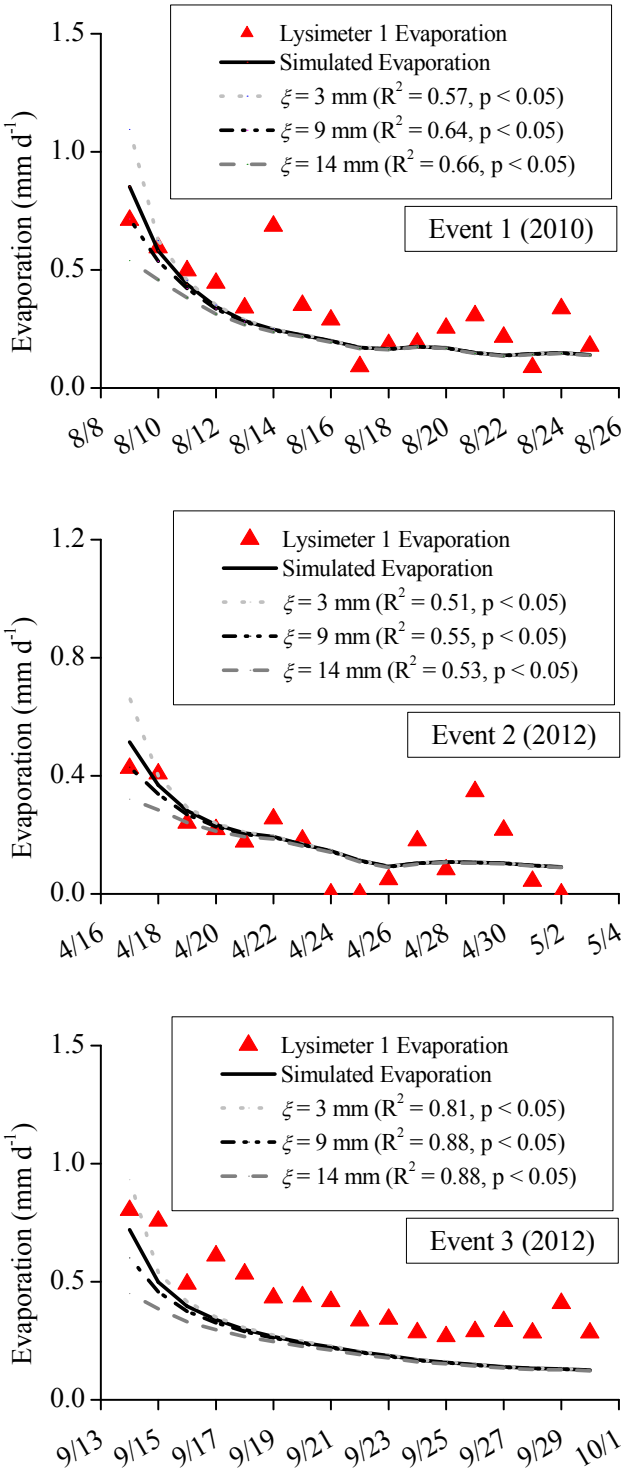

rate in Equation (3) shows a non-linear dependence on soil porosity – small differences in total porosity may have considerable impacts on simulated fluxes. Varying φ between 0.20 and 0.40 has a considerable influence on the evaporation rate during the entire simulation period, indicating that the model is indeed sensitive to total porosity. The goodness-of-fit (Table 5) does not improve when varying porosity for Events 1 and 2, but Event 3 is more accurately simulated by porosities of 0.30 and 0.40 $m^3\ m^{-3}$ (RMSE of 0.144 and 0.134 mm d^{-1}, respectively) than the measured value of 0.24 $m^3\ m^{-3}$ (RMSE of 0.181 mm d^{-1}). Based on Events 1 and 2, the porosity seems to be between 0.24 and 0.30 $m^3\ m^{-3}$; considering Event 3 (Figure 14), however, the best fit would be achieved for a porosity of 0.40. Since Event 3 is the last of the three studied events, porosity could have changed due to structure formation. It is unlikely though, that near surface porosity increased from 0.24 (Events 1 and 2) to 0.4 (Event 3) within 26 months.

The final parameter considered was $\Delta\theta$, the difference in soil moisture content between the capillary zone and the dry zone; measured $\Delta\theta$ values were adjusted by -0.02, +0.02, and +0.04 $m^3\ m^{-3}$. As shown in Figure 15, changes in $\Delta\theta$ have little effect at the beginning of Stage II evaporation, but have a greater effect after a few days. Goodness-of-fit improves for Events 1 and 3 if $\Delta\theta$ is increased by +0.02 and +0.04, respectively, but does not improve for Event 2 (Table 5). Overall, the analysis shows that $\Delta\theta$ is a sensitive parameter for the later part of Stage II, and affects evaporation rates to a similar extent as φ.

As would be expected from inspection of equations 3.1 and 3.2, sensitivity to t_0 and ξ is highest at the beginning of Stage II evaporation, while sensitivity to φ and $\Delta\theta$ shows little dependence on time. In addition, we found that φ and $\Delta\theta$ are the two most sensitive parameters in the model by Shokri et al. (2009) and Or et al. (2013). Because φ can be determined rather accurately, and likely remains constant over longer periods of time, $\Delta\theta$ might be the main reason

Figure 14. Lysimeter 1 measured (triangle) and simulated evaporation rates using Equations 3.1 and 3.2 (line) for Events 1-3 and porosity, φ, ranging from 0.2 to 0.4.

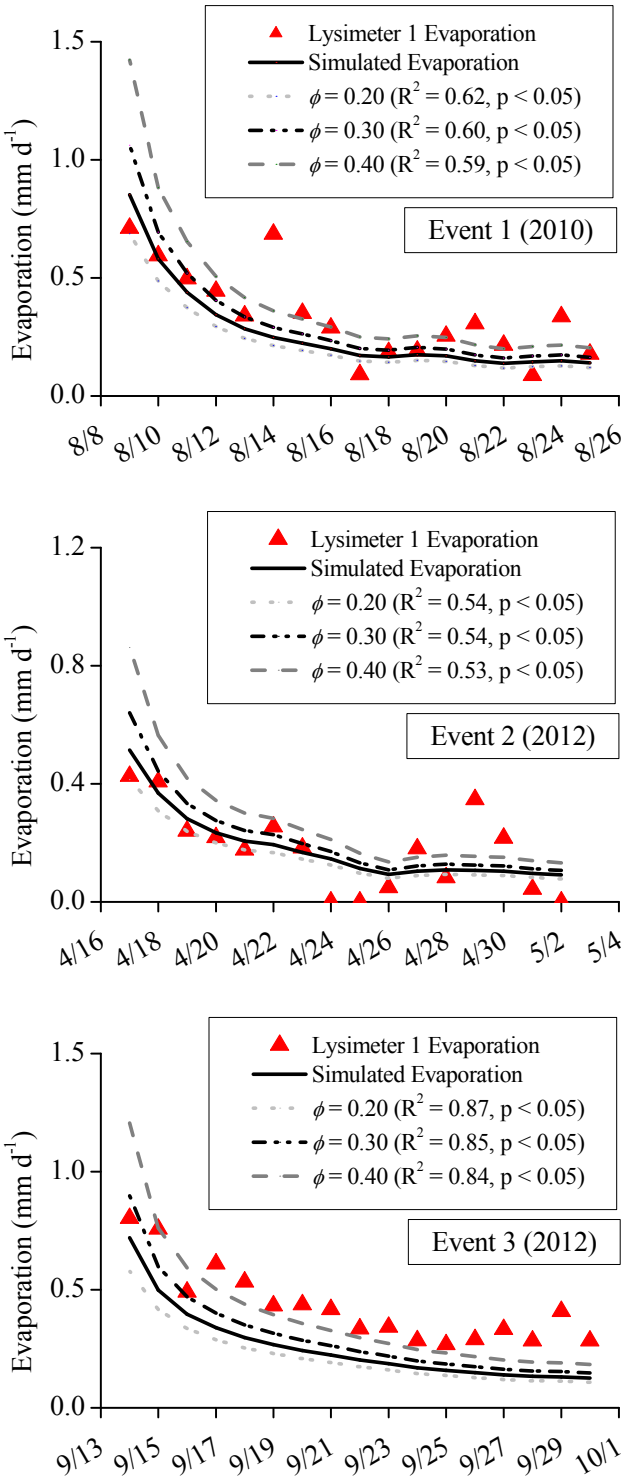

Figure 15. Lysimeter 1 measured (triangle) and simulated evaporation (line) for different values of $\Delta\theta$ for Events 1-3.

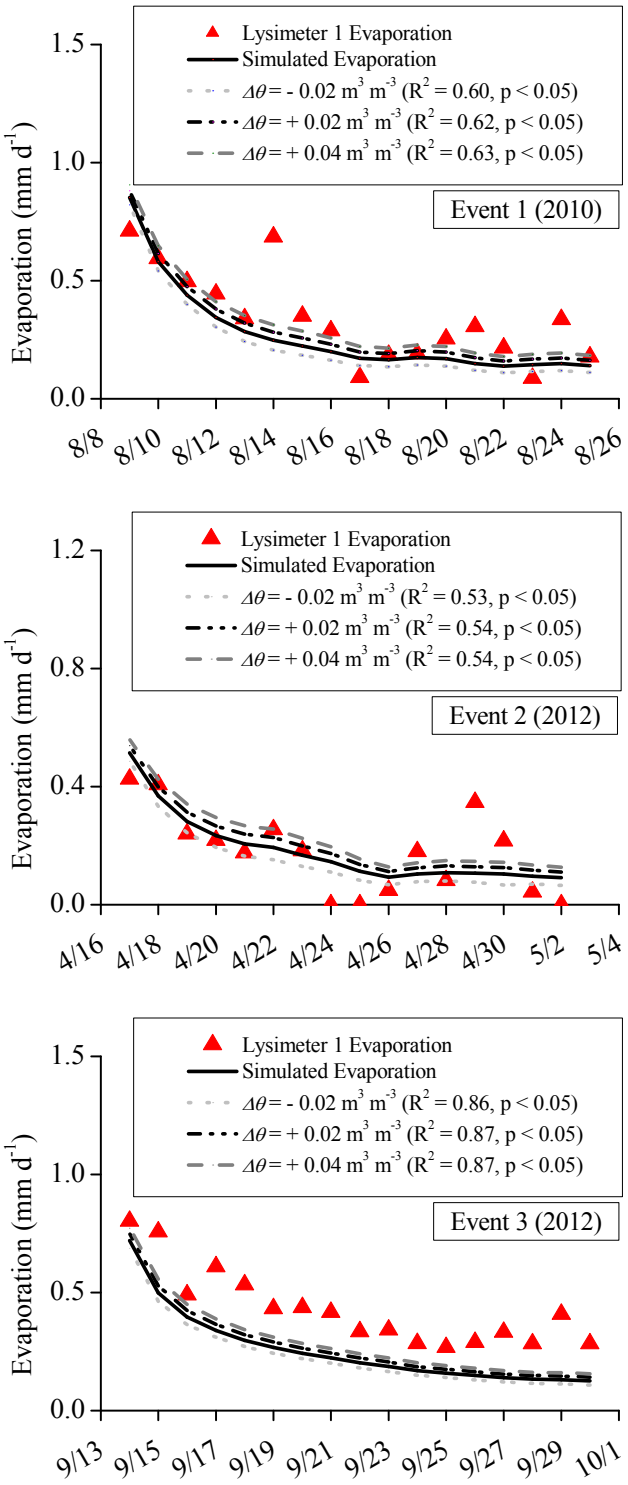

for the difference between measured and simulated Stage II evaporation rates. None of the parameters seemed to effect response to short term fluctuations.

One of the main differences between the laboratory experiments by Shokri et al. (2008) and the lysimeter experiments are their different moisture content profiles. In their experiments Shokri et al. (2008) found a moisture distribution with depth similar to a step function with zero moisture content above the 2° drying front, constant (non-zero) moisture content between the first and the second drying front, and saturated conditions below the first drying front. In the lysimeter soil, however, the shape of the moisture content profile differs considerably from a step function. Figure 16 shows moisture content profiles in Lysimeter 1 between 12 mm and 250 mm depth for Events 1-3. Immediately after the precipitation event, moisture content is highest near the surface and decreases with depth. With increasing time, the near surface soil dries out faster than the deeper soil, leading to a moisture content minimum at 12 mm and a maximum below 100 mm. Also the near surface volumetric moisture content is higher than zero during the study period. A more sophisticated model of the actual soil moisture profile might improve evaporation simulations.

3.5.3 Sensitivity Analysis using Monte Carlo Simulations

In this section we employ a two-step Monte Carlo method to first determine the optimal value of t_0 and then to consider the model's sensitivity to simultaneous variations in multiple parameters. Monte Carlo data are available in the online supplemental material. For Events 1 and 3, the Monte Carlo analyses yielded the same dates of Stage II onset (9 August 2010 and 14 September 2012, respectively) as the initial simulations. Monte Carlo RMSE for Events 1 and 3 was 0.2876 and 0.2538 mm d^{-1}, respectively. In Event 2, the initial simulation found the onset of Stage II evaporation on 17 April 2012. The Monte Carlo analysis, however, showed a better fit

Figure 16. Lysimeter 1 soil profiles of moisture content distribution from 12-250 mm following Events 1-3.

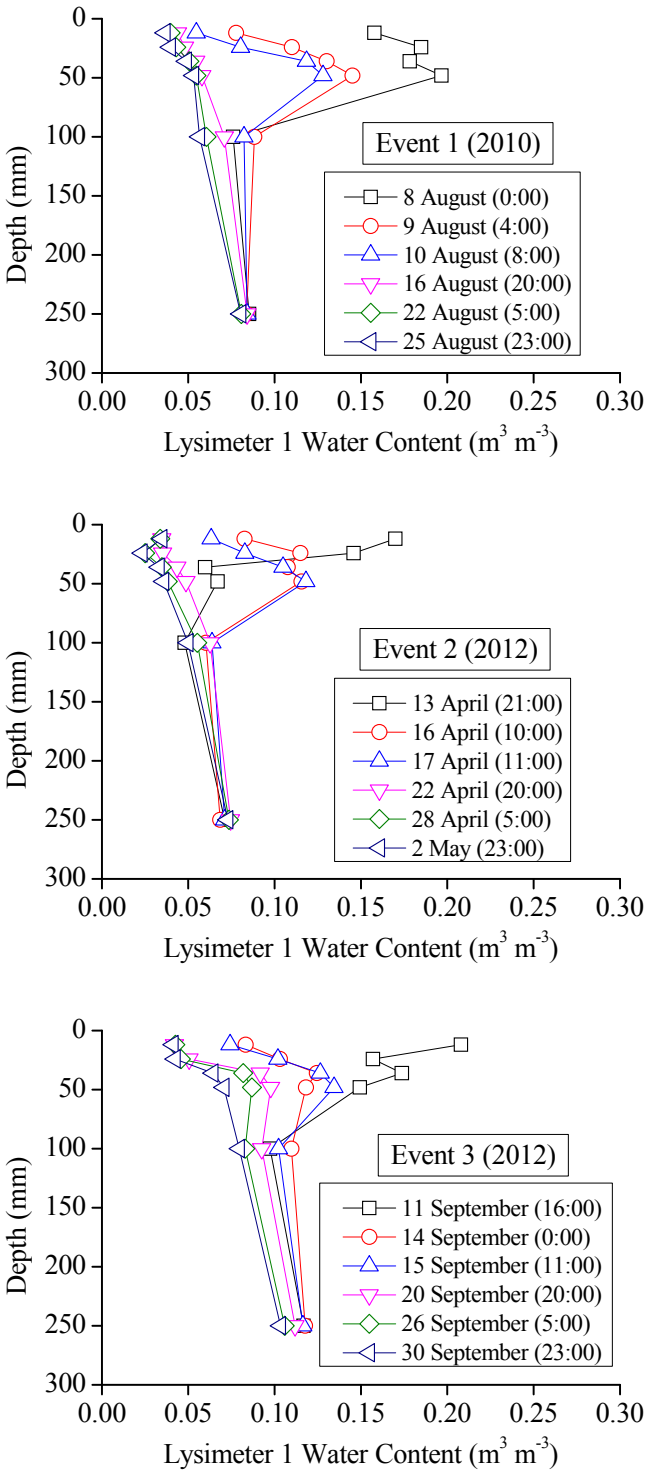

for Stage II evaporation beginning 16 April 2012. The mean Monte Carlo RMSE for 16 April was 0.2008 mm d^{-1} compared to 0.2620 mm d^{-1} for 17 April 2012. The Monte Carlo simulations are based on daily rather than hourly data; this difference makes the Monte Carlo simulations somewhat less accurate, but may also be responsible for the difference in optimal t_0 for Event 2.

With the onset of Stage II evaporation set as 9 August 2010, 16 April 2012, and 14 September 2012 for Events 1-3, respectively, optimum values for ξ, φ, and $\Delta\theta$ were determined based on the lowest RMSE values. Table 6 provides arithmetic mean, minimum, and maximum ξ, φ, and $\Delta\theta$ values for the lowest 1% and 5% RMSE values from the 1000 realizations. Monte Carlo simulations were run for the entire observation periods after precipitation Events 1-3, as well as only for the last ten days of Stage II evaporation. Looking only at the lowest 1% of RMSE values, we see ξ ranging between 9 and 13 mm, 4.6 and 10.5 mm, and 10.6 and 13.3 mm, for Events 1-3, respectively; the initial ξ value of 6.3 mm falls within this range only for Event 2. The total porosities for Events 1-3 range from 0.22 to 0.38, which matches the range of total porosities observed in Lysimeter 1 (Shillito, R., unpub. data, 2015). The total porosity of 0.24 measured for the top 60 mm of the soil is within range but at the lower end of the Monte Carlo simulated values. There was no common value of $\Delta\theta$ among all events, but values for the lowest 1% and 5% were no greater than 0.29 m^3 m^{-3}. The Monte Carlo analysis, however, failed to converge on any particular set of parameters. With the 4 lowest RMSE values in Event 1, for example, there is a negligible difference in RMSE between them (0.1064 – 0.1066 mm d^{-1}), yet ξ, φ, and $\Delta\theta$ show ranges of 9.0-13.0 mm, 0.22-0.29, and 0.11-0.19 m^3 m^{-3}, respectively. Similar parameter ranges are also found for Events 2 and 3. The lowest 1% of RMSE values provide improved goodness-of-fit using a more narrow range of values for ξ, φ, and $\Delta\theta$.

The Monte Carlo method provides some insight into potential values for the variables when the entire observation period is considered for all events. If only considering the last ten days of Stage II evaporation for the Monte Carlo simulations, however, ranges for ξ, φ, and $\Delta\theta$ could be narrowed down. As observed in the individual sensitivity analysis completed above, the variables t_0 and ξ have little impact on evaporation simulations during the last ten days of diffusive evaporation. The lowest 1% of RMSE values for the last ten days provides an improved goodness-of-fit with a narrower range of values for both φ and $\Delta\theta$ (Table 6). Events 1-3 have average φ of 0.22, 0.21, and 0.32, respectively (all with standard deviations of 0.01), and average $\Delta\theta$ values of 0.14, 0.07, and 0.27 $m^3\ m^{-3}$, respectively (standard deviations of 0.02, 0.01, and 0.02 $m^3\ m^{-3}$, respectively). The measured porosity used for the simulations was 0.24, which is within the range (0.20-0.25) from the 10-day Monte Carlo simulations for Events 1 and 2. Since the porosity likely did not change much between all three events, an average porosity between 0.2 and 0.25 might also apply to Event 3 and the average porosity of 0.32 simulated for Event 3 is less likely to be real. Simulated $\Delta\theta$ values for all three events were within the range of measured data between 6 mm and 54 mm depth. On average, the Monte Carlo analysis yields higher $\Delta\theta$ values than used in the initial simulations as well as a wider range of $\Delta\theta$ values between 0.07 and 0.15 $m^3\ m^{-3}$.

As discussed above, the soil moisture profiles assumed by the model and those actually found in the lysimeter (Figure 16) are very different. $\Delta\theta$ therefore is a poorly-defined parameter in terms of the lysimeter moisture profiles. When applied to the lysimeter soil profiles, $\Delta\theta$ may be acting more as a fudge factor than as a physical descriptor. Even if $\Delta\theta$ but does not accurately characterize the actual soil moisture profile, it may describe it sufficiently for modelling purposes.

3.6 Conclusions

The goal of this study was to evaluate the stage II evaporation models by Shokri et al. (2009) and Or et al. (2013) on an arid soil system under-well controlled boundary conditions as provided by a weighing lysimeter. Stage II evaporation rates were simulated after three storm events in August 2010, April 2012, and September 2012, and compared with measured evaporation rates from the weighing lysimeter. Good agreement between measurements and simulations was found for two out of the three events (evaporation rate RMSEs of 0.141 and 0.093 mm d^{-1}). For the third event, simulations systematically underestimated measured evaporation rates (evaporation rate RMSE of 0.181 mm d^{-1}). The latter is likely due to significant differences between the soil moisture profile in the lysimeter and that assumed by the model. A sensitivity analysis on the four major input parameters for the models by Shokri et al. (2009) and Or et al. (2013) (onset of stage II evaporation, t_0, vapor diffusion length, ξ, total porosity, φ, and difference in moisture content above and below the second drying front, $\Delta\theta$) showed that φ and $\Delta\theta$ are the most sensitive parameters in the model. Since φ can be determined rather accurately, improving the soil moisture profile characterization would likely need more scrutiny to further improve the model predictions for arid soils.

Considering their simplicity, the models by Shokri et al. (2009) and Or et al. (2013) provide a very good estimate for stage II evaporation rates from bare arid soil, especially for low antecedent moisture contents (Events 1 and 2). For high antecedent moisture content (Event 3), the models under predict actual evaporation rates. Due to its simplicity, these models have potential to be used in many different simulation environments (e.g., arid land modules in climate change models) while still simulating the actual physical processes controlling stage II evaporation. The good agreement between measured and simulated evaporation rates also indicates that the models by

Shokri et al. (2009) and Or et al. (2013) can be applied at the plot scale, since the lysimeter has a soil surface area of 4 m^2. Finally, since arid environments are precipitation-free throughout most of the year, stage II evaporation likely dominates over evaporation under wet surface conditions in terms of time and potentially water loss (Chapter 2). Therefore the stage II models by Shokri et al. (2009) and Or et al. (2013) may provide a considerable contribution towards closing the water balance for arid environments.

Table 6. Events 1-3 RMSE for Monte Carlo sensitivity analysis using 1000 realizations for three variables (ξ, φ, and $\Delta\theta$) in Equations (3.1) and (3.2). Only the top 5% and 1% RMSE are shown with the variable's respective ranges. In addition, RMSE (and variable ranges) for the last ten days of diffusive evaporation were also included.

Lowest 5% RMSE values of 1000 realizations

	RMSE (mm d^{-1})				Vapor Diffusion Length, ξ (mm)				Porosity, φ (--)				Soil Moisture Difference, $\Delta\theta$ (m^3 m^{-3})			
Event	Min	Max	Ave	StDev	Min	Max	Ave	StDev	Min	Max	Ave	StDe	Min	Max	Ave	StDev
1	0.106	0.114	0.110	0.002	7.7	14.0	11.1	1.6	0.20	0.32	0.25	0.03	0.09	0.22	0.15	0.04
2	0.096	0.105	0.101	0.003	4.0	13.5	7.9	2.1	0.21	0.40	0.30	0.06	0.02	0.11	0.06	0.02
3	0.052	0.083	0.068	0.009	9.1	13.7	11.7	1.4	0.25	0.37	0.31	0.03	0.15	0.29	0.23	0.04

Lowest 1% RMSE values of 1000 realizations

	RMSE (mm d^{-1})				Vapor Diffusion Length, ξ (mm)				Porosity, φ (--)				Soil Moisture Difference, $\Delta\theta$ (m^3 m^{-3})			
Event	Min	Max	Ave	StDev	Min	Max	Ave	StDev	Min	Max	Ave	StDe	Min	Max	Ave	StDev
1	0.106	0.108	0.107	0.001	9.0	13.0	10.8	1.3	0.22	0.29	0.25	0.02	0.11	0.20	0.16	0.03
2	0.096	0.098	0.097	0.001	4.6	10.5	7.2	2.0	0.23	0.38	0.28	0.05	0.03	0.08	0.06	0.02
3	0.052	0.058	0.054	0.002	10.6	13.3	12.0	0.9	0.28	0.33	0.30	0.02	0.21	0.29	0.26	0.03

Lowest 1% RMSE values of 1000 realizations using the last 10 days of diffusive evaporation

	RMSE (mm d^{-1})				Vapor Diffusion Length, ξ (mm)				Porosity, φ (--)				Soil Moisture Difference, $\Delta\theta$ (m^3 m^{-3})			
Event	Min	Max	Ave	StDev	Min	Max	Ave	StDev	Min	Max	Ave	StDe	Min	Max	Ave	StDev
1	0.080	0.081	0.081	0.000	11.0	13.8	12.9	0.8	0.20	0.25	0.22	0.01	0.10	0.17	0.14	0.02
2	0.108	0.109	0.109	0.000	9.1	13.9	11.0	1.9	0.20	0.23	0.21	0.01	0.06	0.08	0.07	0.01
3	0.046	0.047	0.047	0.000	9.3	13.4	11.4	1.5	0.30	0.33	0.32	0.01	0.25	0.30	0.27	0.02

3.7 Acknowledgements

This research was supported in part by the National Science Foundation funded program entitled Scaling Environmental Processes in Heterogeneous Arid Soils, or SEPHAS (EPS-0447416). We would like to acknowledge Peter Lehmann and Mark Hausner for their valuable comments and contributions to the discussion of the paper. Special thanks go to Karletta Chief, Jeff Daniels, Karen and Stephen Gray, John Healey, Emily Kaminski, Brad Lyles, Karl Pohlmann, and Rose Shillito for their support developing this manuscript. We would like to acknowledge Desert Research Institute and in particular the Division of Hydrologic Sciences and Jim Thomas for their continuous support of the SEPHAS weighing lysimeters.

CHAPTER 4

SOIL MOISTURE AND TEMPERATURE AS A FUNCTION OF PRECIPITATION, ET, AND GROUNDWATER LEVEL IN SPRING VALLEY, NV

4.1 Abstract

Understanding the interaction between precipitation, evapotranspiration (ET) and groundwater levels is critical where an increased demand for water resources meets an uncertain supply. In the case of Spring Valley, NV, decreasing groundwater levels could lead to an undesired shift in vegetation because of decreasing water supply for phreatophytes, one of the dominant shrub species. This study focuses on the effect of inter-annual variability of precipitation, evapotranspiration (ET) and groundwater level on moisture content and temperature of the unsaturated root zone in the valley floor of Spring Valley. A study site (SV6) was instrumented to monitor soil moisture content, temperature, precipitation, ET, and groundwater level from July 2010 to June 2011. Precipitation and ET were monitored from an already existing meteorological tower and eddy covariance (EC) system. Groundwater depth was measured using a pressure transducer in an existing well. Soil moisture was measured at 30, 100, 200, 300, 400, and 500 cm depth using TDR probes. Soil temperatures were measured using thermocouples at depths of 3, 29, 49, 69, 89, 109, 209, 309, 409, and 509 cm. Soil temperature was measured using a novel Fiber Optic Distributed Temperature Sensing (FO DTS) technique concurrently to the thermocouple measurements. The results show that ET dominates water loss at the site from March through September. Soil moisture data indicates that snowmelt and precipitation may percolate as deep as ~400 cm but does not reach the phreatic zone. Changes in

soil moisture content in 500 cm depth were likely due to changes in groundwater table. The latter was fluctuating between 5.4 m and 6.0 m below surface during the study period. For example, the gradual soil moisture content increases at 500 cm were measured; however, groundwater levels rose sharply from early October 2010 to approximately mid-June 2011, suggesting a high capillary fringe. There were periods of time when shrub roots, such as phreatophytes, obtained water from deeper in the soil profile as inferred by observable dips in moisture content at 3, 4, and 5 m. Diurnal variation of soil temperatures were observed to ~50 cm depth and seasonal variation were observed down to ~500 cm. Sensors recorded multiple cold wetting fronts in March through April 2011. Changes in soil temperatures were observed that related to changes in soil water storage; however, this occurred only near the surface.

4.2 Introduction

Precipitation, soil water availability and soil temperature variability are important to mass and energy balance studies, particularly to processes involving evapotranspiration (ET), as phreatophytes have substantial influence on water budgets in shallow arid and semi-arid groundwater basins (Cooper et al., 2006; Steinwand et al., 2006; Devitt et al., 2010; Kray et al., 2012). With large uncertainty in precipitation rates from inter-annual variability and potential changes brought on by climate change, understanding these processes is critical for assessing the movement of mass and energy through the vadose zone and into the phreatic zone. This is particularly true in the arid and semi-arid western United States (e.g., Great Basin) where ET can dominate the loss of water from ground surface. Studies have shown that declining water tables in riparian and non-riparian environments can decouple the connection between phreatophytes and groundwater (Cooper et al., 2006), reduce ET (Nichols, 1994; Cooper et al., 2006), change

or reduce plant diversity (Cooper et al., 2006; Patten et al., 2008), and reduce spring discharge (Patten et al., 2008). Furthermore, phreatophytes in arid and semi-arid basins vary considerably in their response to changes in precipitation (Kray et al., 2012). Inaccurate estimates of the water balance can present difficulties when predicting and understanding potential climate change outcomes.

For processes such as infiltration, percolation, recharge and discharge as the dominating mass exchange within a semi-arid valley floor, soil temperature can act as a good tracer for water movement (Constantz et al., 2003; Constantz, 2008). For example, streambed temperatures and water temperature have been used to identify losing and gaining streams (Silliman and Booth, 1993; Scanlon et al., 2002; Constantz and Stonestrom, 2003; Constantz, 2008) and estimating water exchange (Constantz and Stonestrom, 2003; Conant, 2004; Constantz, 2008). Anderson (2005) provides a detailed review on using temperature as a tracer in saturated environments. Constantz et al. (2003) provides a detailed synthesis estimating percolation rates in arid environments. Although Anderson (2005) and Constantz et al. (2003) suggest using temperature to provide estimates in the surficial zone, very few studies (Taniguchi and Sharma, 1993; Tabbagh et al., 1999) have been reported using temperature as a tracer to estimate water flux, and subsequently changes in soil water storage, in the vadose zone without a constant source of water (e.g., below a streambed).

Methods to measure water movement using temperature as a tracer have been hampered by the relatively discrete nature of the methods themselves (i.e., point-scale measurements with thermocouples). However, new advances in temperature measuring technologies, such as fiber optic distributed temperature sensing (FO DTS), has allowed for greater spatial resolution while maintaining excellent temporal resolution (Selker et al., 2006a; Tyler et al., 2009). FO DTS has

only recently been applied to the field of near-surface hydrology including stream temperature dynamics and exchange (Selker et al., 2006a, 2006b; Tyler et al., 2009), leachate through landfill (Weiss, 2003), and more recently estimating soil moisture (Steele-Dunne et al., 2010; Sayde et al., 2010). Although DTS has been used in many hydrologic applications, very little work has been completed using it in the vadose zone.

This study emphasizes the processes that affect soil water and temperature from a shallow water table to near surface and the effects of inter-annual precipitation and ET variability in a semi-arid climate. This study was conducted between 1 July 2010 and 30 June 2011 where daily ET, precipitation, soil moisture, and depth to groundwater were evaluated to examine seasonal trends within a Great Basin valley. Soil temperature analysis using FO DTS was conducted during early spring and summer seasons of 2011 where ET was at its highest. We use a field-based approach to observe seasonal water fluxes into (infiltration), through (percolation), and out (evapotranspiration) of the vadose zone. Inter-annual and seasonal variability can provide insight as to potential climate change outcomes in the vadose zone, as variability is expected to increase if the climate continues to warm. This research hypothesizes that there is a limited connection between the atmosphere and groundwater ET (under specific conditions) as well as valley-fill recharge. Furthermore, soil temperature signals will follow shifts in water storage and provide soil temperature extinction depths (maximum depth of daily temperature variation). Goals of this research include: (i) analyze inter-annual and seasonal precipitation and ET with changes in soil water storage; (ii) determine depth of wetting front and whether or not it reaches the phreatic zone during the study period; and (iii) provide soil temperature extinction depths.

4.3 Study Area

Field investigations took place in valley-fill sediments at the Spring Valley 6 (SV6) field site located in East-Central Nevada (39.043°N, - 114.482°W). The site is at an elevation of 1,753 m above sea level within the Great Basin (Figure 17). The site is surrounded by north trending mountain ranges and alluvial valleys typical of the Great Basin (Hunt, 1967; Stewart, 1980). According to Mifflin (1988), Houghton et al. (1975), and Elliot et al. (2006), climates vary from the very dry and hot desert climate in the smaller and lower basins, to steppe-like climates in the higher basins where Site SV6 is located, to the humid continental and eventually alpine tundra climates in the mountains (e.g., Snake Range). Table 17 in Houghton et al. (1975) characterizes the mid-latitude steppe as having a moisture deficit (annual precipitation of 152 – 381 mm), with cold winters (-7 – 4 °C) and warm summers (18 – 27 °C) while the high latitude is characterized as having heavy precipitation (annual precipitation of 381 – 1143 mm), cold winters (-18-1 °C), and mild summers (4 – 21 °C). According to Elliot et al. (2006), snow accumulation occurs from November to March with melting occurring from March through the summer. Snow melt from these upland areas (predominantly from the Schell Creek and Snake Ranges) is the dominant recharge mechanism of the deeper carbonate aquifers while recharge in the basin-fill sediments occurs as upward discharge from the carbonate aquifer and along the interface of the mountains and valley alluvium through a series of springs (Welch et al., 2007). The area is considered a closed basin, and valley-fill recharge is typically consumed by ET.

Greasewood (*Sarcobatus vermiculatus*) and Sagebrush (*Artemisia tridentata*), or Big Sage, are the dominant plants in Spring Valley and would provide the largest loss of water from the subsurface due to high ground cover percentages and (presumably) root distribution. A plant and ground cover assessment (D.A. Devitt, unpub. data, 2012) within the study area showed bare soil

Figure 17. Map of the Great Basin Region and Site SV6 located in Spring Valley, Nevada.

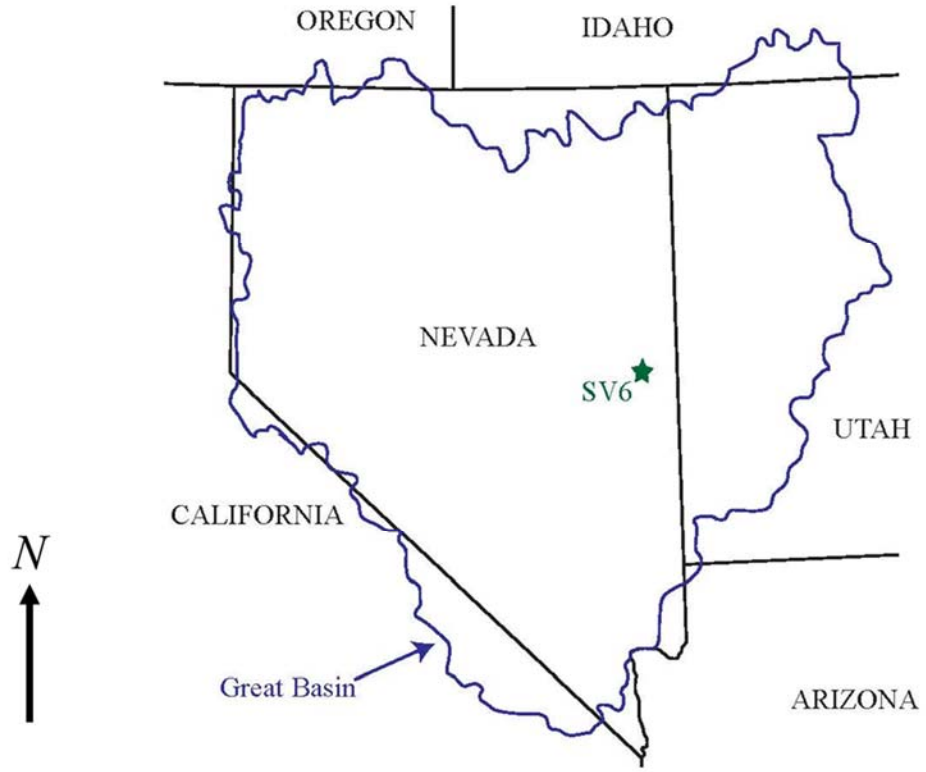

(~55%), Greasewood (~20%), Sagebrush (~16%), Shadscale (*Atriplex confertifolia* ~1%), Rabbitbrush (*Chrycothammus nauseosus* ~1%), and unknown dead plants (~7%). Although phreatophyte roots can extend to depths greater than 3 m (Groeneveld, 1990), maximum lateral root densities are typically above 3 m for Big Sage (Richards and Caldwell, 1987) and Greasewood, which was shown to have ~ 65% of roots within the upper 0.75 m (Donovan et al., 1996). Well SV6, located within the study area (Figure 18) was installed in May 2007, with roots observed down to 3.6 m (Arnone et al., 2008); although density of root distribution was not provided. The depth to groundwater within a shrubland valley is typically between 2 and 10 m below ground surface (Moreo et al., 2007). During Well SV6 installation, depth to groundwater

was 5.4 m (Arnone et al., 2008). The area is considered to be a dense desert shrubland (Arnone et al., 2008) with average annual ET rates between 305 – 549 mm yr^{-1}, or an area-weighted average of 378 mm yr^{-1} (Welch et al., 2007). According to Arnone et al. (2008), ET rates from April 2007 to April 2008 at Site SV6 were 238 mm yr^{-1}. Soil textures observed during the construction of Well SV6 include silt-loam (0 – 0.6 m), clay (1.5 – 2.1 m), silt (3.0 – 3.6 m), sand and clay (4.5 – 5.1 m), clay (6.0 – 6.7 m), and sand, clay, and gravel (7.6 – 8.2 m) (Arnone et al., 2008). For a full synthesis of the physiography, climate, geology, hydrology, and plant community described in the context of both regional and local scales, the reader is referred to Appendix D.

4.4 Field Methods and Data Collection

4.4.1 Soil Moisture and Groundwater Monitoring

On 17-18 August 2009, a borehole was advanced at Site SV6 between plant canopies (Figure 18) down to approximately 6.2 m using a drilling rig setup with both solid-stem and hollow-stem augers. Into the borehole, time domain reflectometry probes (TDR, CS-605, Campbell Scientific, Inc., Logan, UT) were installed to measure soil moisture in the unsaturated zone at 0.3, 1.0, 2.0, 3.0, 4.0 and 5.0 m depth (the boring was backfilled with fine grain sediments from 6.2 to 5.85 m). Although this technique is invasive, it allows for deeper access to absolute change in soil moisture, rather than absolute soil moisture values. This technique is also less expensive as compared to excavation down to the same depth (which would inevitably include shoring to support the excavated sidewalls) where we would install probes into the sidewall (less invasive).

The probes with 30 cm long prongs were installed vertically providing average moisture content of the soil 0.15 m above and below the respective depths where the probes were placed.

Following individual probe installation, the boring was backfilled with fine-grain sediments from the surface of the surrounding area. The TDR probes were connected via a Campbell Scientific SDMX50 multiplexers to a Campbell Scientific CR1000 datalogger. Data were collected every 24 hours (0:00 hour) from 1 July 2010 through 30 June 2011. Soil moisture was determined using Topps equation (Topp et al., 1980) via double tangent waveform analysis (Herkelrath et al., 1991). The reader is referred to Topp et al. (1980) and Herkelrath et al. (1991) for details on TDR theory, and Young et al. (1997) for analysis and calibration of TDR probe signals. Groundwater was continuously monitored using a submersible pressure transducer (Pressure Systems, Inc., Hampton, Virginia) in the existing groundwater Well SV6 (screened from 4.5 – 8.8 m) and is connected to a Campbell Scientific CR3000 datalogger (Figure 18). Data were collected every 30 minutes from 1 July 2010 to 30 June 2011. For well specific details, the reader is referred to Arnone et al. (2008).

4.4.2 Soil Temperature

A second borehole was originally advanced between plant canopies on 17-18 August 2009 (Figure 18); however, due to initial issues with FO DTS technology, the borehole was covered and not instrumented until 6-7 April 2010, until a DTS fiber optic (FO) cable (model DNS-1068, AFL Telecommunications LLC, Duncan, South Carolina) was placed into the borehole using a threaded 0.075 m diameter PVC pipe, around which the cable was wrapped, providing improved vertical resolution of soil temperature (i.e., a temperature reading every per 0.0114 m) from approximately 0.12 to 6.05 m (this depth range was due to settlement of the FO DTS and PVC structure). PVC was used due to its low thermal conductivity, similar to a very dry mineral soil (Evett et al., 1995), and rigid nature. The cable was comprised of two 50 μm multimode fibers housed in a 2.0 mm outer-diameter loose blue plastic buffer tube filled with hydrophobic gel.

The two cables were spliced together at the base of the PVC pole and housed in a protectable wooden casing. Following installation and backfill of the annular space, the DTS system was calibrated on 8 April 2010 using an ice bath and logger (model N4386A, AP Sensing,

Figure 18. Instrumentation plan (a) and cross sectional (b) views of Site SV6 (not to scale).

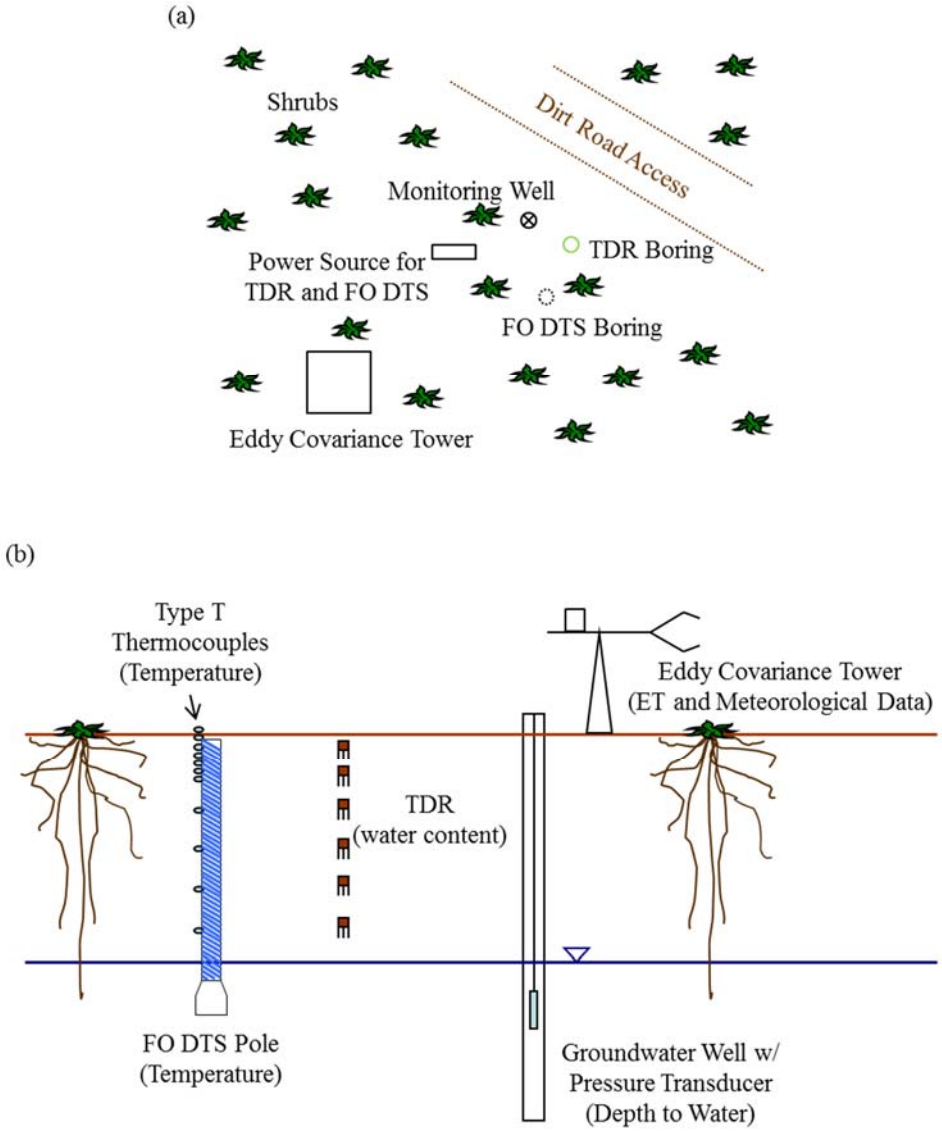

Boeblingen, Germany). Approximately 20 m of FO cable was placed in the calibration bath. A temporal resolution of 10 minutes, sampling interval of 1.0 m, and a spatial resolution of 1.5 m were used to collect temperatures from 24 March through 25 April and 29 May through 29 June 2011. Ten minute measurements were then averaged over an hour.

In addition to the FO cable, the PVC pipe was instrumented with thermocouples (Type T, Omega Engineering, Stamford, CT) at increments of 0.2 m for the first 1.0 m, and increments of 1.0 m for the next 4.0 m. Due to settlement, the final depths of the thermocouples were 0.29, 0.49, 0.69, 0.89, 1.09, 2.09, 3.09, 4.09, and 5.09 m. Two additional thermocouples were added at 0.03 m below surface and 0.01 m above surface on 16 March 2011. Thermocouples were connected via one Campbell Scientific AM25T multiplexer to a Campbell Scientific CR1000 datalogger. Thermocouples were used during the study period to compare with, and eventually correct for, soil temperatures measured using FO DTS. The corrections were needed to account for variations in the internal temperature of the DTS logger and direct pressure on the cable at the base of the pole; as these can cause large (±1° to 2°C) instrument drift (Tyler et al., 2009).

Temperature readings from thermocouples were matched with readings from FO DTS by comparing differences in 24-hour running average temperatures at depths of 0.29, 0.49, 0.69, 0.89, 1.09, 2.09, 3.09, 4.09, and 5.09 m. Two second order polynomials were fitted to the data, one for the shallow zone (0.29, 0.49, 0.69, 0.89, 1.09, and 2.09 m) and one for the deep zone (2.09, 3.09, 4.09, and 5.09 m). Two polynomials were used due to increased attenuation with increased length of the FO cable (Tyler et al., 2009) and pressure at the base of the PVC pole. The polynomials were then used to calculate temperature differences along the entire DTS cable. The differences were then added (or subtracted) to the original DTS data. To correct for diurnal fluctuations caused by temperature variations inside the instrument box, differences between

depth-corrected DTS temperatures and depth-corrected 24-hour running average DTS temperatures were calculated for depths 2.09, 3.09, 4.09, and 5.09 m. The calculated differences were averaged and then subtracted from the depth-corrected soil temperatures.

4.4.3 Soil Sampling and Analysis

One soil sample was collected during drilling efforts on 18 August 2009 from a depth of approximately 5.6 – 6.2 m (in the phreatic zone). Additional soil samples were collected from 0 to 3.4 m using a hand-auger in September 2010 and April 2011. All samples were submitted to A&L Western Laboratories, Inc. (Modesto, CA) and analyzed for soil texture (% Sand, % Silt, and % Clay).

4.4.4 Atmospheric and Weather Measurements

Site SV6 (Figure 18) is installed with eddy covariance (EC) and meteorological instrumentation towers (installed in April 2007) (Arnone et al., 2008). These towers consisted of sensors to measure wind speed (3D Sonic Anemometer, model CSAT3, Campbell Scientific, Inc., Logan, UT), air temperature and relative humidity (Temperature and Relative Humidity Probe, model HMP45C Campbell Scientific, Inc., Logan, UT), and solar radiation (Net Radiometer, model NR-LITE, Campbell Scientific, Inc., Logan, UT). In addition, a tipping bucket rain gage was used to measure precipitation. Average ET fluxes were measured using the methods by Baldocchi et al. (2001) and Baldocchi (2003). Data from these towers were collected continuously from 1 July 2010 through 30 June 2011. The system was set up to meet fetch requirements and allow for minimal obstructions (e.g., hills, depressions, etc.). For a detailed description of the installation and setup of the EC Tower, readers are referred to Arnone et al. (2008).

4.4.5 Field Complications

Instrumentation for soil moisture and temperature sensing was invasive with multiple instruments (TDR, thermistors, Type T thermocouples, and FO DTS) placed in boreholes down to 6 m. The soil around the probes within the borehole was repacked and therefore disturbed. In addition, the clayey soil from within the borehole could not be used for backfill and instead, sand from the surface was used. Textures observed during drilling and sampling included a large percentage of very fine grains in addition to caliche; both of which can impact both heat and water flow through the soil (slow it down). Additional problems also occurred from 24 July to 24 August 2010 and again from 25 February to 22 March 2011, due to datalogger issues (soil moisture data are missing).

Difficulties arose during the installation of the FO DTS pole. The weight of the PVC pole was too much on the protectable wooden casing at the base (location of FO cable splice). Signal attenuation (loss) from the backscatter of the laser in the FO cable increases with increasing length of cable and increased pressures leading to incorrect temperature calculations (Tyler et al., 2009). Furthermore, due to the placement of the DTS system in a warm environment (inside the instrument box), diurnal variation occurred throughout the profile. Nevertheless, calibration and curve fitting using thermocouples were still completed to provide soil temperature profiles during spring and summer, where diurnal temperature extinction depths could be estimated.

4.5 Results

4.5.1 Soil Texture

Near surface soil samples collected during field activities were characterized as loam (0-0.4 m) and sandy clay loam (0.4-0.8 m). Below 0.8 m, soil textures were characterized as clay

or heavy clay (0.8-3.0, 3.2-3.4, and 5.6-6.2 m) or clay loam (3.0-3.2 m). Clay and caliche were observed between 3.4-5.6 m during drilling activities conducted on 17-18 August 2009; although samples were not taken. According to Arnone et al. (2008), sand lenses were observed between 4.6-5.2 m during installation of Well SV6.

4.5.2 Precipitation and Evapotranspiration

A total of 247.7 mm of precipitation and 433.9 mm of ET were observed at Site SV6. October 2010 (31.8 mm), December 2010 (41.9 mm), and May 2011 (66.0 mm) represents the three largest monthly totals, while monthly total ET varied throughout the year ranging from 8.7 mm (January 2011) to 69.4 mm (May 2011) (Table 7). Precipitation was greatest during spring months (108.7 mm), followed by winter (54.6 mm), autumn (51.3 mm), and summer (33.0 mm). ET rates were the largest during spring (175.3 mm) and summer (151.5 mm) while autumn and winter were the lowest (58.6 and 48.4 mm, respectively). Precipitation events were recorded for 80 days with daily precipitation ranging from 0.0 to 16.0 mm d^{-1} (Figure 19, top). Daily ET fluctuated between -0.4 to 5.9 mm d^{-1} (Figure 19, bottom). Negative ET values indicate net water vapor uptake via condensation due to colder temperatures (Arnone et al., 2008).

Measured annual precipitation and ET during this study were similar to previous annual measurements from other studies; however, ranges of precipitation and ET vary greatly throughout Spring Valley. Moreo et al. (2007) reported 202.4 to 232.9 mm of precipitation and 254.5 to 684.3 mm of ET from 1 September 2005 to 31 August 2006 at three different sites. Devitt et al. (2010) reported 306.5 mm of precipitation (combination of two separate sites) in 2005 and 155.5 mm of precipitation and 240.4 mm of ET in 2006 (at one site); ET was not measured in 2005. Arnone et al. (2008) reported approximately 91 to 150 mm of precipitation and 172 to 659 mm of ET between 20 April 2007 and 20 April 2008 at four different sites in

Spring Valley, one of which is Site SV6, the same site of this study (127 mm of precipitation and 238 mm of ET).

Table 7. Monthly and yearly measured precipitation (P) and ET, and P/ET ratios, for the study period of 1 July 2010 through 30 June 2011.

Month	Total Precipitation (mm)	Total ET (mm)	Monthly P/ET Ratio (--)
Jul-10	26.2	49.9	0.5
Aug-10	4.3	32.4	0.1
Sep-10	0.0	15.5	0.0
Oct-10	31.8	26.1	1.2
Nov-10	19.6	17.0	1.1
Dec-10	41.9	12.5	3.4
Jan-11	4.8	8.7	0.6
Feb-11	7.9	27.2	0.3
Mar-11	17.5	53.2	0.3
Apr-11	25.1	52.7	0.5
May-11	66.0	69.4	1.0
Jun-11	2.5	69.1	0.0
Summer (Jun, Jul, Aug):	**33.0**	**151.5**	**0.2**
Autumn (Sep, Oct, Nov):	**51.3**	**58.6**	**0.9**
Winter (Dec, Jan, Feb):	**54.6**	**48.4**	**1.1**
Spring (Mar, Apr, May):	**108.7**	**175.3**	**0.6**
Year:	**247.7**	**433.9**	**0.6**

In addition to monthly, seasonal, and annual totals, ratios of precipitation to ET were calculated (Table 7) to assess the impact precipitation had on the soil and root zone. Ratios reflect simple supply and demand relationships of water usage and provide periods of time of potential recharge (Devitt et al., 2010). A ratio > 1 indicates more precipitation than ET and a ratio < 1 more ET than precipitation. An annual ratio of 0.6 was calculated during the study period, while seasonal ratios of 0.2, 0.9, 1.1, and 0.6, were calculated for summer, autumn, winter, and spring, respectively. Winter was the only season with a ratio greater than 1, but was

heavily influenced by December 2010 (ratio of 3.4), as January and February 2011 had ratios of 0.6 and 0.3, respectively. Also October and November 2010 (1.2 and 1.1, respectively) had ratios above 1 but the zero ratio for September yielded an overall ratio smaller than 1 for autumn. Monthly ratios in spring ranged from 0.3 to 1.0 (although, the ratio is slightly lower than 1.0, as May had less precipitation than ET), while ratios in summer ranged from 0.0 to 0.5. Subsequently, most of the precipitation comes in late fall through early winter, and again in late spring through early summer.

Figure 19. Measured daily precipitation and ET for the study period of 1 July 2010 through 30 June 2011.

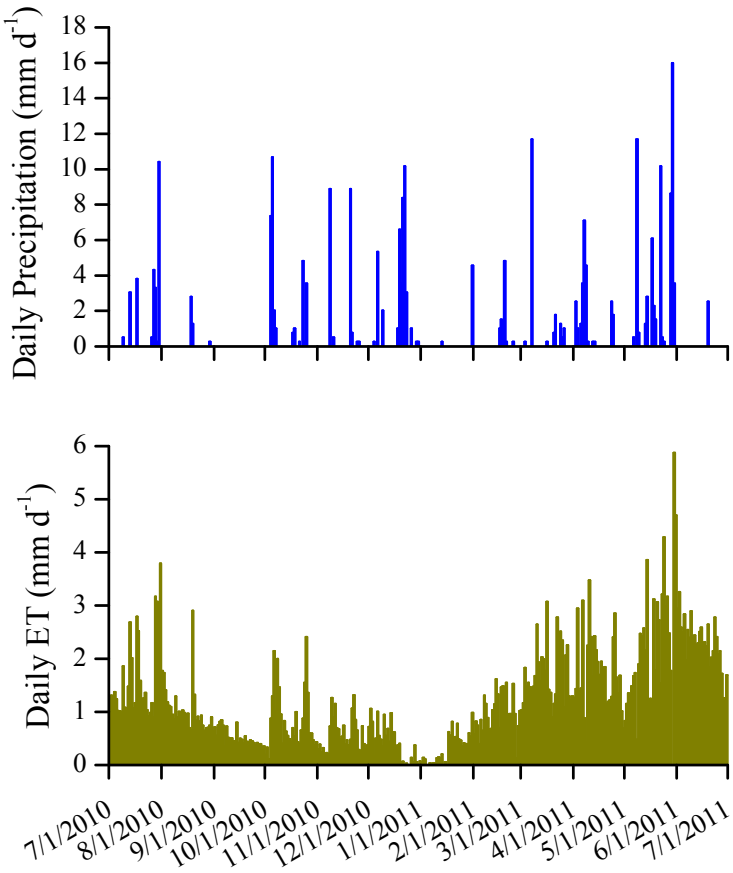

4.5.3 Soil Moisture

Figure 20 provides soil moisture time series down to m. Shallow depths of 0.3 and 1.0 m (Figure 20a) show the greatest variation in soil moisture throughout the year with ranges of 0.07-0.22 m^3 m^{-3} and 0.12-0.29 m^3 m^{-3}, respectively. Beginning on 1 July 2010, soil moisture in 0.3 m was 0.12 m^3 m^{-3} but then decreased to a low of 0.07 m^3 m^{-3} in autumn 2010. The missing data from 22 July to 24 August 2010 does not allow further analysis of soil moisture content during that time. But the general trend of soil moisture at 0.3 m depth indicates a continuous decrease in moisture content from summer to fall 2010. Soil moisture in 0.3 m depth remained relatively constant throughout fall until 24 December 2010, where it markedly increased following multiple days of precipitation (32.8 mm between 18 and 23 December 2010), reaching a first maximum of 0.14 m^3 m^{-3} on 2 January 2011. During the months of January and February, soil moisture fluctuated between 0.13 and 0.15 m^3 m^{-3} due to 8 precipitation events ranging between 0.3 and 4.8 mm of total precipitation. Soil moisture content continuously increases to 0.22 m^3 m^{-3} by 25 March 2011, although data is missing from 24 February to 23 March 2011. The 0.22 m^3 m^{-3} was most likely due to a 3-hour, 3.8 mm hr^{-1} intensity precipitation event on 7 March 2011 and a few smaller events (seven events with intensities between 0.3-1.5 mm hr^{-1}). From March to early June, soil moisture ranged from 0.18 to 0.22 m^3 m^{-3} at the 0.3 m depth with increases following precipitation events and decreases due to ET during periods of little to no precipitation. Between 7 March and 19 June 2011, there were 52 additional events recorded ranging between 0.3 to 11.7 mm in total precipitation. There were only 3 events occurring in June 2011 ranging between 0.3 and 1.8 mm in total precipitation. During this month (which is the last month of the study), soil moisture decreases from 0.21 to 0.10 m^3 m^{-3}. As expected, soil moisture at 1.0 m depth did not change as quickly as soil moisture at 0.3 m depth. Interestingly,

and in contrast to 0.3 m depth, soil moisture increases from a low of 0.15 m^3 m^{-3} to a high of 0.21 m^3 m^{-3} during July and August 2010, then decreases to 0.12 m^3 m^{-3} by January 2011 and increases to a high of 0.29 m^3 m^{-3} by June 2011. Day-to-day variability in soil moisture content is largest during the wettest periods at 1.0 m, which coincides with higher saline solutions in soil (D.A. Devitt, unpub. data, 2012). Soil moisture at 1.0 m was observed to be at its highest during late spring and/or early summer, likely due to infiltrating water from the late fall and winter precipitation events as well as the spring snow melt. Subsequently, soil moisture in the first top 1 m is controlled by precipitation.

Smaller changes in soil moisture over the one year study period were observed at 2.0 m and 3.0 m (Figure 20b). Soil moisture at 2.0 m ranges from 0.10-0.18 m^3 m^{-3}; however, the variability observed from July through September (values greater than 0.14 m^3 m^{-3}) may be attributed to salinity, similar to that observed at 1.0 m. The general trend of soil moisture increases from summer (0.10 m^3 m^{-3}) to autumn (0.14 m^3 m^{-3}) 2010 and then decreases to 0.11 m^3 m^{-3} by winter 2010-2011, at which point it remains constant through the remainder of the study. Soil moisture at 3.0 m ranges from 0.05-0.14 m^3 m^{-3}. The maximum value of 0.14 m^3 m^{-3} occurred on 1 October 2010; if this data point were to be removed (value most likely not real due to salinity, or a problem with the TDR sensor), the new maximum is 0.10 m^3 m^{-3}. Soil moisture remains fairly constant (between 0.05-0.06 m^3 m^{-3}) until mid-October 2010, at which point increases steadily to 0.10 m^3 m^{-3} by 23 May 2011. Soil moisture then decreases to 0.06 m^3 m^{-3} by the end of the study. The temporal changes of soil moisture content in 2.0 and 3.0 m depth are noticeable even though quite a bit smaller than in 0.3 and 1.0 m depth. The observed changes indicate some systematic annual fluctuation, possibly representing infiltration fronts from winter storm events and snow melt of the previous year(s).

Figure 20. Measured soil moisture content at (a) 0.3 and 1.0 m, (b) 2.0 and 3.0 m, and (c) 4.0 and 5.0 m at Site SV6 from 1 July 2010 through 30 June 2011.

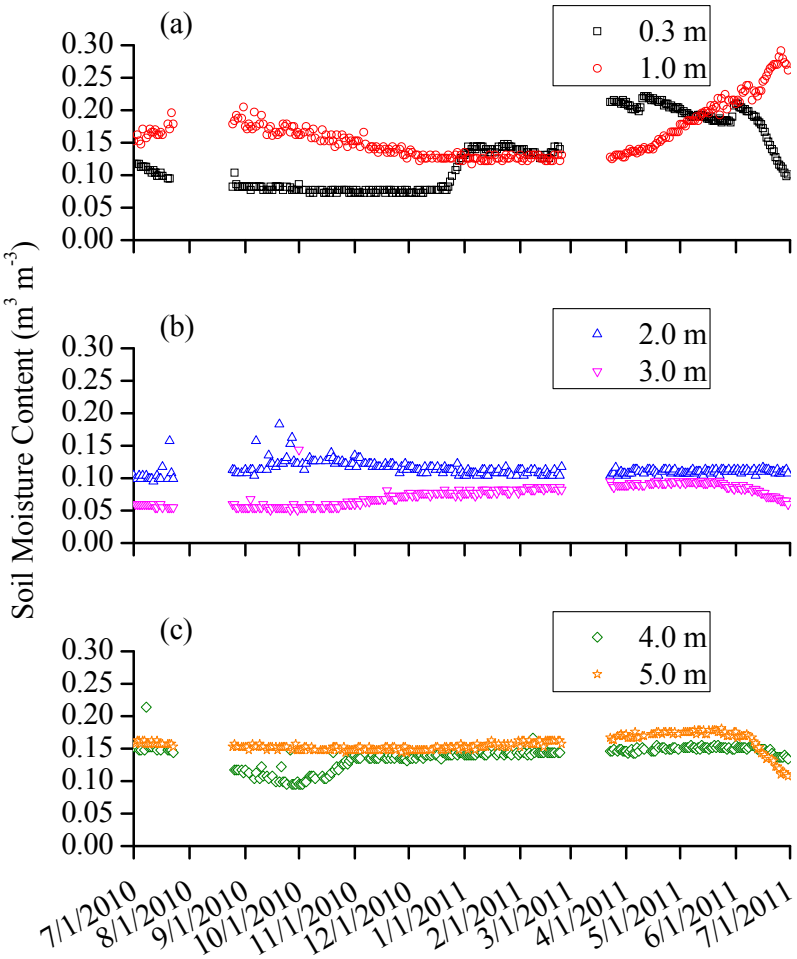

Soil moisture deeper within the soil profile (4.0 and 5.0 m) is presented in Figure 20c. At 4.0 m, soil moisture decreases from 0.15 m^3 m^{-3} to a low of 0.10 m^3 m^{-3} from 1 July through 28 September 2010, then increases to 0.14 m^3 m^{-3} by 30 October 2010. Following this sharp dip, soil moisture at 4.0 m slowly increases to 0.16 m^3 m^{-3} by 12 June 2011; at which point, decreases to 0.14 m^3 m^{-3} by the end of the study. Soil moisture at 5.0 m decreases from 0.16 to 0.15 m^3 m^{-3} from July through September 2010, remains constant until December 2010, and then increases

steadily to 0.18 m^3 m^{-3} by 21 May 2011. Soil moisture then decreases to 0.11 m^3 m^{-3} by the end of the study. At these depths, not much influence from precipitation on soil moisture content is expected. It is, however, quite remarkable that there seems to be some influence of the ground water table (Figure 21) on the soil moisture above, at least at 5.0 m depth (see also next section). It remains unclear what might have caused the "dip" in soil moisture content during June 2011. High ET rates and dips in soil moisture content at 3, 4, and 5 m in June 2011 indicates possible phreatophytes, and other deep-rooted species (not just phreatophytes), removing water at these depths.

4.5.4 Depth to Groundwater

Depth to groundwater measured in Well SV6 is provided in Figure 21. Increases in water table depth occurred predominantly during the summer months and into autumn representing a period of discharge from the alluvial fill aquifer. From 1 July to 9 October 2010 and again from 16 to 30 June 2011, depth to water increased from 5.54 to 5.97 m below ground surface (bgs) and from 5.39 to 5.44 m bgs, respectively. Decreases in water depth occurred during the winter and spring months from 9 October 2010 to 16 June 2011. During this period of recharge, depth to water decreased from 5.97 to 5.39 m bgs, with three different observable trends (based on different slopes of the water depth curve in Figure 21). Using linear regression, individual slopes were calculated for 18 October 2010 through 2 March 2011 (136 days), 3 March through 9 May 2011 (68 days), and 10 May through 12 June 2011 (34 days), representing decreasing water depth. Slopes (and correlation coefficients, R2) were -0.002 m d^{-1} (R2=0.9995), -0.003 m d^{-1} (R2=0.9976), and -0.002 m d^{-1} (R2=0.9758), respectively. In addition to seasonal groundwater trends, small daily trends were also observed with maximum changes of 0.01 m within a 24 hour period.

With the groundwater table oscillating between 6.0 m (October 2010) and 5.4 m below surface (July 2011), one would expect to see concurrent fluctuations in soil moisture content at 5 m depth (soil moisture content minimum around October 2010 and maximum around July 2011). Soil moisture minima and maxima in 5 m depth occur during September 2010 and May 2011, indicating that the soil moisture fluctuations in 5.0 m depth are not necessarily, or at least not exclusively, driven by groundwater table fluctuations.

Figure 21. Depth to groundwater at Site SV6 from 1 July 2010 through 30 June 2011. Using linear regression, slopes (negative value represents decreasing water table in m d^{-1}) and R2 values were calculated for three periods of time during the decreasing trend: 18 October 2010 to 2 March 2011, 3 March to 9 May 2011, and 10 May to 12 June 2.

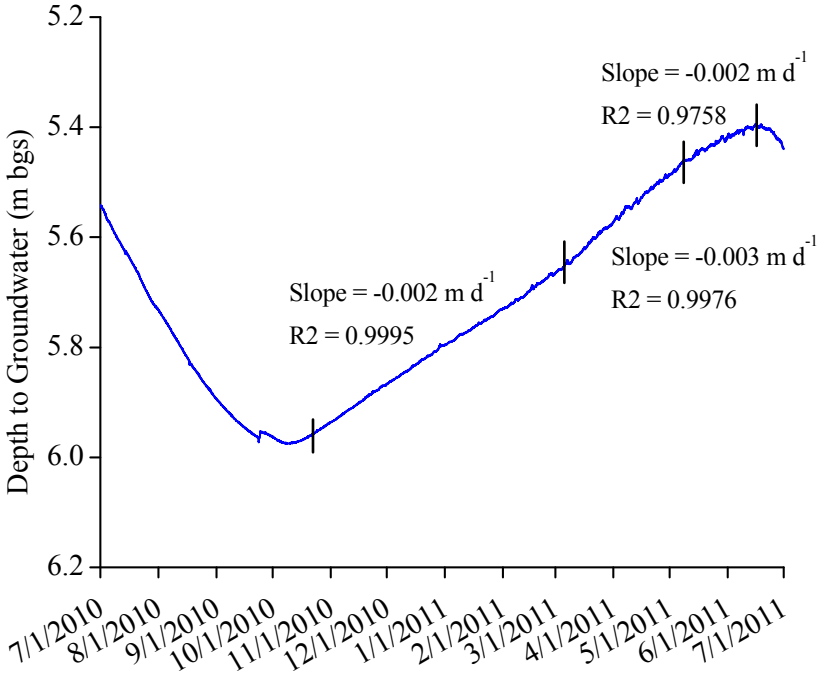

4.5.5 Air-Soil Temperature Profiles (Spring and Summer 2011)

Air-soil temperature profiles collected during the most active growing period in Spring Valley (Moreo et al., 2007; Devitt et al., 2010), display both diurnal and seasonal variation for both spring (Figures 22a-22b) and summer 2011 (Figures 23a-23b). The profiles provide ambient air temperature, collected approximately 0.01 m above soil surface, and soil temperature collected at 0.03 m and 0.12 through 6.0 m on the 4th (4:00) and 16th (16:00) hour of every day from 24 March through 25 April 2011 (early spring) and 29 May through 30 June 2011 (early summer). Times were chosen to represent contrasting temperatures of a cool morning and warm afternoon.

Ambient air temperatures at 0.01 m above land surface range from -6.2°C to 35.0°C for spring 2011 and -1.9°C to 54.1°C for summer 2011. Soil temperature ranges decrease deeper within the profile with the smallest ranges of 7.4 to 7.6°C during spring 2011 and 9.6 to 9.9°C during summer 2011 at depths of 2.7 and 5.0 m, respectively. Temperatures deeper in the soil profile display slightly higher ranges but whose differences are less than 1.0°C, with the greatest variation between 5.5 and 6.0 cm, as this is close to the base of the DTS pole where signal attenuation (loss) from the backscatter of the laser in the FO cable increases due to increasing length of cable and increased pressures placed on the cable (Tyler et al., 2009). Soil temperature responds to atmospheric conditions with the typical damping and phase shift of the temperature signal with increasing depth. Depending on atmospheric conditions, diurnal temperature changes occurred down to a depth ranging between 0.50 and 1.0 m below surface for both seasons; however, amplitudes are larger in the summer compared to the winter time. As diurnal changes dampen to a depth where amplitudes are zero, only seasonal changes are observed. At 1.0 m, soil temperature continues to increase with increasingly warmer weather for spring (4.1°C to 7.2°C)

and summer (9.4°C to 13.9°C); however, the increase is greater during the summer period. The increases were also observed at a depth of 2.0 m for spring (5.9°C to 6.7°C) and summer (8.2°C to 10.0°C). At a depth of 3.0 m, soil temperature remains relatively constant during spring (7.8°C and 8.2°C) but increases during summer (8.3°C to 9.1°C). At a depth of 4.0 m, soil temperatures decrease during spring (9.5°C to 8.9°C) and remain relatively constant in summer (between 8.9°C and 9.3°C). At a depth of 5.0 m, soil temperatures remain relatively constant in spring (between 9.9°C and 10.4°C) and summer (between 9.6°C and 9.9°C).

Figure 22. Air (0.01 m above land surface) and soil temperature (0.03 and 0.12 – 6.0 m bgs) profiles using Tc's and FO DTS for spring at (a) 4:00 and (b) 16:00, from 24 March - 25 April 2011 (early spring).

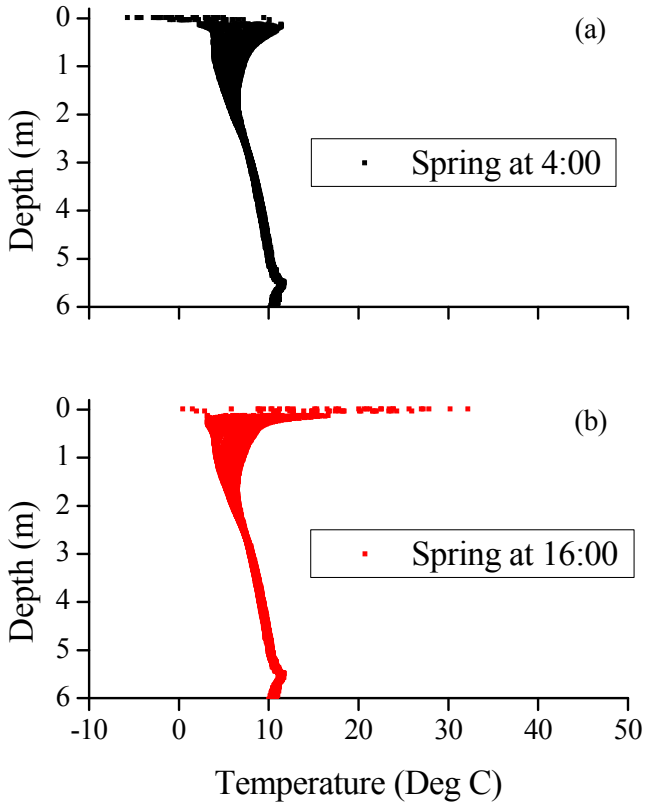

Figure 23. Air (0.01 m above land surface) and soil temperature (0.03 and 0.12 – 6.0 m bgs) profiles using Tc's and FO DTS for summer at (a) 4:00 and (b) 16:00 from 29 May - 30 June 2011 (early summer 2011).

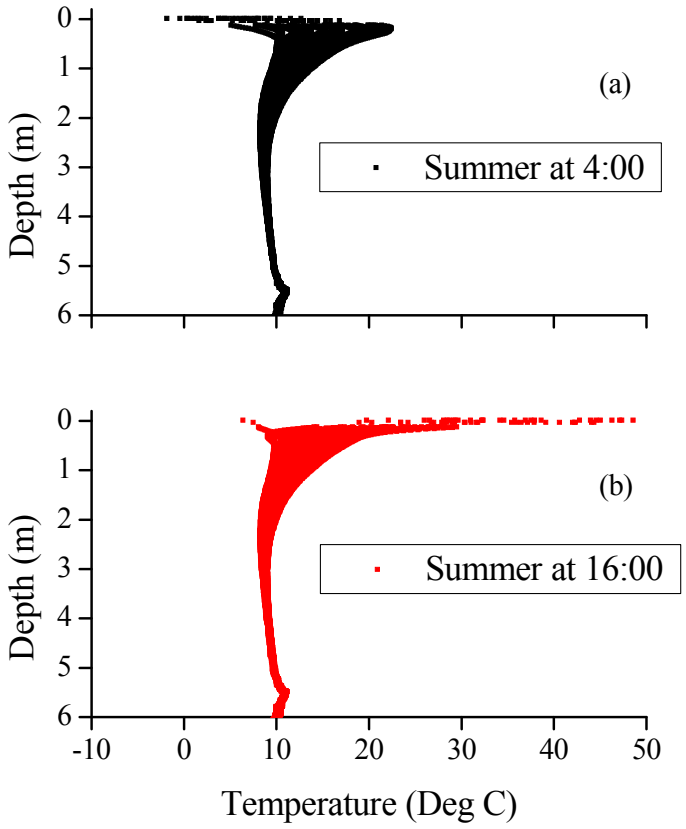

4.6 Discussion

4.6.1 Inter-Annual Variation in Soil Water along the Soil-Plant-Atmosphere Continuum

Annual precipitation and ET measured during this study were within past ranges reported at multiple stations throughout Spring Valley (Moreo et al., 2007; Arnone et al., 2008; Devitt et al., 2010). Although Site SV6 falls within the annual ranges of precipitation and ET, values are dependent on many factors, including location and elevation within the valley, depth to

groundwater, plant cover and root distribution, atmospheric conditions, and edaphic properties. At the site alone, Arnone et al. (2008) reported approximately 127 mm of precipitation and 238 mm of ET from 20 April 2007 to 20 April 2008, which is approximately 49% and 45% less than what this study reported, respectively. This variation makes basin-wide precipitation and ET estimation difficult, and subsequently, makes estimation of plant water availability and potential recharge difficult to predict.

Infiltration into, and percolation through soil, is evident as soil moisture increased throughout this study, particularly at 0.3 and 1.0 m (near surface) following high intensity and/or long duration precipitation events. In addition, recharge is occurring as evident in the rising water table from October 2010 to June 2011; however, this is most likely associated with mountain block recharge (Welch et al., 2007). Subsequently, groundwater discharge at Site SV6 occurred via ET as evident in decreases in soil moisture and decreasing water table. With all of this stated, instruments installed at the site were invasive and required drilling to depths of approximately 6 m, and backfilling with sediment. The backfilled sediments were predominantly fine to large grain sands thus changing the soil texture at the site. Although the near-surface soil (top 0.8 m) consisted of sand, below the texture was dominated by clay.

Summer precipitation provided little opportunity for groundwater recharge through valley floor deposits as precipitation was limited in July-August 2010 and June 2011. No increases in soil moisture were observed at 0.3 m during these months; instead, soil moisture decreased to 0.07-0.08 m^3 m^{-3} in August 2010 and to 0.10 m^3 m^{-3} by the end of July 2011. Increases in soil moisture were observed during the summer at 1 m (and what appears to begin increasing at 2 m), but are related to percolation and/or redistribution of storms outside this study period (before 1 July 2010) or spring 2011 storms. On the other hand, water discharge via ET from both saturated

and unsaturated zones is occurring as plant activity is at the tail-end of the most active growing period. During the summer, after water in the shallow soil is depleted, phreatophytes with deep tap roots will use soil water deeper in the profile, including groundwater from the capillary fringe and saturated zone (Sorenson et al., 1991; Cooper et al., 2006). Groundwater depth increased in July and August 2010 and began increasing in June 2011. The relatively low ratio of total precipitation to ET (0.2) for summer suggests that after the shrubs remove water from the seasonal wetting front, they supplement water from soil moisture at different depths as well as increasingly rely on groundwater. Furthermore, as decreasing soil moisture at 0.3 m in July 2010 and June 2011, and soil water beginning to decrease at 1.0 m by the end of July 2011, phreatophytic roots in and around Site SV6 appear to have reached 3.0, 4.0, and 5.0 m during the summer, as inferred from lowest soil moisture values and/or decreasing soil moisture at depth.

Other than September, ratios of precipitation to ET increased during autumn months, showing increasing precipitation and decreasing ET; yet little activity occurred in the top 100 cm with respect to soil moisture. Soil moisture at 0.3 m remained constant while soil moisture at 1.0 m decreased. A total of 21.1 mm of precipitation occurred between 4 and 7 October 2010, yet Figure 20a showed no increases in soil moisture at either 0.3 m or 1.0 m depth. Although the most active growing season in the area is typically April through June (Devitt et al., 2010), evaporative demand and plant activity were still high following large events like those in October subsequently removing water from the soil faster than percolation to 0.3 and 1.0 m. A slight increase in soil moisture at 2.0 m was observed, but was most likely related to the slow moving front observed at 1.0 m during August 2010, and appears to continue down to 3.0 m by November 2010. Soil water at 4.0 m continues to be depleted during autumn as it did during the summer suggesting a potential for localized phreatophytic roots reaching this depth. After all,

soil moisture in autumn was typically at its lowest at 0.3, 3.0, and 4.0 m, decreasing at 1.0 m, and limited changes at 2.0 and 5.0 m. Furthermore, groundwater reached the transition period during these months from increasing to decreasing water depth. This is most likely due to the non-growing season of phreatophytes when they shut off ET sometime in October and the aquifer equilibrates allowing the water table to rise to normal levels.

The amount of precipitation and ET that occurred during winter months were similar to autumn; although, ET during winter was approximately 17% lower than the average ET value for autumn. Winter provides an optimal time for soil water and valley-fill recharge as the amount of precipitation is typically moderate to high and ET is low (precipitation to ET ratio of 1.1, Table 7); however, very little soil moisture change occurred within the soil profile. Although there were 41.9 mm of precipitation in December, some of it was most likely snow and temperatures were too cold for deep percolation. Only soil at 0.3 m saw increases in soil moisture greater than 0.01 m^3 m^{-3}. Depth to groundwater continues to decrease through winter at a similar rate observed in late October and November (0.002 m d^{-1}).

The total amount of precipitation during spring months was approximately 100% more than winter, while the amount of ET was more than 300% of the winter value. Similar to winter, most of the soil moisture changes occurred near surface, although a bit more at 1.0 m than at 0.3 m compared to winter. Soil moisture at 2.0, 3.0, and 4.0 m remains relatively constant, while soil moisture at 5.0 increases to a high of 0.18 m^3 m^{-3} by the end of May. Depth to groundwater continues to decrease throughout spring; however, the rate of increase is at its highest from early March to early May. According to Welch et al. (2007), recharge occurs at the mountain and alluvial fan connection. I speculate that the rate of groundwater depth decrease is most likely related to the melting of snow, thus increasing the amount of recharge into the groundwater;

although the amount of precipitation was high too and could also contribute to recharge at the mountain and alluvial fan connection. Due to limited amount of soil moisture changes between 2.0 and 4.0 m, yet increasing atmospheric demand and therefore higher ET of spring, most of the soil water for the plants likely comes from the top 1.0 m. By early- to mid-May 2011, the rate of decrease in groundwater depth is back to 0.002 m d^{-1}. Then in June, depth to groundwater increases again, as does soil moisture at 3.0, 4.0, and 5.0 m, suggesting phreatophytes begin to use deeper sources of soil water, particularly from the saturated zone, similar to what Devitt et al. (2010) found.

Although changes in water content (both increases and decreases) occurred at all depths monitored, snow melt and precipitation percolated as deep as ~400 cm but does not reach the phreatic zone. This is a bit surprising considering the amount of water taken up from phreatophytes and the layers of clay observed throughout the soil profile. Furthermore, work presented in Chapter 2 showed that after four years of precipitation on an arid soil, water only percolated to a maximum depth of 2.5 m and there were no plants at the site. Of course there is a possibility that due to the invasive nature of the work conducted at the site, a conduit was created for water movement down to 4.0 m. Changes in soil moisture content observed at 5.0 m depth were likely due to changes in groundwater table rather than percolating water from the soil above. There is, however, a potential connection to ET via groundwater from the phreatic zone.

4.6.2 Spring and Summer Soil Temperature

Soil temperatures deeper within the profile do not provide any insight regarding soil moisture movement and. Temperatures in the shallower soil do provide potential extinction depths with and without infiltration and percolation; however, not enough time was allowed in this study to determine seasonal extinction depths. Seasonal temperature extinction depths are typically at

about 30 m below surface (and the DTS pole only went down to ~6 m). Below these depths, variation may be attributed to variations in the internal temperature of the DTS logger and the increased pressure towards the base of the DTS pole (i.e., below 5.0 m). Large ranges of soil temperatures are observed near surface due to diurnal and seasonal atmospheric conditions (e.g., radiation, ambient temperature, etc.). Temperature ranges decrease with increasing depth in the profile, as diurnal temperatures are dampened and only seasonal temperatures are observed. The depth where daily changes are no longer observed and only seasonal changes occur depends on atmospheric conditions (e.g., precipitation amount and intensity, net radiation) and soil properties (e.g., hydraulic conductivity, soil texture). Constantz et al. (2003) suggested that, in the absence of infiltration and percolation, diurnal variation is detected down to a depth of 0.5 m where it reaches the soil's temperature extinction depth; however, with the influence of percolation, diurnal variation is detected down to an extinction depth of 2 m. Variation below 3.0 m can be attributed to variations in the internal temperature of the DTS logger and the increased pressure towards the base of the DTS pole. As water is released back into the atmosphere via ET, diurnal variations in soil temperature increase, as the volumetric heat capacity of wet soil is much larger than dry soil, thereby taking a large amount of energy to raise the temperature of wet soil 1 degree than it is a drier soil. The summer brings increasing radiation and temperature, as well as increasing activity from the phreatophytes. Not only do the phreatophytes (as well as evaporation) remove water from near surface, water eventually is removed from below the water table; as the roots of Greasewood are known to reach these deeper levels (Devitt et al., 2010). As the soil water decreases due to phreatophyte activity, diurnal variations increase, due to increases in soil surface temperatures, and decreasing volumetric heat capacity of the soil. The study shows that the use of temperature as an indicator for water movement is limited, even if highly

sensitive instrument as FO DTS is employed. In particularly for measurements deeper within a soil profile without a constant/perennial water source (e.g., stream) as a control.

4.7 Conclusions

The intensity and duration of precipitation events in the semi-arid southwest is likely to change with changes in climate, which will subsequently change the amount of water storage in the subsurface. The results of this study suggest that only large intensity storms, particularly winter storms, infiltrate deep into the subsurface. Phreatophytes, and other deep-rooted shrubs, remove substantial amounts of water during the summer thereby preventing water from summer storms to infiltrate deeper into the profile. Furthermore, the rate of percolation at the study site is slow due to the low hydraulic conductivity of the predominantly clayey soil. If winter valley storms do not replenish the deeper subsurface, and the plants rely more on the saturated zone during the spring and summer, groundwater water levels will drop, which can create a tipping point where phreatophytes will be decoupled from the water table, changing or reducing plant diversity (Cooper et al., 2006; Patten et al., 2008) and reducing spring discharge (Patten et al., 2008).

Groundwater table readings over one year showed that recharge is occurring; however, it is most likely coming from areas of higher elevation where alluvium meets with the basement, and not through basin fill (i.e. infiltration through the unsaturated soil on site). This study was limited to one year. But based on the soil moisture content changes at 2.0 and 3.0 m depth, and maybe 4.0 m depth, water infiltrating from the soil above may, over a longer period, and depending on the amount of rainfall (both duration and intensity) eventually reach the aquifer.

Similarly, many shrubs in the Great Basin, and subsequently Spring Valley, have high density root distributions within the top 0.75 to 3.0 m (Groeneveld, 1990; Richards and Caldwell, 1987; Donovan et al., 1996). Although the increases in soil moisture at 2.0 and 3.0 m appears to be due to percolation and/or redistribution of water from higher up in the soil profile, it is rather surprising percolation penetrates to depths of 2.0 and 3.0 m within one year. In a similar study described in Chapter 2, it took approximately 3.5 years for water to percolate down to a depth of 2.5 m within a bare, sandy soil under arid conditions (annual precipitation of 141 mm).

Although care was taken to backfill the borehole where the TDR probes were placed in, backfilling with clayey soil was not possible and a more sandy soil material from the local surface location was used. Arrangement of the TDR probes in a vertical borehole and imperfection in the backfill may have created a preferential flow path. Clearly it is difficult to determine constant patterns within one year, but even within one year, we can see how complex and different the connection between soil-plant-atmosphere is from a month to month basis.

Even though the study unveiled many of the shortcomings of the applied methods as well as the study site as a less than perfect location to test this experimental setup, it also shows some potential of the experimental setup to be applied in a different environment. A better location for a similar experimental setup could be an area near a sand bank adjacent to a river with a well-defined, shallow water table and the soil texture is fairly homogenous sand, such as the Virgin River in S. Nevada where salt cedar dominates the shores of this bank. Using the same setup as SV6, and with a better idea on protecting the DTS cable, and having a shallow water table, diurnal changes in water level due to these phreatophytes, we can set up an experiment that shows that changes in these water levels will cause changes in both sensible and latent heat flux, thereby providing a better result for ET measurements.

4.8 Acknowledgements

This research was supported in part by Gayle Dana and the National Science Foundation (NSF) Experimental Program to Stimulate Competitive Research (EPSCoR) Cooperative Support Agreement EPS-0814372 with Desert Research Institute. The authors would like to acknowledge Mark Hausner, Brad Lyles, Richard Jasoni, and Jay Arnone at Desert Research Institute, and Amanda Wagner and Mike Nicholl at University of Nevada, Las Vegas, for their contributions to this work. Dr. Yu's work during sabbatical leave has been supported by University of Nevada, Las Vegas.

CHAPTER 5

CONCLUSIONS

This study examined the water balance (precipitation, evaporation and evapotranspiration) and moisture dynamics of two soils in the US Southwest: (1) a bare arid soil at the SEPHAS Weighing Lysimeter Facility in Boulder City, Nevada; and (2) a vegetated semi-arid soil with a shallow water table in the valley floor of Spring Valley (site no. SV6), Nevada.

Chapter 2 presents a 4-yr baseline study (1 October 2008 to 30 September 2012) on precipitation, evaporation, and water storage, as well as soil moisture dynamics of bare arid soil installed in the SEPHAS weighing lysimeters. During the four year observation period, 180 precipitation events were recorded with a 4-yr annual average of 130.3 mm (7.6% below the 70 year average reported for a nearby location). Precipitation intensity was generally higher during summer whereas precipitation duration was higher in the winter. Total precipitation was greatest during winter (44.8% of annual precipitation), followed by summer (29.6% of annual precipitation), autumn (16.7% of annual precipitation), and spring (8.8% of annual precipitation). Of the 130.3 mm 4-yr annual average precipitation, between 69% and 90% was found to evaporate back into the atmosphere during the course of a water year. High annual total evaporation was related to lower annual precipitation, low antecedent water content (observation year 1 only) and the absence of large winter storm events during the respective water year. Approximately two-thirds of annual evaporation occurred immediately or within a few days after storm events at rates of about 1 mm d^{-1}, when the near-surface soil was moist due to most recent precipitation. Approximately one-third of the annual evaporation occurred during the precipitation free weeks and months between storm events and at a fairly constant rate of about

0.1 mm d^{-1}. In other words, evaporation occurred even though near surface soil was dry, indicating that evaporation in such an arid environment may remain driven by atmospheric demand but is primarily controlled by water supply from within the soil. Although not evaluated in this study, soil texture could also play a role (which can provide work for future graduate students).

From the 130 mm of average annual precipitation, between 10 and 31% remained in the soil and led to an increase in soil water storage throughout the four year study period. Higher amounts of annual water storage were related to the occurrence of large winter storms (water years 2010 and 2011). Increases in water storage coincided with storm events that were large enough (in terms of total amount of precipitation) to lead to infiltration deeper than 25 cm. A threshold could be established on the smallest amount of total daily precipitation needed to reach 25 cm and below (i.e. change in daily average soil moisture values > 0.01 m^3 m^{-3} in 25 cm depth). The amount of precipitation needed to see changes of soil moisture at 25 cm and deeper ranged between 14.1-30.9 mm for winter storms, 24.5-41.6 mm for summer storms, 15.9 mm for spring, and 11.9-13.9 mm for fall. Smaller events with infiltration depth less than 25 cm tended to evaporate back into the atmosphere without increasing soil water storage at an annual scale. For water storage changes at a daily scale, a precipitation threshold could be established based on the smallest amount of total daily precipitation necessary to see an effect in soil moisture at 2.4 cm depth (change in daily average soil moisture values > 0.01 m^3 m^{-3} 2.4 cm depth). This threshold ranged between 0.5 mm in winter and 2 mm in spring, summer and fall. Besides the seasons, both threshold were found to depend on antecedent soil moisture conditions, and the amount of time between previous and successive events. It took just under 4 years for water to percolate down to a depth of 250 cm in one lysimeter.

Chapter 3 evaluated the evaporation model by Shokri et al. (2009) and Or et al. (2013) that simulates vapor diffusion-controlled (or Stage II) evaporation by comparing simulated with measured Stage II evaporation rates from the lysimeter. As indicated in Chapter 2, about one third of all the annual evaporation occurs under Stage II evaporation conditions. Measurements and simulations using first-principal soil physical parameters (e.g., porosity, moisture content, etc.) agreed well for two out of three studied precipitation events (evaporation rate RMSEs of 0.141 and 0.093 mm d^{-1}). Simulations for the third event systematically underestimated measured evaporation rates (evaporation rate RMSE of 0.181 mm d^{-1}). The latter is likely due to significant differences between the soil moisture profile in the lysimeter and that assumed by the model. A sensitivity analysis showed that the soil water content profile, besides soil porosity, is the most sensitive parameters in the model. Since porosity can be determined rather accurately, improving the soil moisture profile characterization would likely need more scrutiny to further improve the model predictions for arid soils. Due to its simplicity, these models have potential to be used in many different simulation environments (e.g., arid land modules in climate change models) while still simulating the actual physical processes controlling Stage II evaporation. The good agreement between measured and simulated evaporation rates also indicates that the models by Shokri et al. (2009) and Or et al. (2013), although initially developed for humid conditions and soil-laboratory scale, can be applied to arid soils and at the plot scale, since the lysimeter has a soil surface area of 4 m^2.

Chapter 4 addressed the increase in complexity when moving from a bare soil in a lysimeter with well controlled initial and boundary conditions to a field soil with the addition of a relatively shallow water table (depth of less than 6 m) and the presence of phreatophytes. This 1-yr study (1 July 2010 and 30 June 2011) was conducted in a semi-arid environment within

Spring Valley of the Great Basin in Nevada (Site SV6) where daily ET, precipitation, volumetric soil moisture, and depth to groundwater were monitored to examine seasonal trends in soil water and temperature responses. Although this study was invasive due to the nature of installing instrumentation in both the vadose and phreatic zones, it provided insight on the processes that affect soil water and temperature from a shallow water table to near surface and the effects of inter-annual precipitation and ET variability. Considering the rather short study period and some technical issues with the monitoring equipment that could not be resolved within the study period, it appeared that, similar to arid bare soils in the lysimeters, very little water infiltrates down to greater depths, likely due to evapotranspiration. In contrast to the lysimeters, deeper infiltration were found during snowmelt in spring rather than in winter, indicating that the snow cover can play a major role in recharging the exiting groundwater system; however, this might have been related to the invasive nature of instrument deployment into the soil creating a conduit. Recharge is primarily from the top of the mountain during early spring. In addition, when water becomes limited for the plants, roots tap into deeper portions of the soil profile including the saturated zone. ET was found to be highest in spring and early summer.

The Spring Valley study also looking into fiber optic (FO) distributed temperature sensing (DTS). FO DTS, a new and exciting technique that allows for temperature measurements at greater spatial resolution while maintaining excellent temporal resolution (Selker et al., 2006a; Tyler et al., 2009). FO DTS was used during early spring and summer seasons of 2011 when ET is at its highest with the goal to analyze inter-annual and seasonal precipitation and ET with changes in soil water storage, determine depth of wetting front and whether or not it reaches the phreatic zone during the study period, and determine soil temperature extinction depths. Although DTS provided soil temperature profiles, due to the sensitivity in the setup, only

approximate daily temperature extinction depths were determined. Due to the nature of the soil (high clay content and layers of caliche) and the fact that in order to place the DTS pole, backfill included sands and silts, thus changing the texture, the instrument was not effective for this type of environment.

This study provides a starting point with some insight into the hydraulic behavior of desert soils and a first set of baseline data. The SEPHAS weighing lysimeter has been in operation since 2008 and there are currently 7.5 years of soil, mass, moisture content, matric potential and temperature data. To date, four years of data analysis have been completed but the methods in place can now easily be applied to the entire seven years. The available four year data set also already provided the foundation for three modeling studies that I have been heavily involved in by Kelleners et al. (2015), Dijkema et al. (2015) and Iden et al. (2015), geared towards further exploring the hydraulics of desert soils.

Results from this study shed some light on how arid and semi-arid soils infiltrate, store and evaporate water as functions of precipitation, atmospheric demand and antecedent soil moisture conditions. By influencing basic hydrologic processes such as surface runoff, infiltration, evapotranspiration (ET) and potential groundwater recharge, arid and semi-arid soils play a critical role in supporting life in dryland environments where water is the limiting resource. Overall, increased knowledge about the role of desert soils in the hydrologic cycle will serve as well in the long run, in particular with the ever increasing pressure on water resources globally, the anticipated shifts in precipitation patterns due to climate change as well as the increasingly frequent and longer droughts.

APPENDIX A

SEPHAS WEIGHING LYSIMETER FACILITY DATA ON CD ROM

APPENDIX B

SPRING VALLEY DATA ON CD ROM

APPENDIX C

SEPHAS BACKGROUND, STATISTICAL VERIFICATION, AND ADDITIONAL TIME SERIES DATA

Lysimeters 1-3 Lift Details

Lysimeters 1-3 were filled from bottom to top (0-300 cm) with soil from the Eldorado Valley excavation site as individual lifts (between 2-22 cm in thickness). Table 8 provides height, bulk density, and porosity for each lift (Chief et al., 2009; Shillito, R., unpub. data, 2015).

Lysimeter and Rain Gauge Verification

Rain gauges provide point measurements of precipitation for a given location, as does the one at the SEPHAS Weighing Lysimeter Facility; however, errors can be associated with rain gauges, particularly during short-duration, high-intensity storms or long-duration, high-intensity storms (Humphrey et al., 1997). Due to potential errors associated with intensity and duration variability, and the fact that the rain gauge is approximately 28.5 m west of Lysimeter 1, daily amounts of precipitation collected via rain gauge were compared to daily amounts of precipitation collected using Lysimeters 1-3. Furthermore, as the lysimeters are being used in this study to evaluate soil moisture dynamics, a comparison is important to the validity of what is measured and observed.

Linear regression was completed for daily precipitation using both rain gauge and lysimeter from 8 November 2008 through 30 September 2012 (Figure 24). Data shows a high correlation in measurement techniques (R^2 of 0.895, 0.906, and 0.901 for Lysimeters 1-3, respectively; significance level of $p<0.001$ for Lysimeters 1-3) and falls just short of a 1:1 ratio. Data

Table 8. Individual lift soil properties measured during installation of soil in Lysimeters 1-3 (Chief et al., 2009; Shillito, R., unpub. data, 2015). Lift #1, the first to be installed, begins at the base of the lysimeter.

Lysimeter 1				Lysimeter 2				Lysimeter 3			
Lift #	Lift Height (m)	ρ_b (g cm^{-3})	φ (--)	Lift #	Lift Height (m)	ρ_b (g cm^{-3})	φ (--)	Lift #	Lift Height (m)	ρ_b (g cm^{-3})	φ (--)
28	0.06	1.90	0.24	32	0.03	1.53	0.40	29	0.02	1.54	0.39
27	0.02	1.75	0.30	31	0.02	1.64	0.35	28	0.02	1.64	0.36
26	0.08	1.70	0.32	30	0.05	1.61	0.37	27	0.04	1.65	0.35
25	0.08	1.70	0.32	29	0.06	1.64	0.36	26	0.06	1.64	0.36
24	0.07	1.73	0.31	28	0.10	1.65	0.35	25	0.09	1.64	0.36
23	0.10	1.73	0.31	27	0.05	1.98	0.22	24	0.06	1.67	0.34
22	0.10	1.74	0.31	26	0.10	1.70	0.34	23	0.11	1.71	0.34
21	0.05	1.75	0.30	25	0.10	1.75	0.32	22	0.07	1.74	0.32
20	0.05	1.89	0.25	24	0.06	1.59	0.38	21	0.08	1.73	0.33
19	0.12	1.70	0.32	23	0.03	1.65	0.36	20	0.09	1.67	0.35
18	0.16	1.58	0.37	22	0.17	1.72	0.33	19	0.09	1.73	0.33
17	0.13	1.81	0.28	21	0.05	1.75	0.32	18	0.04	1.56	0.40
16	0.12	1.88	0.25	20	0.10	1.83	0.28	17	0.15	1.80	0.29
15	0.14	1.80	0.28	19	0.10	1.78	0.30	16	0.06	1.99	0.22
14	0.13	1.70	0.32	18	0.11	1.88	0.26	15	0.14	1.81	0.29
13	0.10	1.70	0.32	17	0.09	1.86	0.27	14	0.08	1.90	0.25
12	0.14	1.73	0.31	16	0.10	1.74	0.31	13	0.18	1.80	0.29
11	0.13	1.73	0.31	15	0.13	1.89	0.26	12	0.11	1.76	0.31
10	0.12	1.73	0.31	14	0.08	2.02	0.21	11	0.14	1.78	0.30
9	0.11	1.73	0.31	13	0.10	1.70	0.34	10	0.09	2.30	0.08
8	0.13	1.73	0.31	12	0.10	2.29	0.08	9	0.10	1.74	0.30
7	0.13	1.73	0.31	11	0.10	1.73	0.30	8	0.08	1.73	0.30
6	0.12	1.73	0.31	10	0.10	1.89	0.24	7	0.10	1.87	0.25
5	0.13	1.76	0.30	9	0.09	1.74	0.30	6	0.22	1.67	0.33
4	0.10	1.74	0.31	8	0.06	1.74	0.31	5	0.13	1.73	0.31
3	0.13	1.73	0.31	7	0.16	1.73	0.31	4	0.15	1.74	0.31
2	0.14	1.73	0.31	6	0.16	1.73	0.31	3	0.22	1.74	0.31
1	0.13	1.73	0.31	5	0.13	1.73	0.31	2	0.16	1.73	0.31
--	--	--	--	4	0.12	1.73	0.31	1	0.14	1.76	0.30
--	--	--	--	3	0.14	1.75	0.30	--	--	--	--
--	--	--	--	2	0.15	1.75	0.30	--	--	--	--
--	--	--	--	1	0.10	1.81	0.28	--	--	--	--
	Average:	1.75	0.30		Average:	1.77	0.30		Average:	1.75	0.31

ρ_b - Total bulk density (Includes fines and gravel)

φ - Total Porosity

deviation from the 1:1 ratio occurs mostly at the lower daily precipitation range, in addition to three days of outlying events. Deviation during low daily precipitation is to be expected for two reasons: 1) resolution of the lysimeters; and 2) low amounts of precipitation is evaporated quickly in a given day, in addition to continued evaporation throughout the day, and therefore shows up as a negative value as measured by the lysimeters. As for the outlying events, data from 17-18 December 2008 and 22 December 2010 (circled on Figure 24) deviate from the 1:1 line due to two separate issues. In the night of 17-18 December 2008 a rare snowfall event occurred in Boulder City which could have caused problems with the rain gauge on a day by day basis; however, the cumulative precipitation for 15-18 December 2008 was approximately 25.6 mm while the cumulative mass flux for Lysimeters 1-3 were 25.5, 25.2, and 25.9, respectively, over the same four days. Subsequently, the cumulative precipitation of these four days would line up much closer to the 1:1 ratio line. As for 22 December 2010, the amount of precipitation was particularly intense and the rain gauge had a malfunction that didn't record the correct amount of rainfall. This is based on the total mass increase in all three lysimeters (all were approximately the same increase) and precipitation data from Community Environmental Monitoring Program (CEMP) meteorological stations (sponsored by Department of Energy) in Boulder City, NV (located approximately 2.4 km north of the lysimeter facility) and Henderson, NV (located approximately 11.8 km northwest of the lysimeter facility) showing similar amounts of precipitation as recorded in the lysimeters. If these three days were removed from Figure 24, new R^2 values would be 0.976, 0.976, and 0.977 for Lysimeter 1-3, respectively.

Figure 24. Comparison of daily precipitation using a rain gauge and flux using lysimeters for (a) Lysimeter 1, (b) Lysimeter 2, and (c) Lysimeter 3. Solid red line is best-fitted regression line, and dashed line is 1:1 line (regression line equation R^2, and three outliers included).

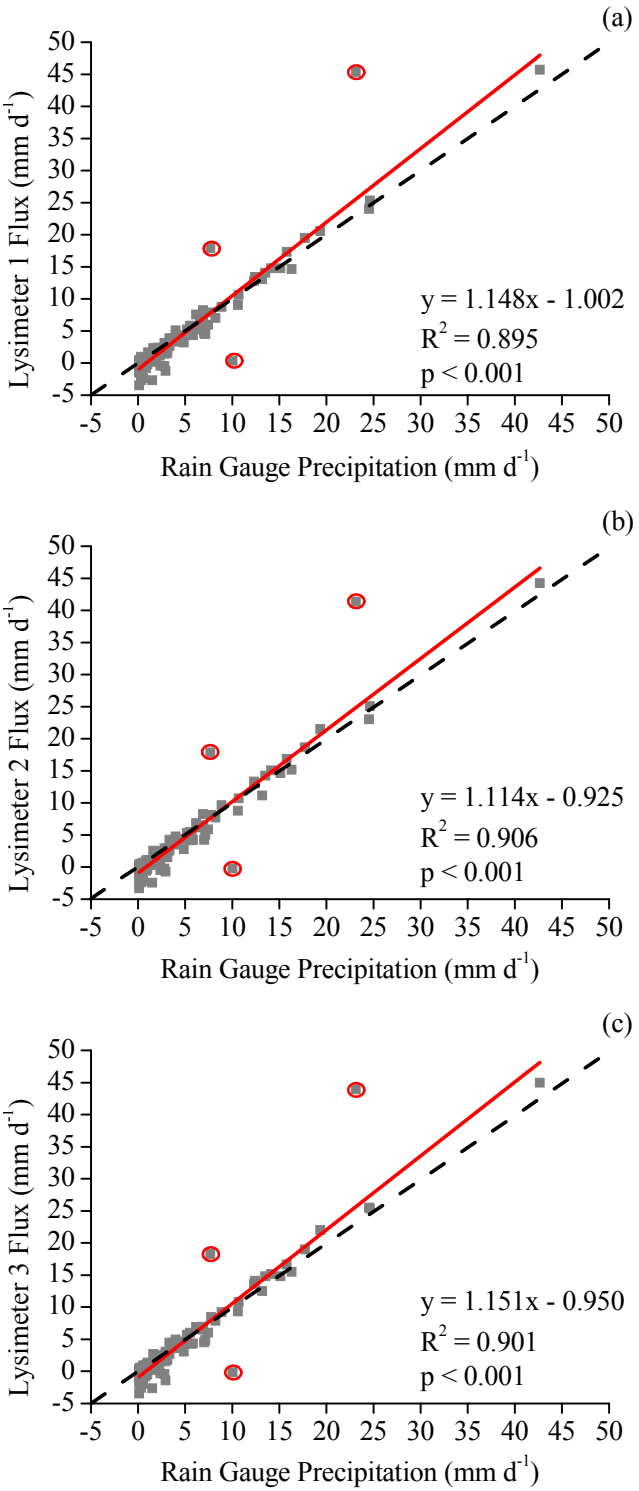

Moisture Content Verification

Initial gravimetric moisture contents collected prior to this study, were compared to moisture contents measured using TDR probes (model CS605, Campbell Scientific Inc., Logan, UT) on 1 October 2008 (first day of this study) to provide both a quantitative and qualitative comparison of direct (gravimetric) and indirect (dielectric) methods and show that the probes provide accurate and reliable volumetric moisture content measurements. Chief et al. (2009) provides details as to the calibration of TDR probes; however, multiple values were determined for the four coefficients (A, B, C, and D) described in Topp's equation (Topp et al., 1980). Multiple values for each coefficient were derived from soil calibration representative of specific soil horizons (25-80, 80-120, 120-160, and 160-200 cm), homogenized soil (0-200 cm), and a combined data set containing all soil (ALL cm). Moisture content was then calculated using all variations of these coefficients for 1 October 2008. As a quantitative comparison, daily average moisture content at each probe depth (10, 25, 50, 75, 100, 150, 200, and 250 cm) were compared to initial moisture content collected for the lift around that depth between 12 March and 1 June 2008. Table 9 provides root mean square statistics for each soil horizon, homogenized mix, and combined data set. Root mean square error is defined as

$$\text{RMSE} = \left(\frac{1}{n}\sum\left(\theta_{probe} - \theta_{initial}\right)^2\right)^{1/2}$$

where θ_{probe} is the soil moisture measured using TDR probe at each depth and $\theta_{initial}$ is the soil moisture content directly measured from a soil lift at each depth. Due to increased soil moisture in the top 50 cm (caused by increased soil moisture in storage bins) at the time of gravimetric sampling, and subsequent evaporation from the soil due to hot and dry temperatures at the facility, RMSE was also calculated removing 10 and 25 cm, as well as 10, 25, and 50 cm moisture contents. When looking at all three sets of data, errors are the lowest using 'ALL cm'

Topp's Coefficients, particularly for Lysimeters 2 and 3. Because the error is so small between coefficients from '0-200 cm' and 'ALL cm' for lysimeter 1 (0.008 and 0.010 $m^3 m^{-3}$, respectively), it is reasonable to use the same coefficients for all sensors and all lysimeters.

A qualitative comparison is provided in Figure 25 showing initial volumetric moisture content profiles determined by TDR probes (using the 'ALL cm' coefficients) on 1 October 2008 and comparing them to volumetric moisture content profiles determined during soil 'lift' installation of Lysimeters 1-3. Profiles are similar in Lysimeter 1 with differences of 0.01 $m^3 m^{-3}$ or less and fall within, or close to, one standard deviation of the 1 October 2008 data (averages and standard deviations were calculated using all instruments and readings every hour for the specific depth; outliers were removed). The initial moisture content for Lysimeter 1 was relatively uniform from near-surface to depth and averaged approximately 0.05 $m^3 m^{-3}$. October 2008 profiles in Lysimeter 2 and 3 were also similar to their respective 2008 initial profiles (differences of 0.01 $m^3 m^{-3}$ or less) except within the upper 25 cm of Lysimeter 2 and upper 10 cm of Lysimeter 3, where near surface initial moisture contents were higher than the 1 October 2008 daily average. Initial moisture content in Lysimeter 2 and Lysimeter 3 showed average moisture contents of 0.04 $m^3 m^{-3}$. Near surface soil in Lysimeter 2 shows approximately 0.03 $m^3 m^{-3}$ difference at 10 and 25 cm, and Lysimeter 3 shows approximately 0.03 $m^3 m^{-3}$ difference at 10 cm. Precipitation did not occur during the installation of individual 'lifts' near the surface; furthermore, lysimeters were covered to prevent additional water to enter into the lysimeters during times of construction hiatus. The higher than usual moisture contents in Lysimeters 2 and 3 could be attributed to poor soil handling, error in gravimetric moisture content measurement, or higher moisture content due to condensation in soil storage, or near surface soil dried out between time of installation and start of observation period. Four months passed since the last lift was installed from the

beginning of this study period; at which time southern Nevada weather (summer) allowed for trapped moisture in the upper lifts of Lysimeters 2 and 3 to evaporate. Overall, measured moisture content measured using TDR probes is very similar to moisture content during soil 'lift' installation and therefore representative of initial conditions.

Table 9. RMSE statistics for initial and 2008 October 1 moisture contents using 6 different Topp's Coefficients obtained during TDR calibration.

Coefficients	**Lysimeter 1**	**Lysimeter 2**	**Lysimeter 3**
All Depths	(m^3 m^{-3})	(m^3 m^{-3})	(m^3 m^{-3})
25-80 cm	0.009	0.017	0.014
80-120 cm	0.016	0.021	0.017
120-160 cm	0.007	0.015	0.013
160-200 cm	0.059	0.059	0.061
0-200 cm	0.008	0.016	0.015
ALL cm	0.010	0.017	0.013
10 and 25 cm Removed	(m^3 m^{-3})	(m^3 m^{-3})	(m^3 m^{-3})
25-80 cm	0.006	0.006	0.008
80-120 cm	0.012	0.007	0.010
120-160 cm	0.006	0.008	0.009
160-200 cm	0.056	0.058	0.058
0-200 cm	0.007	0.012	0.012
ALL cm	0.007	0.005	0.008
10, 25, and 50 cm Removed	(m^3 m^{-3})	(m^3 m^{-3})	(m^3 m^{-3})
25-80 cm	0.006	0.005	0.008
80-120 cm	0.011	0.007	0.008
120-160 cm	0.005	0.006	0.009
160-200 cm	0.052	0.054	0.056
0-200 cm	0.006	0.010	0.012
ALL cm	0.007	0.004	0.007

Figure 25. Comparison of initial volumetric moisture contents (calculated from gravimetric moisture samples and bulk density) prior to start of this study and daily average volumetric moisture content (using TDR probes) on 1 October 2008 for (a) Lysimeter 1, (b) Lysimeter 2, and (c) Lysimeter 3. Error bars with 1 standard deviation included for volumetric moisture contents on 1 October 2008.

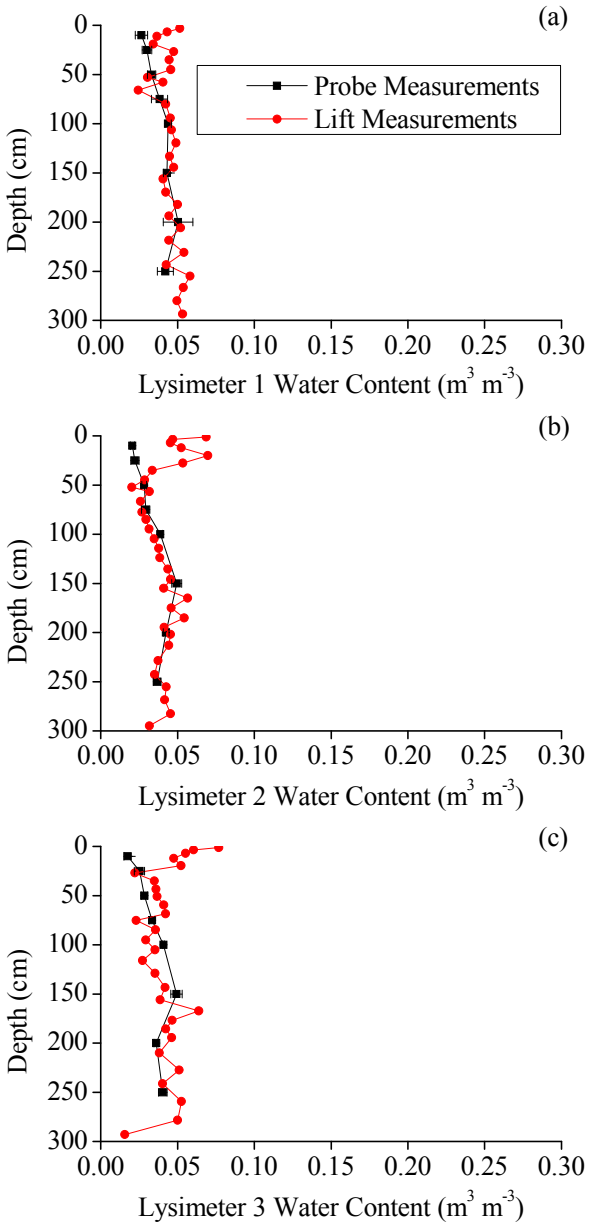

Shallow Moisture Content Time Series for Lysimeter 1

Figure 26 provide times series soil moisture response in Lysimeter 1 due to precipitation and subsequent evaporation. Readings from TPHP probes at 1.2, 3.6, and 4.8 cm depth were used.

Figure 26. Daily average Lysimeter 1 soil moisture content at 1.2, 3.6, and 4.8 cm using TPHP sensors for the study period of 1 October 2008 through 30 September 2012.

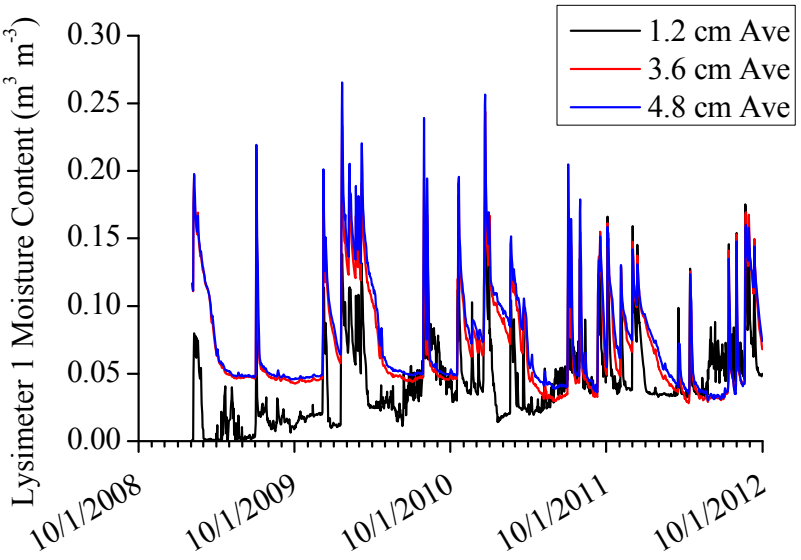

Moisture Content Time Series for Lysimeters 2 and 3

Figures 27 and 28 provide times series soil moisture response in Lysimeters 2 and 3, respectively, due to precipitation and subsequent evaporation. TDR probes at depths of 10, 25, 50, 75, 100, 150, 200, and 250 cm were used.

Figure 27. Daily average Lysimeter 2 soil moisture content at (a) 10 and 25 cm, (b) 50, 75, and 100 cm, and (c) 150, 200, and 250 cm using TDR sensors for the study period of 1 October 2008 through 30 September 2012.

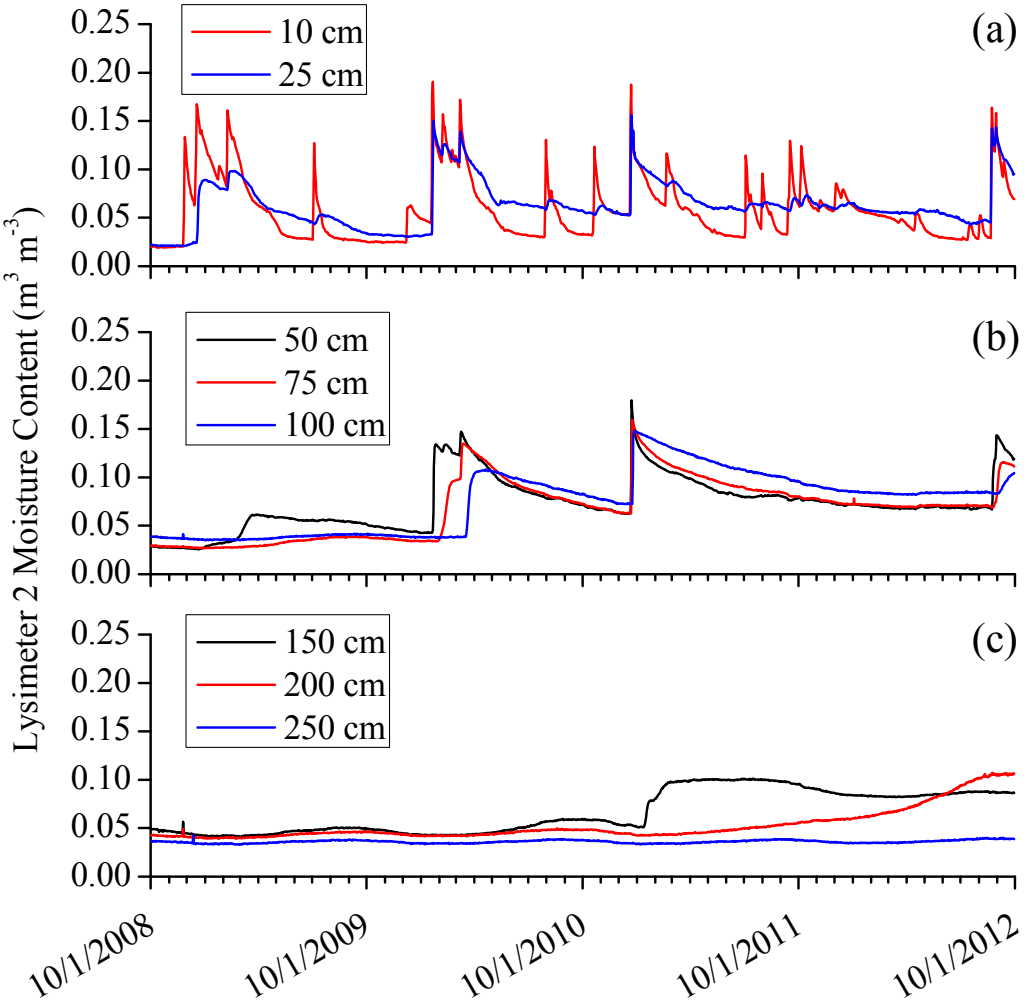

Figure 28. Daily average Lysimeter 3 soil moisture content at (a) 10 and 25 cm, (b) 50, 75, and 100 cm, and (c) 150, 200, and 250 cm using TDR sensors for the study period of 1 October 2008 through 30 September 2012.

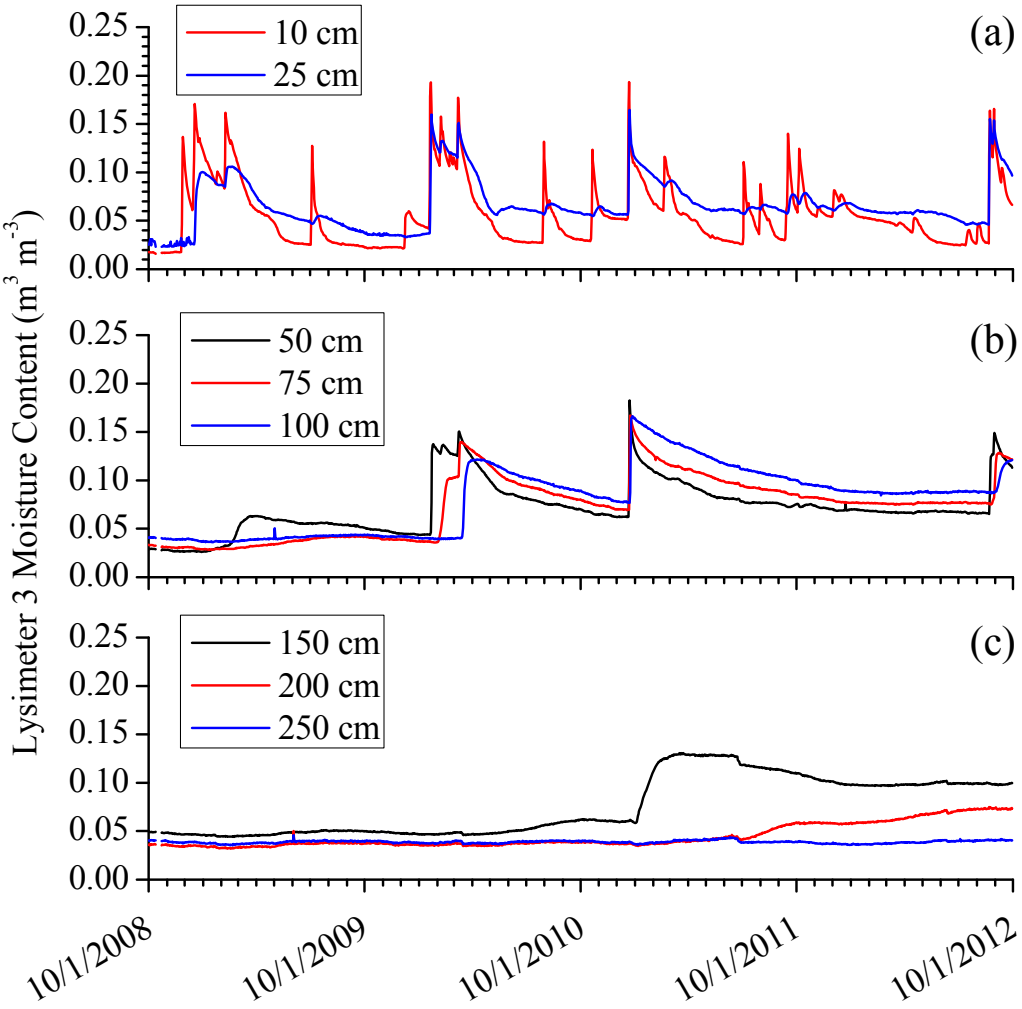

Matric Potential Time Series for Lysimeters 1-3

Figures 29-31 provide times series matric potential response to precipitation infiltration and subsequent evaporation from Lysimeters 1-3. HDU sensors at depths of 5, 10, 25, 50, 75, 100, 150, 200, and 250 cm were used.

Figure 29. Daily average Lysimeter 1 matric potential at (a) 5, 10 and 25 cm, (b) 50, 75, and 100 cm, and (c) 150, 200, and 250 cm using HDU sensors for the study period of 1 October 2008 through 30 September 2012.

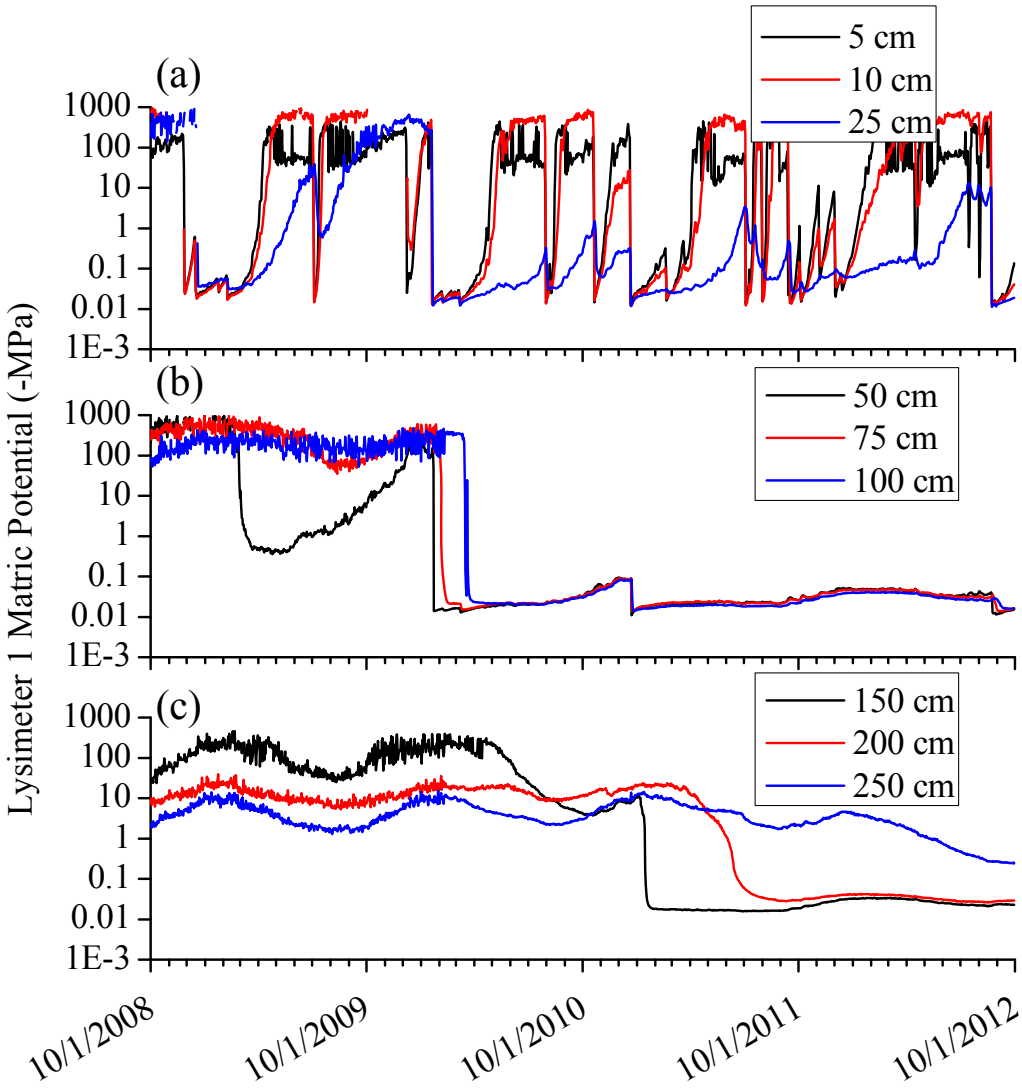

Figure 30. Daily average Lysimeter 2 matric potential at (a) 5, 10 and 25 cm, (b) 50, 75, and 100 cm, and (c) 150, 200, and 250 cm using HDU sensors for the study period of 1 October 2008 through 30 September 2012.

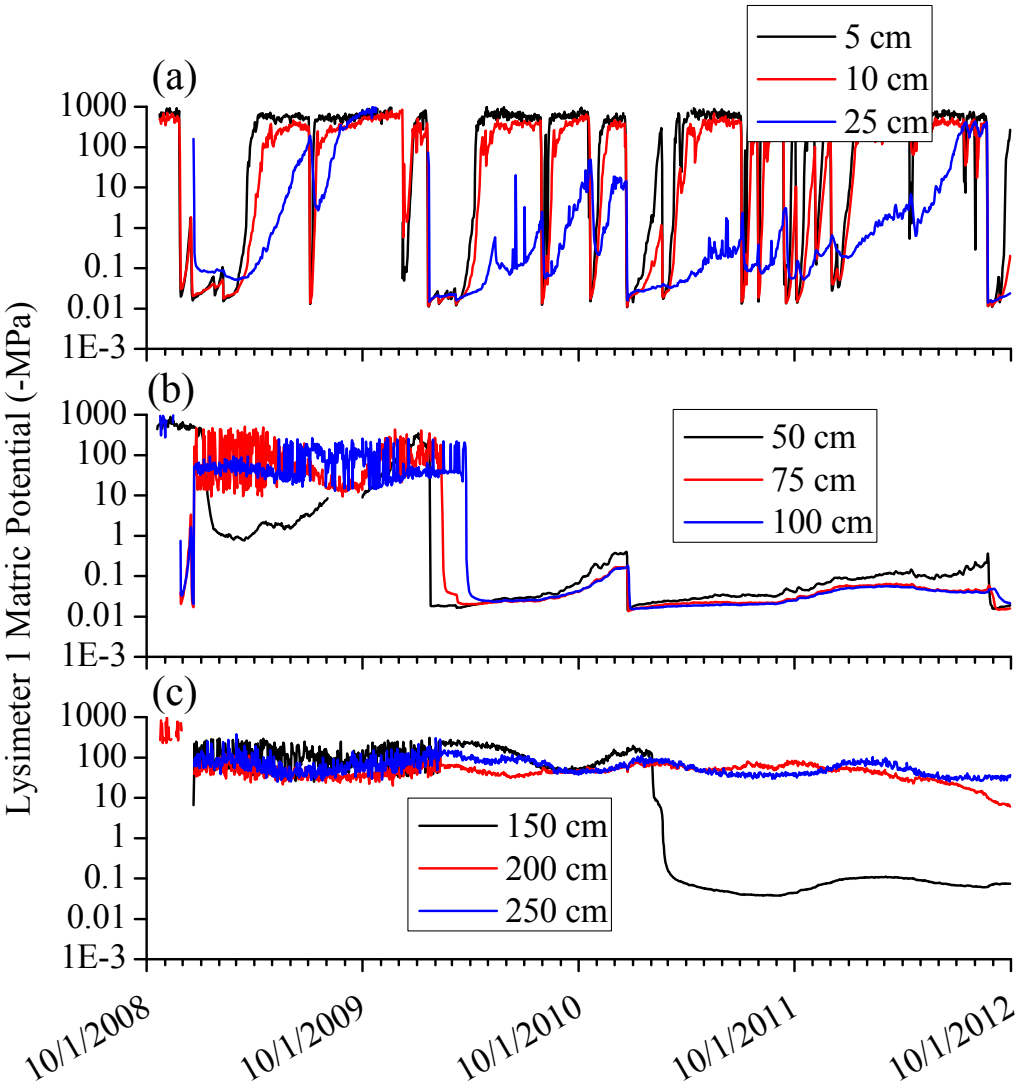

Figure 31. Daily average Lysimeter 3 matric potential at (a) 5, 10 and 25 cm, (b) 50, 75, and 100 cm, and (c) 150, 200, and 250 cm using HDU sensors for the study period of 1 October 2008 through 30 September 2012.

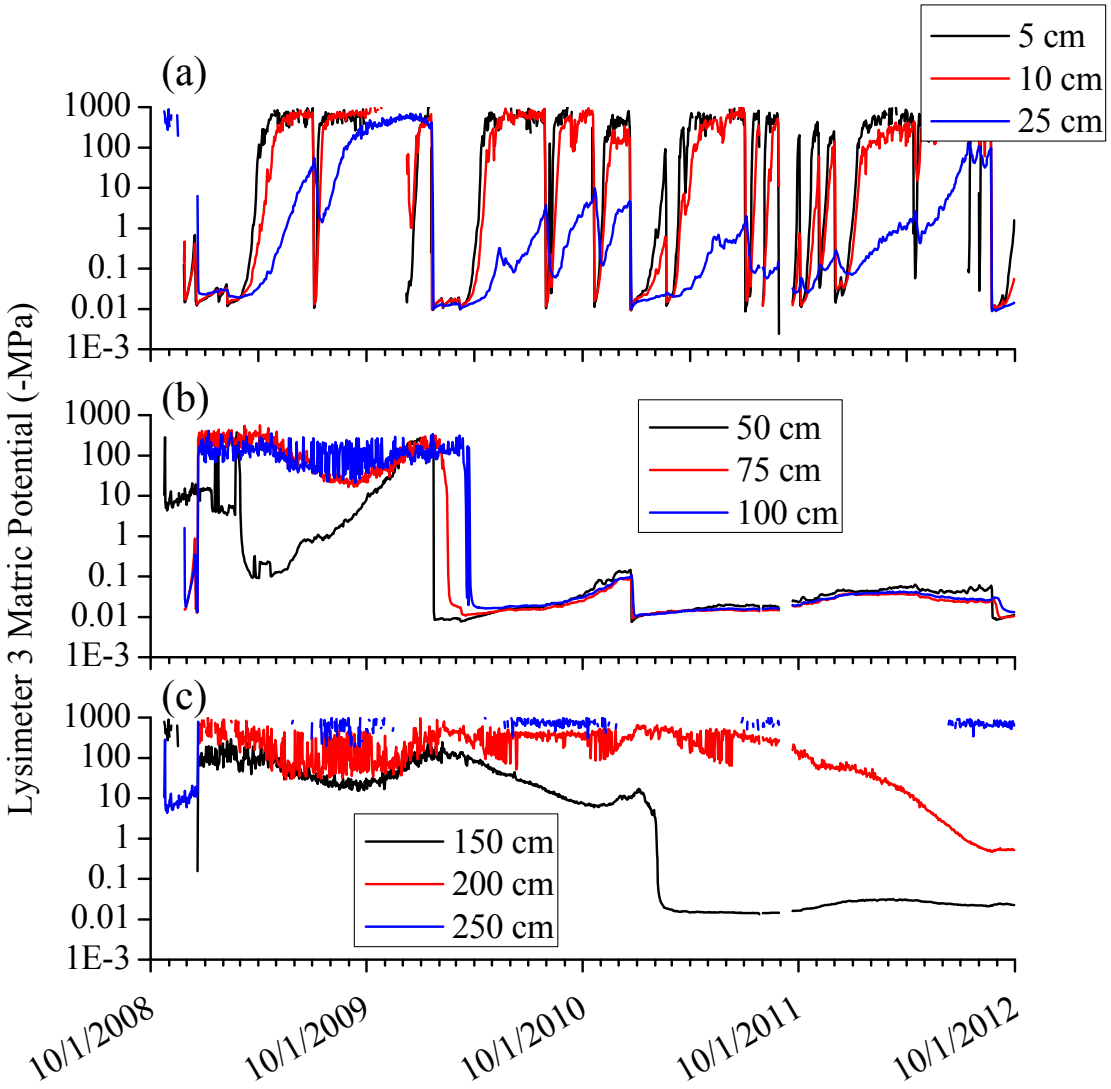

Soil Temperature Time Series for Lysimeters 1-3

Figures 32-34 provide times series soil temperature response in Lysimeters 1-3. HDU sensors at depths of 5, 10, 25, 50, 75, 100, 150, 200, and 250 cm were used.

Figure 32. Daily average Lysimeter 1 soil temperature at (a) 5, 10 and 25 cm, (b) 50, 75, and 100 cm, and (c) 150, 200, and 250 cm using HDU sensors for the study period of 1 October 2008 through 30 September 2012.

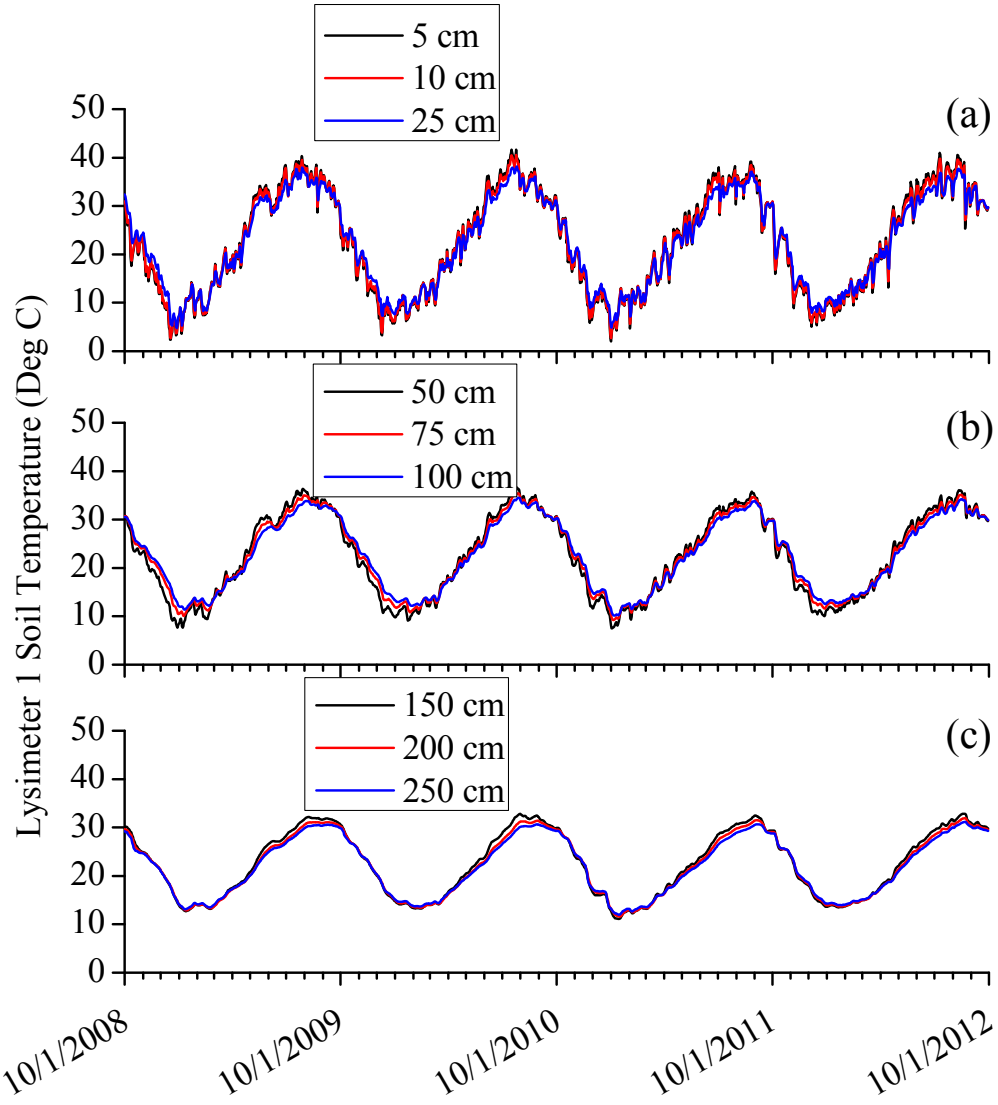

Figure 33. Daily average Lysimeter 2 soil temperature at (a) 5, 10 and 25 cm, (b) 50, 75, and 100 cm, and (c) 150, 200, and 250 cm using HDU sensors for the study period of 1 October 2008 through 30 September 2012.

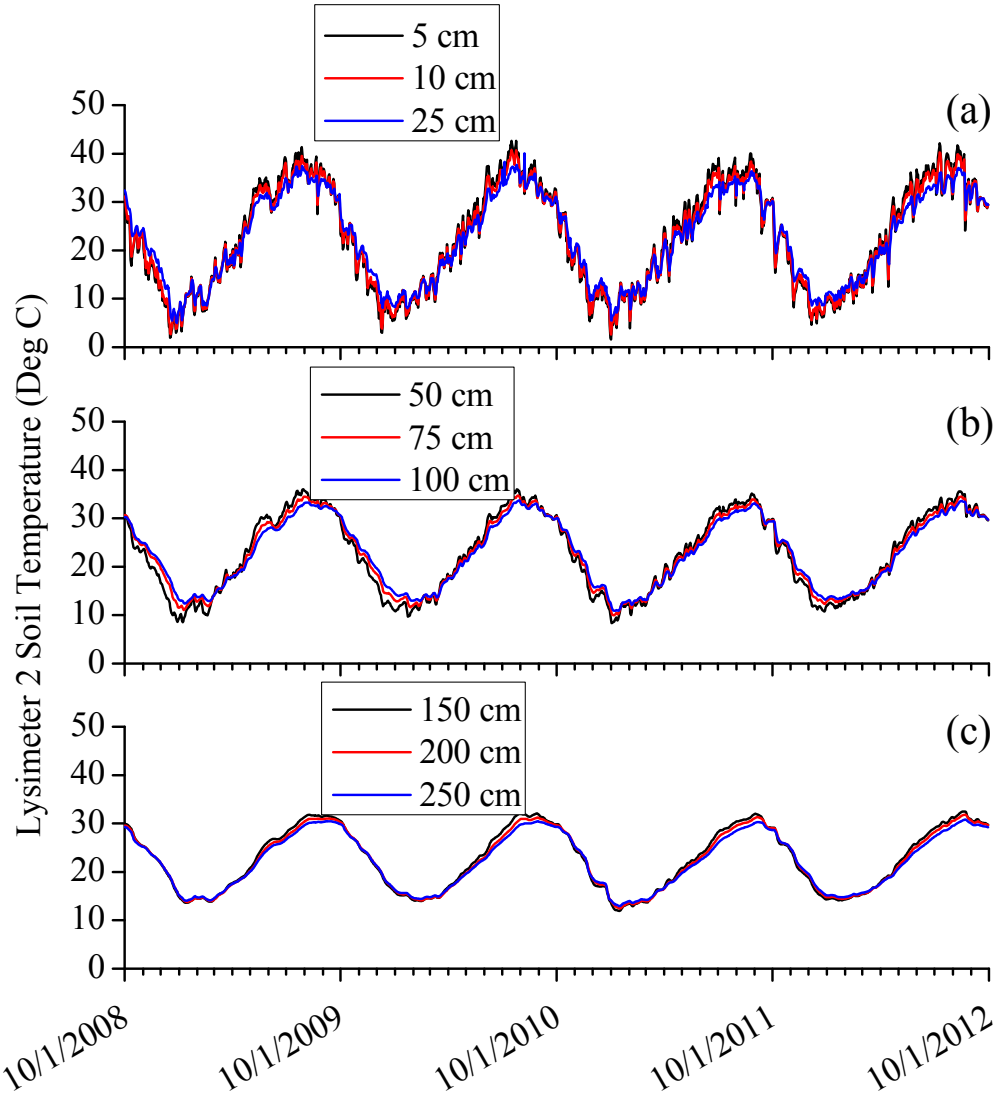

Figure 34. Daily average Lysimeter 3 soil temperature at (a) 5, 10 and 25 cm, (b) 50, 75, and 100 cm, and (c) 150, 200, and 250 cm using HDU sensors for the study period of 1 October 2008 through 30 September 2012.

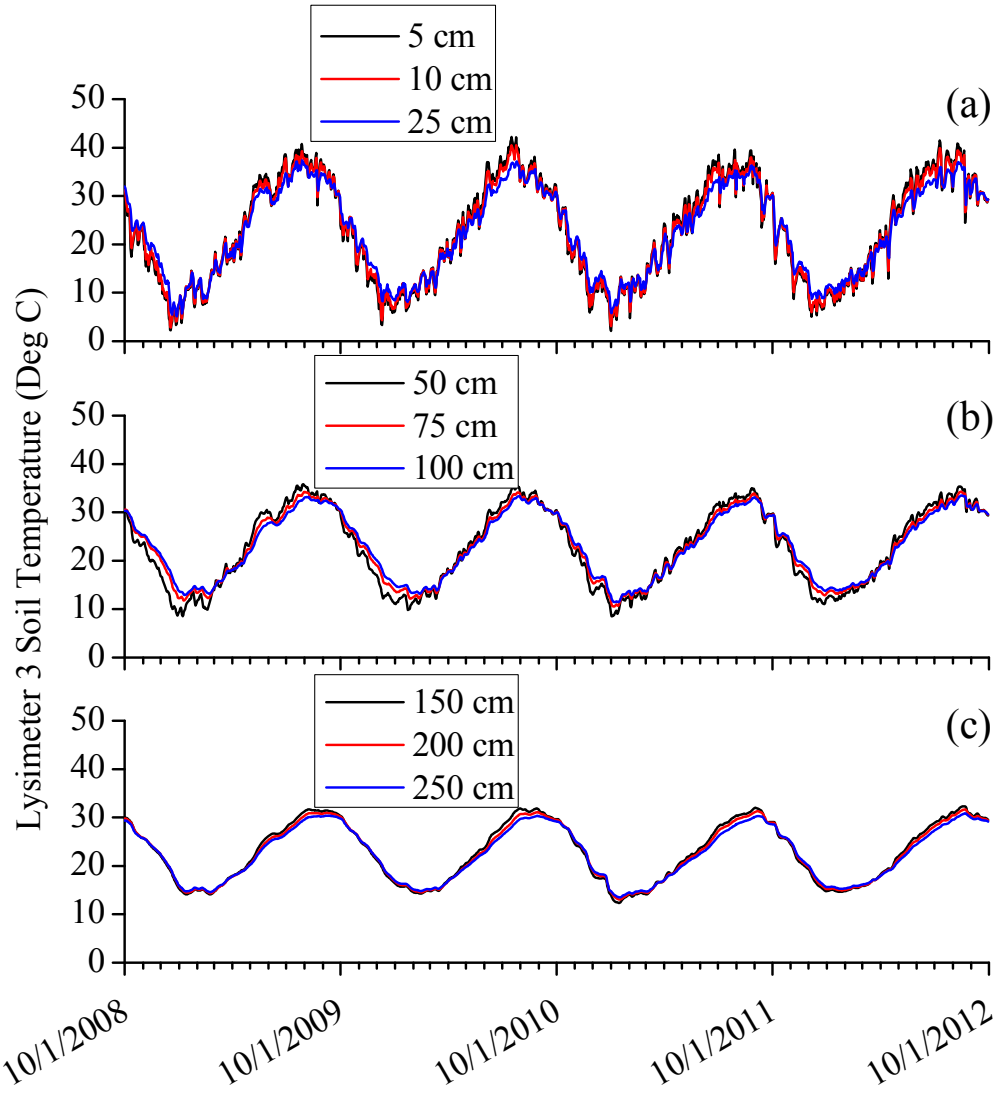

APPENDIX D

SPRING VALLEY FIELD SITE SV6 SYNTHESIS

Physiography

SV6 is located within the Basin and Range Province (Figure 35), one of many provinces in the United States outlined by Hunt (1967). The United States was divided into 11 major divisions which encompass 34 provinces delineated primarily by geologic structure; each characterized with distinctive climate, vegetation, soils, water, and other resources, as well as its own economy and cultural traits. The Basin and Range Province area covers ~800,000 km^2 (Hunt, 1967; Eaton, 1982) that expands over two countries (United States and Mexico) and eight states (Arizona, California, Idaho, Nevada, New Mexico, Oregon, Texas, and Utah). This region is characterized by horst and graben terrain providing long parallel mountain ranges and alluvial valleys. Due to the topography and the control it has over the climate, the Basin and Range Province is home to four major deserts: the Great Basin, Mojave, Sonoran, and Chihuahuan (Figure 35).

The Basin and Range Province is further divided into five arbitrary divisions, one of which is the Great Basin, centering on Nevada (and including parts of Oregon, Idaho, Utah, Arizona, and California) and making up half of the Basin and Range Province (Hunt, 1967). SV6 is located within this division, and as such, the physical characteristics of the Great Basin subdivision will be the primary focus of this synthesis; however, large scale physical conditions and forces (e.g., climate, tectonics) that occur in the Great Basin affect other divisions and provinces.

Figure 35. Map of the subdivision outlined by Hunt (1967) and location of SV6.

The mountain ranges and alluvial valleys in the Great Basin generally trend north (Hunt, 1967; Stewart, 1980), with altitudes ranging from below sea level to more than 4,000 m (Hunt, 1967; Stewart, 1980). Death Valley, California is the lowest altitude (~85 m below sea level) in the Great Basin, and the United States. The two highest peaks in the state of Nevada include Wheeler Peak at ~3,984 m and Boundary Peak at ~4,009 m (Stewart, 1980). Wheeler Peak is part of the Snake Range that bounds SV6 to the east (SV6 is bound by the Schell Creek Range to the west, Antelope Range to the north, and the Fortification and Wilson Creek Ranges to the south). The Sierra Nevada and Cascade ranges bound the western portion of the Great Basin and the Wasatch Mountains and southern Utah plateaus bound the eastern portions. The Great Basin is bounded by the low ridges of Tertiary and Quaternary disrupted lava flows of the Columbia Plateau to the north; however, this delineation is arbitrary due to the grading into the Basin and Range (Hunt, 1967). The Great Basin is bordered by the Sonoran Desert subdivision to the south.

The Great Basin was so named by John C. Fremont (1845) because water did not drain to the ocean from this region. This in effect is what is known as a closed basin; however, there are a few rivers that drain outwards including a few streams in southeast Idaho (most of which empty into the Snake River) and Virgin River which empties into Lake Mead and is further carried away down the Colorado River (Stewart, 1980).

Climate

The Basin and Range Province, and particularly the Great Basin, is defined by Hunt (1967) as an arid climate; however, the Great Basin is much more varied and extreme (Hidy and Klieforth, 1990; Mac et al., 1998). Due to the large mountain ranges west (Sierra Nevada and Cascade ranges) and east (Rocky Mountains) of the Great Basin, and the mountain ranges and alluvial valleys in between, climates vary from the very dry and hot desert climate in the smaller and lower basins, to steppe-like climates in the higher basins, to the humid alpine climates in the mountains (Mifflin, 1988). Climates ranging from mid-latitude steppe in the valleys (e.g., Spring Valley and SV6) to humid continental climate in the high latitudes (e.g., Snake Range) are typical (Houghton et al., 1975; Elliot et al., 2006). The mid-latitude steppe is characterized as having a moisture deficit (annual precipitation of 150 to 380 mm), with cold winters (-6 to 4 °C) and warm summers (18 to 27 °C); and the high latitude is characterized as having heavy precipitation (annual precipitation of 630 to 1140 mm), cold winters (-12 to -1 °C), and mild summers (10 to 21 °C) (Houghton et al., 1975). According to Western Regional Climate Center (WRCC) meteorological Station # 267450 (38.92°, -114.4°), ~15 km southeast of SV6, the average annual minimum and maximum temperatures are 0.4°C and 18.0°C, respectively, for the period of record 1 October 1988 through 31 May 2007 (WRCC, 2007). Station # 267450 is

located at an elevation of 1,807 m. According to Elliot et al. (2006), snow accumulation occurs from November to March with melting occurring from March through the summer.

According to Houghton et al. (1975), three types of storms impact the area. The first is a low pressure storm where warm, moist air from the Pacific Ocean moves across the shore and up over the Sierra and Cascade Ranges. This warm, moist oceanic air rises up along the west-facing Sierra Nevada Mountains, cools due to the high elevation and condenses to form rain and snow. The dry, dense air sinks, warms via compression, and creates the rain-shadow deserts of the Great Basin and Mojave (Figure 36). However, if enough moisture coalesces from the Pacific, the air mass can move over the ranges and carry enough precipitation to Spring Valley (Houghton et al., 1975). The second type of storm system is the Great Basin low, or continental storm. These storms occur due to the combination of a cold front from the Pacific Ocean and polar-air mass from the north replacing the warm air and creating a low pressure system within the area (Houghton et al., 1975). Low pressure and continental storms occur throughout the year, but are rare during the summer (Houghton et al., 1975). The third storm is convective, formed from moist tropical air from the southeast (Gulf of Mexico and Gulf of California), and hot days and strong surface heating (Houghton et al., 1975). Convective storms create afternoon and evening thunderstorms during July and August.

Although the most of the Great Basin is generally considered an arid environment, this was not always the case (Hunt, 1967). The Pleistocene Epoch (3 Ma to 11 ka) consisted of major glaciation and deglaciation events allowing for multiple lakes to develop (Hunt, 1967; Mac et al., 1998); while the last 11,000 years is characterized by recession of glaciers and warmer and drier climate (Mac et al., 1998).

Figure 36. Conceptual diagram of the Great Basin rain shadow.

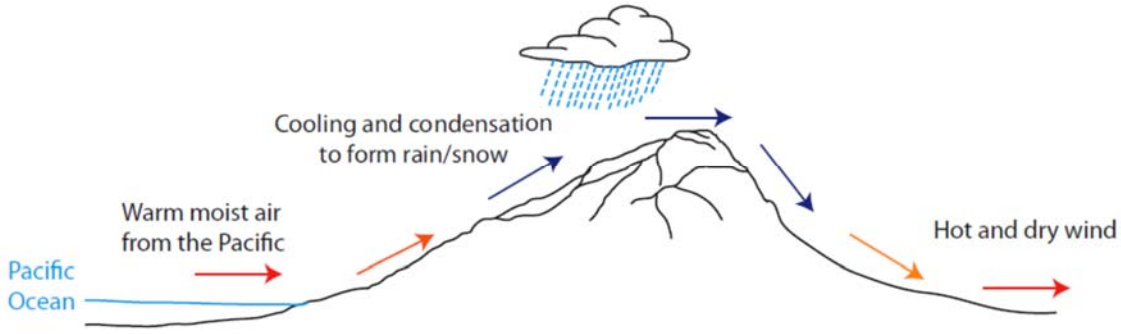

Geology

The geology of the area resulted from an array of complex events characteristic of the Great Basin. The region displays a record of marine sedimentation, compression, island-arc plutonism and volcanism, volcanism of both mafic and felsic lava, extension, and the weathering, erosion, transportation, deposition, and lithification of terrestrial sediments (Mifflin, 1988). Little is known of the Precambrian, but according to Fiero (1986), rifting of a supercontinent (Columbia) occurred something around 2 Ga (Early/Middle Proterozoic). The southern half of the land mass moved south allowing for the deposition of Middle and Late Proterozoic sediments to lie unconformably on top of the Early Proterozoic and Archean crystalline basement. Beginning ~1.75 million years ago, plate movement changed direction creating a subduction zone of oceanic crust between the margins of the split supercontinent (Fiero, 1986). Eventually the island arcs reached the continent where accretion occurred, forming new crust in the southern border of the North American continent (Fiero, 1986). Isotopic dating also found additional intrusive rocks that found their way up through the crust ~1.45 Ga; as plate movement continued towards the

same direction, island arc subduction continued to repeat in the southern portion of the Great Basin (Fiero, 1986).

Another rifting event occurred during the Late Proterozoic, splitting along a North-South direction in Central Nevada. This was the beginning of what Levy and Christie-Blick (1989) considered the first of three phases of Great Basin evolution. This period of intracontinental extension created what is known as the miogeocline (Stewart and Poole, 1974; Bond et al., 1985; Levy and Christie-Blick, 1989); sedimentary rocks forming in shallow water along a passive continental margin. Using tectonic subsidence curves for Early Paleozoic strata in the miogeocline from Canada to Mexico, Bond et al. (1985) found evidence of Late Proterozoic rifting events beginning sometime between 800 to 900 Ma. This first phase (Levy and Christie-Blick, 1989) continued into the Middle Paleozoic with continued marine deposition along the passive continental margin (Figure 37). A stable shelf allowed for the deposition of thick and extensive siltstone and quartzite to the east, siltstone, carbonate, and quartzite in the central Great Basin, and chert, shale and volcanic rocks to the west (Stewart and Poole, 1974; Levy and Christie-Blick, 1989; Welch et al., 2007). Deposition of these rocks formed a miogeoclinal wedge, thickening from east to west from <150 m to >6000 m of the Great Basin (Stewart and Poole, 1974). The thicker section of this wedge consisted of mostly carbonate rocks and mudstones (Middle Cambrian to Devonian) (Levy and Christie-Blick, 1989). The vast carbonates that deposited during this period are characteristic of the Great Basin carbonate aquifer (Winograd and Thordarson, 1975; Harrill and Prudic, 1998). Siliceous sediments and volcanics deposited in the deeper ocean to the west, while colder water dissolved out the carbonates (Fiero, 1986). These deposits are known as the siliceous, or western, assemblage.

Figure 37. Middle Paleozoic Era (Silurian) of the Great Basin with marine deposition along a passive continental margin (modified from Blakely, 1997 and Welch et al., 2007).

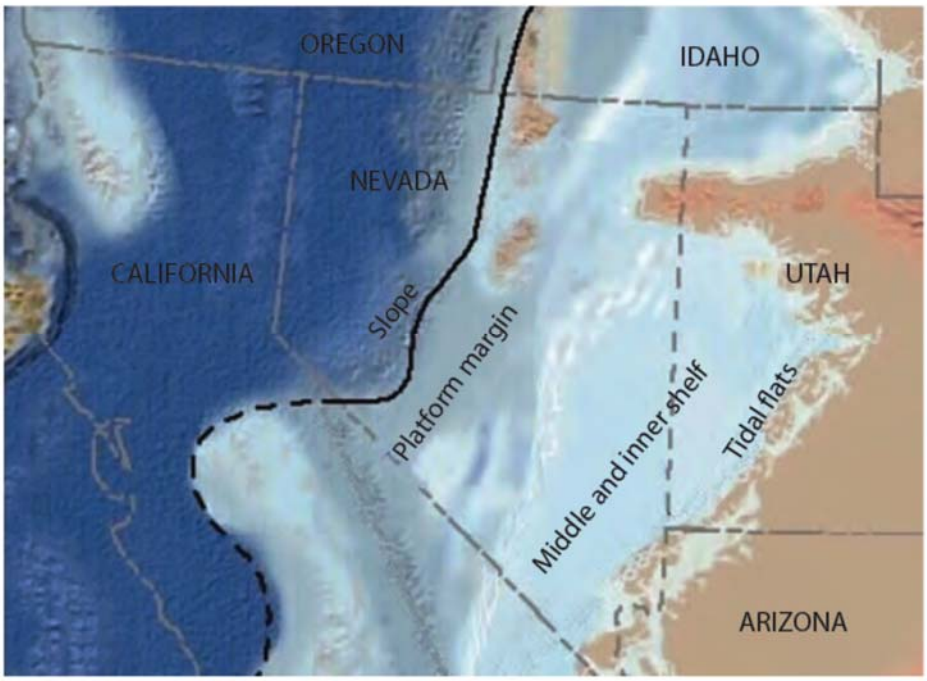

The second phase outlined by Levy and Christie-Blick (1989) was during the Late Devonian to Eocene (~375 to 50 Ma). The continental margin was passive until the Late Devonian when large-scale compression and mountain building occurred (Levy and Christie-Blick, 1989). Although the second phase was tectonically active, Paleozoic deformational events were focused in the central and western portions of the Great Basin and did not affect the eastern portion (Levy and Christie-Blick, 1989). This large scale compression brought forth one of the major Great Basin mountain building events (Late Devonian to Late Mississippian) known as the Antler Orogeny. Less dense continental crust was subducted under an oceanic volcanic arc (Antler Arc) during compressive deformation affecting the northwestern part of the Great Basin (Stewart, 1980; Fiero, 1986). This event formed folds and thrusts of the Roberts Mountain, which was at least 2,400 m thick and passed through the western side of Eureka, Nevada, thus creating a

north-trending highland (Stewart, 1980; Fiero, 1986). During the Carboniferous, the Antler Foreland Basin formed a shallow water environment, or seaway (Lane et al., 1999). Deposition of ~3,500 m of Mississippian sedimentary rocks was deposited in eastern Nevada (Speed and Sleep, 1982).

During the Early Mesozoic, ~9100 m of sediments, most of which were volcanic, overlapped the Paleozoic miogeocline's flank (Hunt, 1967). A batholith formed the Sierra Nevada during the Middle and Late Mesozoic; in addition, the Early Mesozoic and Paleozoic formations were folded with resulting thrust faults and uplift (Hunt, 1967). Continued igneous intrusive activity spread eastward into the deformed Mesozoic and Paleozoic rocks creating stocks and laccoliths (Hunt, 1967). During the Middle Jurassic to Early Tertiary, compressive deformation occurred in the east, resulting in a north-northeast Cordilleran fold and thrust belt (Fiero, 1986; Levy and Christie-Blick, 1989).

Thick blankets of lava and ash-flow tuff developed during the Eocene to Middle Miocene, including many calderas, in the north (Hunt, 1967) and was followed by lithospheric extension of the entire region between the Colorado Plateau and the Sierra Nevada, additional volcanic eruptions in the southwest, and continental sedimentation causing the horst and grabben topography of today (Hunt, 1967; Levy and Christie-Blick, 1989; Welch et al., 2007). The margins of these calderas formed new groundwater flow paths and barriers within the Great Basin (SNWA, 2008). The lithospheric extension during the Middle to Late Cenozoic (37 Ma to present) was the third phase as defined by Levy and Christie-Blick (1989) that occurred between the Colorado Plateau and Sierra Nevada (Eaton, 1982). Block faulting (normal faulting) continues to today.

SV6 is located in Spring Valley, one of many grabens in the Great Basin that holds basin-fill deposits from erosion of the nearby ranges. Lithology of Spring Valley basin-fill includes both volcanic rocks, sedimentary rocks, and lake sediments (Welch et al., 2007), holding ~610 m of basin-fill deposits in the north and ~1,829 m in the south (SNWA, 2008). Along the flanks of the mountain ranges towards the bottom of the basin, sediments generally decrease in size and sorting. Occasional fault scarps interrupt the basin fill, as do alluvial fans at the canyons mouth (Eaton, 1982). Fine-grained material and evaporites (lacustrine deposits) are also found within the basin-fill of Spring Valley, including caliche and anhydrite (Hunt, 1967; Mifflin, 1968; Morrison, 1991; Welch et al., 2007).

Hydrology

Surface Water

Most of the valleys within the Great Basin show evidence of a large number of pluvial lakes, some extensive in size, formed during the Late Pleistocene (Hunt, 1967; Mifflin, 1988; Morrison, 1991). Morrison (1991) estimated ~120 lakes during this time. Evidence is supported by the lacustrine features throughout the Great Basin. Mifflin (1988) and Morrison (1991) identified strandlines, fine-grained lacustrine deposits, spits, embankments, evaporites and saline groundwater, terraces, deltas, and/or wave-cut cliffs. Most evidence comes from Lakes Lahontan and Bonneville located in the western and eastern Great Basin, respectively. Lake Bonneville was the largest lake in the Western Hemisphere. During the period from ~17,000 to 15,000 years ago, it reached an area of ~51,800 km^2, similar size as present day Lake Michigan (Hunt, 1967; Morrison, 1991). Lake Lahonton was considered the second-largest pluvial lake in the Western Hemisphere covering ~21,000 km^2 (13,000 ka). Permanent natural lakes still in existence today

(in the Great Basin) include Great Salt, Bear, Utah, Pyramid, Walker, Tahoe, Mono, Abert, Crump, Harney, Malheur, and Summer Lakes (Morrison, 1991).

Despite the aridity of the region, there are many perennial rivers within the Great Basin. Some of the larger rivers include the Bear (largest river draining into or within the Great Basin), Sevier, Humboldt (longest river with a length of ~ 620 km), Truckee, Carson, and Walker Rivers (Morrison, 1991). The Truckee, Carson, and Walker Rivers supply potable water for the residents, industry, and agriculture in northwestern Nevada, while the Humboldt River supplies much of northeastern Nevada with water (Morrison, 1991). Although generally acknowledged as a closed basin, water does drain out of the Great Basin via a few streams in southeast Idaho, most of which empty into the Snake River, Pit River located in northwest California, and Virgin River which empties into Lake Mead and is further carried away down the Colorado River (Hunt, 1967; Stewart, 1980). Snowpack provides melt-water runoff for most of these rivers. Where runoff does not reach the larger rivers, some infiltrates in the mountain source areas, some reaches basin margins and infiltrates into the vadose zone, and the rest is lost to evapotranspiration (ET) (Mifflin, 1988). ET can dominate the loss of water from ground surface in arid and semi-arid regions.

In addition to lakes and rivers, numerous desert springs within the boundary of the Great Basin exist. Spring brooks, or small streams, usually accompany the springs. Water emanating from springs is provided by groundwater from the basin-fill and/or carbonate aquifers. Springs provide a water source for wildlife and a habitat for numerous plants, including rare and endemic species within the Great Basin (Patten et al., 2008). The primary source of water for springs in the area is from the carbonate aquifer; however, the basin-fill aquifer also supplies numerous springs (Welch et al., 2007; Patten et al., 2008). SNWA (2008) inventoried 503 springs in Spring

Valley, with most located along the western side of the northern half of the valley. No springs are within the vicinity of SV6.

Groundwater

Two primary aquifers dominate the Great Basin area, including the Cenozoic valley or basin-fill aquifer (eroded carbonate and volcanic rock) which is hydraulically connected to other basin-fill aquifers or the second dominant aquifer the fractured, highly permeable carbonate rock aquifer that is hydraulically connected to large mountains (Plume, 1996; Welch et al., 2007). Harrill et al. (1988) groups the rocks within the Great Basin into three categories: 1) high permeable basin fill, 2) low permeable consolidated rock, and 3) moderate to high permeable consolidated rock. There are numerous flow systems throughout the Great Basin that are governed by the geologic and climatic history. According to Mifflin (1988), the structure and related topography of the Great Basin determines the hydrogeology of the region, and includes the following factors that have created current hydrogeologic conditions:

I. Extensional faulting during the last 37 Ma providing the basin and range topography;

II. Regional atmospheric circulation due to rain-shadow effect that produce humid alpine in high altitudes and arid/semi-arid climate in the basins;

III. Numerous closed basins preventing both surface and groundwater external drainage; and

IV. Quaternary climate (pluvial lakes) providing more water today.

Harrill et al. (1988) lists 39 major flow systems incorporating 260 Great Basin hydrographic areas. Each hydrographic area is typically one topographic basin (e.g., Spring Valley, Snake Valley), following the basic premise that the discharge area is the location of termination of these flow systems (Harrill et al., 1988). Basin-fill aquifers are typically present within each individual hydrographic area; however, the major flow systems are typically delineated by multiple

hydrographic areas, ranging from ~78 to 46,620 km^2 in area (Harrill et al., 1988). In the eastern portion of the Great Basin, flow systems governed by the carbonate-rock province (aquifer) typically discharge from springs and do not coincide with surface flow; in the west, large flow systems do coincide with surface flow (Harrill et al., 1988). Figure 38 provides a conceptual model (modified from Welch et al., 2007) of groundwater flow in the Great Basin. Ranges of transmissivity and hydraulic conductivity for the dominant aquifers in the Great Basin are 10-10000 m^2 day^{-1} and 10-500 m day^{-1}, respectively (Heath, 1988).

Figure 38. Great Basin conceptual groundwater flow model (modified from Welch et al., 2007)

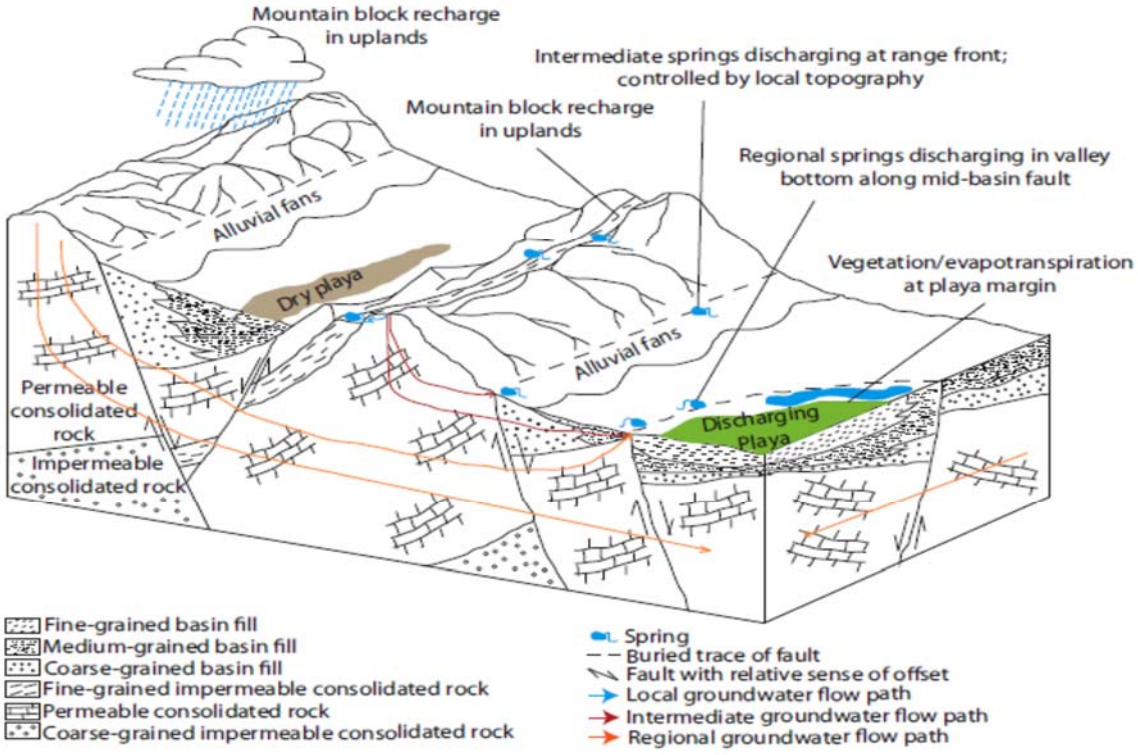

Recharge in the basin-fill occurs from upward discharge from the carbonate aquifer and along the interface of the mountains and valley alluvium (Welch et al., 2007) through a series of springs. The deep carbonate aquifer is recharged primarily through the mountain blocks, flowing from east-central Nevada and western Utah toward the south, discharging from springs in Ash Meadows, Death Valley, and Lake Mead (Laczniak et al., 1996; Plume, 1996). Range of recharge for the dominant aquifers in the Great Basin is 5-50 mm yr^{-1} (Heath, 1988). The climate during the Quaternary, particularly the Pleistocene, varied providing more moisture for the pluvial environments discussed above, both small and large, thus determining the patterns of groundwater, discharge, and water quality of today (Mifflin, 1988). Due to more prominent rainfall and wetter conditions of this time, increased distribution of well-sorted river and delta deposits have formed "favorable aquifers" for the basin-fill (Arnow et al., 1970).

Lithologic descriptions and previous studies describe the basin-fill aquifer for both Spring and Snake Valleys as having interbedded silts, clays, sands, and gravels, with increasing grain size from the central valleys to the valley margins (Rush and Kazmi, 1965; SNWA, 2008). Groundwater reaches the surface from springs, but reaches depths over 122 m below surface in Spring Valley (SNWA, 2008). Groundwater is typically deeper along the valley margins. Two gradients were observed in Spring Valley by SNWA (2008), one from north to south in the northern section (~4.7-5.7 m km^{-1}) and one from south to north in the southern portion (~1 m km^{-1}). SNWA (2008) suggest regional groundwater movement from the southern portion of Spring Valley to the middle portion, based on limited data. Most of the recharge in Spring Valley comes from the Schell Creek and Snake Ranges; furthermore, interbasin flow is believed to occur from Steptoe and Lake Valleys into Spring Valley, and Spring Valley into Snake Valley (Welch et al.,

2007). Investigations have been conducted by Laczniak et al. (1996), Prudic et al. (1995), Welch et al. (2007), and SNWA (2008) for the given area groundwater systems.

Plant Community

Climate partly controls the distribution of plants. Hunt (1967) identifies four principal climate factors that affect plant growth: light, temperature, precipitation, and wind. The Great Basin topography, particularly the altitude, influences these four factors creating life zones. For example, the Upper Sonoran Zone identified in Hunt (1967), is dominated by Sagebrush (*Artemisia L.*) in the valleys and pinyon-juniper in the mountains. Others have also stated that the dominant vegetation in the Great Basin is mostly shrub land, predominantly Sagebrush (*Artemisia L.*), in the valleys, and pinyon (*Pinus monophylla*)-juniper (*Juniperus L.*) woodlands and aspen (*Populus tremuloides*)-coniferous forests in the mountains; although alpine tundra dominates very high altitudes (U.S. Department of the Interior, 1992; Orndorff et al., 2001; Elliot et al., 2006). Although climate influences the distribution of different species following an elevational transect, differences within the individual zones primarily depends on the ground's ability to control water. Finer materials (i.e., clays and silts) have a higher water capacity whereas coarser materials not as much. Moving from the valley margins to the center, soil grain size typically decreases, thereby increasing the amount of water that can be held in the subsurface soil. In addition, the water table becomes shallower, where it may reach the surface as spring discharge. The amount of ET, an important component in nature's water balance (particularly in arid and semi-arid environments), will depend on the amount of water near the surface which is also controlled by the local plant diversity. Moreo et al. (2007) identified 10 ET units within the basins that included xerophytes, open water, marshes, meadows, grass, moist

bare soil, dense shrubland, moderately dense shrubland, sparse shrubland, dry playa, and recently irrigated cropland.

Greasewood (*Sarcobatus vermiculatus*) and Big Sage (*Artemisia Tridentata*) are the dominant plants in Spring Valley. Although phreatophyte roots can extend to depths greater than 3 m (Groeneveld, 1990), maximum lateral root density are typically above 3 m for Big Sage (Richards and Caldwell, 1987) and Greasewood, which was shown to have ~ 65% of roots within the upper 75 cm (Donovan et al., 1996). Other shrubs found in the Great Basin specific to the site include rabbitbrush (*Chrycothammus nauseosus*), and shadscale (*Atriplex confertifolia*) (Nichols, 1994; Welch et al., 2007). Plants rely on both groundwater and soil water simultaneously; as opposed to soil water in the summer and groundwater later in the growing season (Steinwand et al., 2006). Accordingly, ~60-81% of ET at the sites was from plant uptake directly from the water table (Steinwand et al., 2006); however, these estimates were from sites with dense cover and shallow water tables (~1 to 3 meters in depth) which is much shallower than SV6.

REFERENCES

Anderson, M.P. 2005. Heat as a ground water tracer. Ground Water 43: 951-968. doi:10.1111/j.1745-6584.2005.00052.x.

Andraski, B.J. 1997. Soil-water movement under natural-site and waste-site conditions: A multiple-year field study in the Mojave Desert, Nevada. Water Resources Research 33: 1901-1916.

Arnone, J. A., R.L. Jasoni, J.D. Larsen, L.F. Fenstermaker, G. Wohlfahrt, C.B. Kratt, B.F. Lyles, J. Healey, M.H. Young, and J.M. Thomas. 2008. Variable evapotranspirative water losses from lowland agricultural and native shrubland ecosystems in the eastern Great Basin of Nevada, USA: DRI Publication No. 655.7250, 97 pp.

Arnow, T., J.H. Feth, and R.W. Mowers. 1970. Ground water in the deltas of the Bonneville Basin, U.S.A, International Association Scientific Hydrology Symposium, 2: 396-407.

Baldocchi, D., E. Falge, L.H. Gu, R. Olson, D. Hollinger, S. Running, et al. 2001. FLUXNET: A new tool to study the temporal and spatial variability of ecosystem-scale carbon dioxide, water vapor, and energy flux densities. Bulletin of the American Meteorological Society 82: 2415-2434. doi:10.1175/1520-0477(2001)082<2415:fantts>2.3.co;2.

Baldocchi, D.D. 2003. Assessing the eddy covariance technique for evaluating carbon dioxide exchange rates of ecosystems: past, present and future. Global Change Biology 9: 479-492. doi:10.1046/j.1365-2486.2003.00629.x.

Bilskie, J., B. Clawson, and J. Ritter. 2007. Calibration of heat pulse sensors for soil water matric potential, *in* Proceedings, American Society of Agronomy, Crop Science Society of America, and Soil Science Society of America International Annual Meeting: New Orleans, LA, 4-8 November.

Blakely, R.C. 1997. Paleographic evolution of the passive-margin to active-margin transition, early Mesozoic, western North America, *in* Proceedings, Annual Meeting of Geological Society of America: http://jan.ucc.nau.edu/rcb7/paleogeogwus.html: Salt Lake City, UT, October (accessed October 2014).

Bond, G.C., N. Christieblick, M.A. Kominz and W.J. Devlin. 1985. An early Cambrian rift to post-rift transition in the Cordillera of Western North-America A. Nature 315: 742-746. doi:10.1038/315742a0.

Bristow, K.L., G.J. Kluitenberg and R. Horton. 1994. Measurement of soil thermal-properties with a dual-probe heat-pulse technique. Soil Science Society of America Journal 58: 1288-1294.

Brutsaert, W. and D.Y. Chen. 1995. Desorption and the 2 stages of drying of natural tallgrass prairie. Water Resources Research 31: 1305-1313. doi:10.1029/95wr00323.

Campbell, G.S., C. Calissendorff and J.H. Williams. 1991. Probe for measuring soil specific-heat using a heat-pulse method. Soil Science Society of America Journal 55: 291-293.

Chief, K., M.H. Young, B.F. Lyles, J. Healey, J. Koonce, E. Knight, E. Johnson, J. Mon, M. Berli, M. Menon, and G. Dana. 2009. Scaling environmental processes in heterogeneous arid soils: construction of large weighing lysimeter facility: Division of Hydrologic Sciences, Desert Research Institute Pub. No. 41249.

Conant, B. 2004. Delineating and quantifying ground water discharge zones using streambed temperatures. Ground Water 42: 243-257. doi:10.1111/j.1745-6584.2004.tb02671.x.

Constantz, J. 2008. Heat as a tracer to determine streambed water exchanges. Water Resources Research 44. doi:10.1029/2008wr006996.

Constantz, J., and D. A. Stonestrom, (2003), Heat as a tracer of water movement near streams *in* D. A. Stonestrom and J. Constantz, eds., Heat as a tool for studying the movement of ground water near streams: U.S. Geological Survey Circular 1260: 96.

Constantz, J., S.W. Tyler and E. Kwicklis. 2003. Temperature-Profile Methods for Estimating Percolation Rates in Arid Environments. Vadose Zone Journal 2: 12-24.

Cooper, D.J., J.S. Sanderson, D.I. Stannard and D.P. Groeneveld. 2006. Effects of long-term water table drawdown on evapotranspiration and vegetation in an arid region phreatophyte community. Journal of Hydrology 325: 21-34. doi:10.1016/j.jhydrol.2005.09.035.

Devitt, D.A., L.F. Fenstermaker, M.H. Young, B. Conrad, M. Baghzouz and B.M. Bird. 2010. Evapotranspiration of mixed shrub communities in phreatophytic zones of the Great Basin region of Nevada (USA). Ecohydrology 4: 807-822. doi:10.1002/eco.169.

Dijkema, J., J. Koonce, T.A. Ghezzehei, M. Berli, M. Van der Ploeg and M.T. Van Genuchten. 2015. Simulating water flow and heat transfer in arid soil using weighing lysimeter data. European Geosciences Union, Vienna: p. EGU2015-8178.

Donovan, L.A., J.H. Richards and M.W. Muller. 1996. Water relations and leaf chemistry of Chrysothamnus nauseosus ssp Consimilis (Asteraceae) and Sarcobatus vermiculatus (Chenopodiaceae). American Journal of Botany 83: 1637-1646.

Dregne, H.E. 1991. Global status of desertification. Annals of Arid Zone 30: 179-185.

Eaton, G.P. 1982. The basin and range province - origin and tectonic significance. Annual Review of Earth and Planetary Sciences 10: 409-440. doi:10.1146/annurev.ea.10.050182.002205.

Ehleringer, J.R., S.L. Phillips, W.S.F. Schuster and D.R. Sandquist. 1991. Differential utilization of summer rains by desert plants. Oecologia 88: 430-434. doi:10.1007/bf00317589.

Elliot, P.E., D.A. Beck, and D.E. Prudic. 2006. Characterization of surface-water resources in the Great Basin National Park area and their susceptibility to ground-water withdrawals in adjacent valleys, White Pine County, Nevada: U.S. Geological Survey, Scientific Investigations Report 2006-5099.

Evett, S.R., A.W. Warrick and A.D. Matthias. 1995. Wall material and capping effects on microlysimeter temperatures and evaporation. Soil Science Society of America Journal 59: 329-336.

Fiero, B. 1986. Geology of the Great Basin, University of Nevada, Reno: 197.

Fremont, J.C. 1845. Report of the exploring expedition to the Rocky Mountains in the year 1842, and to Oregon and North California in the years 1843-1844: Washington, Blair and Rives, Printers: 583.

Garcia, C.A., B.J. Andraski, D.A. Stonestrom, C.A. Cooper, J. Simunek and S.W. Wheatcraft. 2011. Interacting Vegetative and Thermal Contributions to Water Movement in Desert Soil. Vadose Zone Journal 10: 552-564. doi:10.2136/vzj2010.0023.

Garnier, M., D.M. Harper, L. Blaskovicova, G. Hancz, G.A. Janauer, Z. Jolankai, E. Lanz, A.L. Porto, M. Mandoki, B. Pataki, J.L. Rahuel, V.J. Robinson, C. Stoate, E. Toth, and G. Jolankai. 2015. Climate Change and European Water Bodies, a Review of Existing Gaps and Future Research Needs: Findings of the ClimateWater Project. Environmental Management 56: 271-285. doi:10.1007/s00267-015-0544-7.

Gee, G.W., P.J. Wierenga, B.J. Andraski, M.H. Young, M.J. Fayer and M.L. Rockhold. 1994. Variations in water-balance and recharge potential at 3 western desert sites. Soil Science Society of America Journal 58: 63-72.

Groeneveld, D.P. 1990. Shrub rooting and water acquisition on threatened shallow groundwater habitats in the Owens Valley, California: USDA Forest Service General Tech. Report INT-276: 221-236.

Harrill, J.R., J.S. Gates, and J.M. Thomas. 1988. Major ground water flow systems in the Great Basin area of Nevada, Utah, and adjacent states: U.S. Geol. Surv. Hydrologic Investigations Atlas 694-C, scale 1:500,000.

Harrill, J.R., and D.E. Prudic. 1998. Aquifer systems in the Great Basin region of Nevada, Utah, and adjacent states, Summary report, U.S. Geol. Surv. Professional Paper 1409-A: 66.

Heath, R.C. 1988. Chapter 3 Hydrogeologic setting of regions, *in* Back, W., Rosenshein, J.S., and Seaber, P.R., eds., The Geology of North America, Hydrogeology, Geological Society of America, Boulder, Colorado, O-2: 15-23.

Heitman, J.L., R. Horton, T.J. Sauer and T.M. Desutter. 2008a. Sensible heat observations reveal soil-water evaporation dynamics. Journal of Hydrometeorology 9: 165-171. doi:10.1175/2007jhm963.1.

Heitman, J.L., X. Xiao, R. Horton and T.J. Sauer. 2008b. Sensible heat measurements indicating depth and magnitude of subsurface soil water evaporation. Water Resources Research 44. doi:10.1029/2008wr006961.

Hendrickx, J.M.H., F.M. Phillips and J.B.J. Harrison. 2003. Water flow processes in arid and semi-arid vadose zones. Understanding Water in a Dry Environment 23: 151-210.

Herkelrath, W.N., S.P. Hamburg and F. Murphy. 1991. Automatic, real-time monitoring of soil-moisture in a remote field area with time domain reflectometry. Water Resources Research 27: 857-864. doi:10.1029/91wr00311.

Hidy, G.M., and H.E. Klieforth. 1990. Atmospheric processes affecting the climate of the Great Basin, 17-45 *in* C. B. Osmond, L. F. Pitelka, and G. M. Hidy, editors, Plant biology of the Basin and Range, Springer-Verlag, New York.

Hillel, D. 1998. Environmental Soil Physics. Academic Press, London: 771.

Houghton, J.G., C.M. Sakamoto, and R.O. Gifford. 1975. Nevada's weather and climate: Nevada Bureau of Mines and Geology, Special Publication 2, 1-78.

Humphrey, M.D., J.D. Istok, J.Y. Lee, J.A. Hevesi, and A.L. Flint. 1997. A new method for automated dynamic calibration of tipping-bucket rain gauges. Journal of Atmospheric and Oceanic Technology 14: 1513-1519.

Hunt, C. B. 1967. Physiography of the United States: New York, W.H. Freeman: 480.

Iden, S., D. Reineke, J. Koonce, M. Berli and W. Durner. 2015. Variably-saturated flow in large weighing lysimeters under dry conditions: inverse and predictive modeling. European Geosciences Union. European Geosciences Union, Vienna. p. EGU2015-9251.

Idso, S.B., R.J. Reginato, R.D. Jackson, B.A. Kimball and F.S. Nakayama. 1974. 3 STAGES OF DRYING OF A FIELD SOIL. Soil Science Society of America Journal 38: 831-837.

Jones, T.L. and R.L. Skaggs. 1989. Influence of hydrologic factors on leaching of solidified low-level waste forms at an arid-site field-scale lysimeter facility *in* Cote, P.L., Gilliam, T.M., eds., Environmental aspects of stabilization and solidification of hazardous and radioactive wastes, ASTM STP 1033, American Society of Testing and Materials, Philadelphia, 358-380.

Kalma, J.D. and S.W. Franks. 2003. Rainfall in arid and semi-arid regions. Understanding Water in a Dry Environment 23: 15-63.

Kelleners, T.J., J. Koonce, R.M. Shillito, J. Dijkema, M. Berli, M.H. Young, J.M. Frank, and W.J. Massman. 2015. Numerical modeling of coupled water flow and heat transport in soil and snow: Soil Science Society America Journal: in press.

Kray, J.A., D.J. Cooper and J.S. Sanderson. 2012. Groundwater use by native plants in response to changes in precipitation in an intermountain basin. Journal of Arid Environments 83: 25-34. doi:10.1016/j.jaridenv.2012.03.009.

Laczniak, R.J., J.C. Cole, D.A. Sawyer, and D.A. Trudeau. 1996. Summary of hydrogeologic controls on ground-water flow at the Nevada Test Site, Nye County, Nevada: U.S. Geological Survey Water-Resources Investigations Report 96-4109: 58.

Lane, H.R., P.L. Brenckle, J.F. Baesemann, and B.F. Richards. 1999. The IUGS boundary in the middle of the Carboniferous: Arrow Canyon, Nevada USA, Episodes 22: 272–283.

Lehmann, P., Assouline, S., and Or, D. 2008. Characteristic lengths affecting evaporative drying of porous media. Physical Review E: 77.

Levy, M. and N. Christieblick. 1989. Pre-Mesozoic palinspastic reconstruction of the Eastern Great-Basin (Western United-States). Science 245: 1454-1462.

Mac, M.J., P.A. Opler, C.E. Puckett Haecker, and P.D. Doran. 1998. Status and trends of the nation's biological resources: U.S. Geological Survey 2: 437-964.

Middleton, N. and D. Thomas. 1997. World atlas of desertification. John Wiley & Sons, Inc.: 182.

Mifflin, M.D. 1988. Chapter 8 Region 5, Great Basin, *in* Back, W., Rosenshein, J.S., and Seaber, P.R., eds., The Geology of North America, Hydrogeology: Geological Society of America, Boulder, Colorado, O-2, 69-78.

Moldrup, P., T. Olesen, J. Gamst, P. Schjonning, T. Yamaguchi and D.E. Rolston. 2000. Predicting the gas diffusion coefficient in repacked soil: Water-induced linear reduction model. Soil Science Society of America Journal 64: 1588-1594.

Moreo, M.T., R.J. Laczniak, and D.I. Stannard. 2007. Evapotranspiration rate measurements of vegetation typical of ground-water discharge areas in the Basin and Range carbonate-rock aquifer system, Nevada and Utah, September 2005–August 2006: U.S. Geological Survey Scientific Investigations Report 2007-5078: 36.

Morrison, R.B. 1991. Quaternary stratigraphic, hydrologic, and climatic history of the Great Basin, with emphasis on Lakes Lahontan, Bonneville, and Tecopa, *in* Morrison, R. B., eds., Quaternary nonglacial geology: Conterminous U.S.: The Geology of North America, K-2.

Nichols, W.D. 1994. Groundwater discharge by phreatophytes shrubs in the Great-Basin as related to depth to groundwater. Water Resources Research 30: 3265-3274. doi:10.1029/94wr02274.

National Security Technologies. 2015. Nevada National Security Site 2014 waste management monitoring report Area 3 and Area 5 Radioactive Waste Management Sites, Prepared for U.S. Department of Energy, National Nuclear Security Administration, Nevada Field Office.

Noy-Meir, I. 1973. Desert ecosystems: Environment and producers, Annual Review of Ecology and Systematics 4: 25-51.

Or, D., P. Lehmann, E. Shahraeeni and N. Shokri. 2013. Advances in Soil Evaporation Physics-A Review. Vadose Zone Journal 12. doi:10.2136/vzj2012.0163.

Orndorff, R.L., R.W. Wieder, and H.F. Filkorn. 2001. Geology underfoot in central Nevada: Missoula, Mountain Press Publishing: 294.

Osborn, H.B. 1983. Timing and duration of high rainfall rates in the Southwestern United-States. Water Resources Research 19: 1036-1042. doi:10.1029/WR019i004p01036.

Patten, D.T., L. Rouse and J.C. Stromberg. 2008. Isolated spring wetlands in the Great Basin and Mojave deserts, USA: Potential response of vegetation to groundwater withdrawal. Environmental Management 41: 398-413. doi:10.1007/s00267-007-9035-9.

Plume, R.W. 1996. Hydrogeologic framework of the Great Basin region of Nevada, Utah, and adjacent states, U.S. Geol. Surv. Professional Paper 1409-B: 64.

Prudic, D.E., J.R. Harrill, and T.J. Burbey (1995), Conceptual evaluation of regional ground-water flow in the carbonate-rock province of the Great Basin, Nevada, Utah, and adjacent states: U.S. Geol. Surv. Professional Paper 1409-D: 102.

Redmond, K.T. 2009. Historic Climate Variability *in* Webb, R.H., L.F. Fenstermaker, J.S. Heaton, D.L. Hughson, E.V. McDonald, and D.M. Miller, eds., The Mojave Desert: Reno, Nevada, University of Nevada Press: 11-30.

Reece, C.F. 1996. Evaluation of a line heat dissipation sensor for measuring soil matric potential. Soil Science Society of America Journal 60: 1022-1028.

Richards, J.H. and M.M. Caldwell. 1987. Hydraulic lift – substantial nocturnal water transport between soil layers by Artemisia-Tridentata roots. Oecologia 73: 486-489.

Rundel, P.W. and A.C. Gibson. 1996. Ecological communities and processes in a Mojave Desert ecosystem: Rock Valley, Nevada, Cambridge University Press: 369.

Rush, F.E., and S.A.T. Kazmi. 1965. Water resources appraisal of Spring Valley, White Pine and Lincoln Counties, Nevada, groundwater resources – Reconnaissance Series Report 33, U. S.

Geological Survey in cooperation with the State of Nevada Department of Conservation and Natural Resources: 36.

Sayde, C., C. Gregory, M. Gil-Rodriguez, N. Tufillaro, S. Tyler, N. van de Giesen, et al. 2010. Feasibility of soil moisture monitoring with heated fiber optics. Water Resources Research 46. doi:10.1029/2009wr007846.

Scanlon, B.R., R.W. Healy and P.G. Cook. 2002. Choosing appropriate techniques for quantifying groundwater recharge. Hydrogeology Journal 10: 18-39. doi:10.1007/s10040-001-0176-2.

Scanlon, B.R., K. Keese, R.C. Reedy, J. Simunek and B.J. Andraski. 2003. Variations in flow and transport in thick desert vadose zones in response to paleoclimatic forcing (0-90 kyr): Field measurements, modeling, and uncertainties. Water Resources Research 39. doi:10.1029/2002wr001604.

Scanlon, B.R., D.G. Levitt, R.C. Reedy, K.E. Keese and M.J. Sully. 2005. Ecological controls on water-cycle response to climate variability in deserts. Proceedings of the National Academy of Sciences of the United States of America 102: 6033-6038. doi:10.1073/pnas.0408571102.

Scherer, G.W. 1990. Theory of drying. Journal of the American Ceramic Society 73: 3-14. doi:10.1111/j.1151-2916.1990.tb05082.x.

Selker, J., N. van de Giesen, M. Westhoff, W. Luxemburg and M.B. Parlange. 2006a. Fiber optics opens window on stream dynamics. Geophysical Research Letters 33. doi:10.1029/2006gl027979.

Selker, J.S., L. Thevenaz, H. Huwald, A. Mallet, W. Luxemburg, N.V. de Giesen, et al. 2006b. Distributed fiber-optic temperature sensing for hydrologic systems. Water Resources Research 42. doi:10.1029/2006wr005326.

Shillito, R. (2015). Soil texture and bulk density data. Unpublished raw data.

Shokri, N., P. Lehmann, P. Vontobel and D. Or. 2008. Drying front and water content dynamics during evaporation from sand delineated by neutron radiography. Water Resources Research 44. doi:10.1029/2007wr006385.

Shokri, N., P. Lehmann and D. Or. 2009. Critical evaluation of enhancement factors for vapor transport through unsaturated porous media. Water Resources Research 45. doi:10.1029/2009wr007769.

Shokri, N. and D. Or. 2011. What determines drying rates at the onset of diffusion controlled stage-2 evaporation from porous media? Water Resources Research 47. doi:10.1029/2010wr010284.

Silliman, S.E. and D.F. Booth. 1993. Analysis of time-series measurements of sediment temperature for identification of gaining vs losing portions of Juday-Creek, Indiana. Journal of Hydrology 146: 131-148. doi:10.1016/0022-1694(93)90273-c.

Simmers, I. 2003. Hydrological processes and water resources management. Understanding Water in a Dry Environment 23: 1-14.

SNWA. 2008. Baseline characterization report for Clark, Lincoln, and White Pine Counties groundwater development project, Prepared in cooperation with the Bureau of Land Management.

Soil Survey Staff. 1993. Soil survey manual: USDA-SCS Agric. Handbook 18, U.S. Gov. Print. Office, Washington, DC.

Sorenson, S.K., P.D. Dileanis, and F.A. Branson. 1991. Soil water and vegetation responses to precipitation and changes in depth to groun water in Owens Valley, California. US Geological Survey Water-Supply Paper 2370.

Speed, R.C. and N.H. Sleep. 1982. Antler orogeny and foreland basin – a model. Geological Society of America Bulletin 93: 815-828.

Steele-Dunne, S.C., M.M. Rutten, D.M. Krzeminska, M. Hausner, S.W. Tyler, J. Selker, et al. 2010. Feasibility of soil moisture estimation using passive distributed temperature sensing. Water Resources Research 46. doi:10.1029/2009wr008272.

Steinwand, A.L., R.F. Harrington and D. Or. 2006. Water balance for Great Basin phreatophytes derived from eddy covariance, soil water, and water table measurements. Journal of Hydrology 329: 595-605. doi:10.1016/j.jhydrol.2006.03.013.

Stewart, J.H. 1980. Geology of Nevada: Nevada Bureau of Mines Geology Special Publications 4.

Stewart, J.H., and F.G. Poole. 1974. Lower Paleozoic and uppermost Precambrian Cordilleran miogeocline, Great Basin, Western United States, *in* Dickinson, W.R., ed., Tectonics and Sedimentation, Society of Economic Paleontologists and Mineralogists Special Publication 22: 28-57.

Tabbagh, A., H. Bendjoudi and Y. Benderitter. 1999. Determination of recharge in unsaturated soils using temperature monitoring. Water Resources Research 35: 2439-2446. doi:10.1029/1999wr900134.

Taniguchi, M. and M.L. Sharma. 1993. Determination of groundwater recharge using the change in soil-temperature. Journal of Hydrology 148: 219-229. doi:10.1016/0022-1694(93)90261-7.

Topp, G.C., J.L. Davis and A.P. Annan. 1980. Electromagnetic determination of soil-water content – measurements in coaxial transmission-lines. Water Resources Research 16: 574-582. doi:10.1029/WR016i003p00574.

Tyler, S.W., J.S. Selker, M.B. Hausner, C.E. Hatch, T. Torgersen, C.E. Thodal, and S.G. Schladow. 2009. Environmental temperature sensing using Raman spectra DTS fiber-optic methods. Water Resources Research 45. doi:10.1029/2008wr007052.

UNESCO. 1979. Map of the world distribution of arid regions: Explanatory note: MAP Technical Notes 7.

U.S. Department of the Interior. 1992. Great Basin National Park, Nevada—Final general management plan, development concept plans, environmental impact statement: Denver, Colo., U.S. Department of the Interior, National Park Service: 434.

van Brakel, J. 1980. Mass transfer in convective drying. Advanced drying 1: 217-267.

Vorosmarty, C.J., P. Green, J. Salisbury and R.B. Lammers. 2000. Global water resources: Vulnerability from climate change and population growth. Science 289: 284-288. doi:10.1126/science.289.5477.284.

Vorosmarty, C.J., P.B. McIntyre, M.O. Gessner, D. Dudgeon, A. Prusevich, P. Green, S. Glidden, S.E. Bunn, C.A. Sullivan, C. Reidy Liermann, and P.M. Davies. 2010. Global threats to human water security and river biodiversity. Nature 467: 555-561. doi:10.1038/nature09440.

Weiss, J.D. 2003. Using fiber optics to detect moisture intrusion into a landfill cap consisting of a vegetative soil barrier. Journal of the Air & Waste Management Association 53: 1130-1148.

Welch, A.H., D.J. Bright, and L.A. Knochenmus. 2007. Water resources of the Basin and Range carbonate-rock aquifer system, White Pine County, Nevada, and adjacent areas in Nevada and Utah: U.S. Geological Survey, Scientific Investigations 2007-5261.

Winograd, I.J., and W. Thordarson. 1975. Hydrogeologic and hydrochemical framework, south-central Great Basin, Nevada-California, with special reference to the Nevada Test Site: U.S. Geological Survey Professional Paper 712-C: 123.

Winograd, I.J. 1981. Radioactive-waste disposal in thick unsaturated zones. Science 212: 1457-1464.

WRCC. 2009. Western Regional Climate Center, http://www.wrcc.dri.edu/cgi-bin/cliMAIN.pl?nv1071 (accessed November 26, 2014).

Wright, L., D.A. Devitt, M.H. Young, J. Gan, B.J. Vanderford, S.S. Snyder, M. McCullough, and L. Dodgen. 2012. Fate and transport of thirteen pharmaceutical and personal care products in a controlled irrigated turfgrass system. Agronomy Journal 104: 1244-1254.

Wythers, K.R., W.K. Lauenroth and J.M. Paruelo. 1999. Bare-soil evaporation under semiarid field conditions. Soil Science Society of America Journal 63: 1341-1349.

Xu, X.Y., R.D. Zhang, X.Z. Xue and M. Zhao. 1998. Determination of evapotranspiration in the desert area using lysimeters. Communications in Soil Science and Plant Analysis 29: 1-13. doi:10.1080/00103629809369924.

Yiotis, A.G., I.N. Tsimpanogiannis, A.K. Stubos and Y.C. Yortsos. 2006. Pore-network study of the characteristic periods in the drying of porous materials. Journal of Colloid and Interface Science 297: 738-748. doi:10.1016/j.jcis.2005.11.043.

Young, M.H., J.B. Fleming, P.J. Wierenga and A.W. Warrick. 1997. Rapid laboratory calibration of time domain reflectometry using upward infiltration. Soil Science Society of America Journal 61: 707-712.

Young, M.H., G.S. Campbell and J. Yin. 2008. Correcting dual-probe heat-pulse readings for changes in ambient temperature. Vadose Zone Journal 7: 22-30. doi:10.2136/vzj2007.0015.

CURRICULUM VITAE

Graduate College
University of Nevada, Las Vegas

Jeremy E. Koonce

Degrees:

Bachelor of Science, Environmental Studies and Physical Geography, 1998
University of California, Santa Barbara

Master of Science, Water Resources Management, 2004
University of Nevada, Las Vegas

Publications:

Kelleners, T.J., J. Koonce, R.M. Shillito, J. Dijkema, M. Berli, M.H. Young, J.M. Frank, and W.J. Massman. Numerical modeling of coupled water flow and heat transport in soil and snow: Soil Science Society of America Journal: in press.

Chief, K., M.H. Young, B.F. Lyles, J. Healey, J. Koonce, E. Knight, E. Johnson, J. Mon, M. Berli, M. Menon, and G. Dana. 2009. Scaling environmental processes in heterogeneous arid soils: construction of large weighing lysimeter facility: Division of Hydrologic Sciences, Desert Research Institute Pub. No. 41249.

Koonce, J.E., Z. Yu, I.M. Farnham, K. Stetzenbach. 2006. Geochemical Interpretation of Groundwater Flow in the Southern Great Basin: Geosphere 2: 88-101.

Dissertation Title: Water Balance and Moisture Dynamics of an Arid and Semi-Arid Soil: A Weighing Lysimeter and Field Study

Dissertation Examination Committee:

Chairperson, Zhongbo Yu, Ph. D.
Committee Member, Markus Berli, Ph. D.
Committee Member, Michael Nicholl, Ph. D.
Committee Member, Ganqing Jiang, Ph. D.
Graduate Faculty Representative, Dale A. Devitt, Ph. D.